NASA Contractor Report 4255

Aircraft Propeller Induced Structure-Borne Noise

James F. Unruh

CONTRACT NAS1-17921
OCTOBER 1989

NASA

AIRCRAFT PROPELLER INDUCED STRUCTURE-BORNE NOISE

NASA Contractor Report 4255

Aircraft Propeller Induced Structure-Borne Noise

James F. Unruh
Southwest Research Institute
San Antonio, Texas

Prepared for
Langley Research Center
under Contract NAS1-17921

National Aeronautics and
Space Administration
Office of Management
Scientific and Technical
Information Division

1989

TABLE OF CONTENTS

LIST OF TABLES

LIST OF FIGURES

NOMENCLATURE

d_p	propeller diameter, test apparatus
f	driving frequency
f_s	engine support frequency
i_e	added engine inertia, test apparatus
i_n	added nacelle inertia, test apparatus
i_{en}	total engine/nacelle inertia, test apparatus
w_t	effective added weight, test apparatus
w_w	bare wing weight, test apparatus
A_n	nacelle frontal area, full scale
D_n	equivalent nacelle diameter
D_p	propeller diameter, full scale
F_m	engine dynamic mass reduction factor
$F(\omega)_i$	input force at the i^{th} location
$HPF(\omega)_{ji}$	force to interior pressure frequency response function
$HPX(\omega)_{ijk}$	structural response to pressure frequency response function
$HXF(\omega)_{ki}$	force to structural response frequency response function
I_e	engine roll inertia, full scale
$P(\omega)_j$	pressure response at the j^{th} microphone
$\overline{P}(\omega)_{ijk}$	computed pressure response at the j^{th} microphone
W_e	engine weight, full scale
W_t	total effective added wing weight, full scale
W_t'	normalized W_t with respect to bare wing weight
W_W	bare wing weight, full scale
$X(\omega)_k$	structural response at the k^{th} location
ρ	engine effective radius of gyration, full scale
ρ'	normalized ρ with respect to propeller diameter

I. INTRODUCTION

A major focus of interior noise control for twin-engine propeller aircraft has been the reduction of the propeller induced direct airborne component via improved sidewall treatments (ref. 1-4). A majority of the research effort in this area has been aimed at the advanced high-speed turboprop aircraft, wherein the direct airborne propeller generated noise is quite intense and appears to be most critical for the success of this new generation aircraft (ref. 5). Continued efforts to develop lightweight sidewall treatments (ref. 6) and the development of improved high-speed, low-noise propeller designs (ref. 7) are presently being pursued. With continued effort in these areas the direct airborne sidewall transmission problem may well be resolved in the near future. However, the potential for other sources and transmission paths to govern the interior noise levels is quite high, based on most recent discoveries and historical data.

Historically speaking, interior noise levels of propeller-driven aircraft continue to be much higher than the acceptable levels of present-day turbofan aircraft, even after apparently ample application of noise control measures. Engine vibration-induced, structure-borne interior noise transmission levels have been shown to be equal to or greater than the direct airborne noise transmission levels in a single-engine, propeller-driven aircraft (ref. 8). The potential for engine vibration as a source of structure-borne interior noise in twin-engine aircraft has not been thoroughly investigated; nevertheless, adequate procedures for engine vibration isolation system evaluation have been developed (ref. 9-10).

A potentially more important source of structure-borne interior noise transmission is provided by the interaction of the propeller wake and aircraft wing structure. The wing surface downstream of the propeller may experience significant aerodynamically-induced, fluctuating pressures due to the propeller wake, especially from the tip vortex (ref. 11). Extensive ground tests of a Twin Otter aircraft revealed that the propeller wake and tip vortex interaction with the wing surface was the major source of interior noise for the aircraft at 50 percent or greater engine torque (ref. 12). The interior noise spectra were dominated by contributions at the propeller blade passage frequency and its harmonics.

The expected levels of propeller wake/vortex-induced, structure-borne noise transmission in an advanced turboprop aircraft are not known, nor can they be determined with use of present-day signal detection technology. It can only be safely assumed that this source of interior noise may well limit achievable interior levels unless several noise control measures are conscientiously incorporated into the aircraft design, or provisions made for incorporation of

such control measures as necessary to achieve acceptable interior noise levels. The purpose of this research program was to develop methods of detection of this potentially important source of structure-borne noise and to evaluate several potential noise control measures.

Early in 1985, a research program was undertaken to develop an understanding of the propeller wake/vortex-induced, structure-borne noise transmission phenomenon. The program approach to achieve this objective was to develop a laboratory-based test apparatus which would allow the study and development of reliable structure-borne noise detection techniques and allow systematic evaluation of potential noise control measures. This report describes the test apparatus and its use in accomplishing the program objectives. It is hoped that the technology gained from this effort will find its way into the aircraft manufacturing community.

II. TEST APPARATUS, INSTRUMENTATION, AND CALIBRATION

A. Test Apparatus Description

In the sections to follow, the major components of the test apparatus, the wing and fuselage structures, the airborne acoustic shield and the propeller source, as pictured in the frontispiece, will be described. The primary approach to the test apparatus design was to provide a physical means of separating the airborne and structure-borne noise components so that the structure-borne noise transmission response could be studied directly without airborne noise contamination. The extent to which this was accomplished is discussed and serves as the apparatus calibration.

1. Wing Structure

The wing structure shown in the frontispiece is a 31 inch constant chord NACA 0012 section airfoil with an exposed span of 80 inches. The structure is of conventional sheet metal and rivet construction with 0.040 inch skin and ribs on 16 inch centers. The wing front and rear spars, at 29 percent and 75 percent chord, extend an additional length of 13.5 inches beyond the skin surface at the fuselage interface, as shown in Figure 1, to accommodate penetration through the fuselage acoustic shield and attachment to the fuselage. The wing structure weighs a total of 29.55 lb.

2. Wing/Fuselage Attachment

The wing-to-fuselage attachment structure is shown in Figures 2 and 3. Spherical bearings were installed at each of the three attachment points to allow only shear energy to be transferred. Wing moments are reacted by lateral differential shear in the front spar only. This physical arrangement confines the structure-borne noise transmission path to well-defined motions at the wing/fuselage attachments. When considering analytical modeling or component impedance testing (ref. 13-14), the moment-free attachment technique greatly simplifies modeling procedures. Rigid attachments, which allow both moment and shear transfer, were achieved by replacing the spherical bearings with solid bushings. Both the front and rear spar fuselage-to-wing attachments are directly secured to the fuselage floor beams and ring frames, as is shown in Figure 3. Additional floor beam cap stiffeners, 1.75 inches deep by 0.032 inches thick, were used to carry the wing loads across the fuselage.

3. Fuselage Structure

The fuselage structure is a 72 inch long and 40 inch diameter cylinder with 0.032 inch thick skin. The cylinder is stiffened by 18 evenly spaced stringers of a cross-section 3/8 x 3/8 x 0.02 inches. The stringers are riveted to the cylinder skin and pass through eight internal ring frames spaced on 8 inch centers. The ring frames are 5/8 x 1-1/2 x 0.032 inch C-channels. A schematic of the fuselage cross-section is shown in Figure 4. The floor of the cylinder, 0.032 inch thick, is supported on continuous floor beams, 0.032 inch thick, extending across the ring frames (see Figure 3) at a distance of 11 inches from the cylinder center. Two longitudinal floor beams, 0.625 x 1.5 x 0.032 inch C-channels, extend the length of the fuselage. The fuselage floor is bolted to the floor support beams and to the cylinder outer skin. The fuselage endcaps are 1/2 inch thick solid aluminum plate.

The fuselage interior trim consists of a 1/2 inch thick fiberglass blanket of density 0.6 lb/cubic ft, with a 0.002 inch thick vinyl film facing on each end cap. Four layers of the fiberglass blanket completely line the walls of the cylinder, including the area below the floor. The cabin sidewall area is finished with a sheet of epoxy/fiberglass material, 0.032 inch thick, of surface density 0.3 lb/square ft. An additional 0.032 inch sheet of vinyl is used in a 120 degree sector as a headliner trim. In this area, the trim has a surface density of 0.371 lb/square ft. The total weight of the fuselage is approximately 241 lb, with 125 lb being the solid aluminium endcaps. Additional details of the fuselage structure and cabin trim properties may be found in References 15 and 16.

4. Fuselage Acoustic Shield

In order to minimize the transmission of airborne propeller noise into the fuselage cabin, a 5-1/2 inch thick, 54 inch inside diameter, 7 ft long, 7000 lb concrete shield is used to house the fuselage (see Figure 5). The acoustic shield has removable endcaps for access to the fuselage. The endcaps are constructed from four sheets of 3/4 inch plywood, two on either side of a 1-1/2 inch thick wood core. The endcaps are bolted to the acoustic shield using a 3/16 inch thick rubber seal to prevent acoustic leakage. The interior of the acoustic shield and endcaps are fitted with 2 inch thick fiberglass, canvas-faced blankets to reduce reverberant sound build-up in the air gap between the shield and fuselage (see Figure 5).

The wing spars penetrate the acoustic shield at only two relatively small areas. An acoustic seal, consisting of a base molded to fit the shield and wing contours, and a pair of 3 inch thick adjustable blocks, also contoured to the wing cross-sectional profile, are used to reduce direct airborne noise radiation. The air gap between the wing and the seal blocks is approximately 3/16 inch around the wing surface and extends into the seal base to a depth of

approximately 4-1/2 inches, after which abrupt transition to the spar penetration holes occurs. The wing acoustic seal provides a rather tortuous sound propagation path, with resulting high transmission loss. In order to maintain the 3/16 inch gap during propeller excitation, the wing tip is fitted with a ground spring of stiffness 350 lb/inch to reduce low frequency wing buffeting which caused impacting of the wing with the acoustic seal. The performance of the seal is addressed in the apparatus calibration section.

The fuselage is supported on either end via four equally spaced elastomeric vibration supports attached to the acoustic shield. These isolators were designed to provide a fuselage/wing support frequency below 15 Hz to reduce flanking vibration. The 7,000 lb acoustic shield provides a considerable blocking mass to floor vibration transmission. In addition approximately 5 square feet of 1 inch thick rubber laminated cork vibration isolation pad was installed between the shield and the floor support stands.

5. Propeller Source

As can be seen in Figure 5, the fuselage is mounted upside down in the acoustic shield to accommodate a high wing position for use of a propeller source. The propeller is 28 inches in diameter, with a modified Clark-Y section of nearly constant 3-1/8 inch chord. The propeller is powered by an 18 horsepower hydraulic motor with a maximum speed of 6,000 rpm. A low-pressure, 9-bladed vane axial fan powered by a 20 horsepower electric motor provides a 33 inch diameter, 70 ft/sec inlet flow to the propeller to simulate forward flight. Flow swirl from the fan is reduced via 12 stationary turning vanes and two downstream 3 inch thick sections of 1/2 inch hexagonal honeycomb. The propeller source and vane axial fan are vibration-isolated and mounted to a common base. The base is on telescoping legs and can be readily positioned. It is important to note that the propeller source is not physically connected to the wing structure, thus, eliminating the propeller and motor structure-borne vibration transmission path.

B. Instrumentation

A three microphone array (see Figure 5) on an automatic traversing mechanism is used in the fuselage cabin to record transmitted sound pressure levels. The microphones are located at simulated passenger head heights: two are symmetrical on each side of the cabin and one in the center. An exterior reference microphone is located adjacent to the wing-to-fuselage acoustic seal. Additional temporary microphones used for particular tests, will be discussed in the various results sections. The interior microphones were Bruel and Kjaer 1/2 inch Type 4166 with B&K 2619 amplifiers. A Bruel and Kjaer 1/4 inch Type 4135 microphone with a B&K 2615 amplifier was used for the external reference.

Various Endevco 2220 type accelerometers were mounted on the wing front and rear spars near the root and within the fuselage cabin to record vibratory response of the structure. Specific details of their locations will be discussed in the various results sections. The wing front and rear spars were also instrumented with EA-13-090EF-120 strain gages for recording lateral strain.

The propeller source is instrumented to measure propeller speed, torque, and thrust. The propeller speed is obtained from a Bently Nevada 3000 proximity transducer and thus provides an accurate timing reference relative to blade passage of the wing plane. A yoke mechanism is used to transfer the propeller loads from the hydraulic motor to an in-line 0-250 in-lb torque cell and 0-50 lb axial load cell. The assembly is housed in the 6 inch diameter by 24 inch center body shown in Figure 6.

All instruments used were calibrated using NBS traceable standards and calibration methods. The gage factors for the strain gages provided calibration for the strain measurements. The assembled propeller loads mechanism was calibrated using known static loads applied to the propeller hub.

C. Data Acquisition and Reduction

Four-channel Zonic 6080 and eight-channel Zonic 6088 fast Fourier transform (FFT) analyzers were used extensively on line to record frequency response functions (FRF) and power spectra of sample averaged data. The spectra were displayed directly and transmitted to a PDP 11/70 digital computer or MicroVAX for further processing. When the number of simultaneous channels exceeded the FFT analyzer capabilities, the data were recorded using a 14-channel FM tape recorder and post processed. Direct data analysis was preferred in order to utilize the 60 dB dynamic range of the FFT analyzers.

D. Apparatus Calibration

1. Acoustic Seal Performance

The performance of the acoustic seal at the wing/fuselage interface was a major concern in the development of the test apparatus. Performance of the seal was evaluated by subjecting the seal to direct airborne noise excitation via a speaker. The test arrangement and microphone locations used during the evaluation are shown schematically in Figure 7. The external microphone in position R2, near the seal gap, was used as a source reference. The speaker was driven with a random noise source with energy in the frequency range from 60 to 2000 Hz. A second microphone was placed just inside the acoustic shield near the wing front spar, where transmission from the acoustic seal leakage would be a maximum, position A in Figure 7. The measured sound pressure level (SPL) spectra at position A and R2 are given in

Figure 8a. These spectra were developed using 1,000 sample averages with a 2.5 Hz analysis bandwidth. The difference in SPL at A to the SPL at R2 is given in Figure 8b. As can be seen by this data, a majority of the spectra exhibit a 20 dB or greater SPL difference.

To evaluate the possibility of improving the seal performance, the 3/16 inch gap was sealed with a putty tape. The high density sealing material resulted in only marginal increases in transmission loss, as is seen by the difference spectrum shown in Figure 8c. At first, it was thought that the sealed gap noise transmission was due to re-radiation of the structure-borne noise from the front spar; however, it was demonstrated that this was not the case by wrapping the wing structure in a high transmission-loss blanket. The blanket had little effect on the closed seal spectrum. Measurements of SPL spectra were also taken at various locations in the air gap between the fuselage and the lined acoustic shield. Consistently, the SPL decreased with increasing distance from the local area where the wing spars penetrate the acoustic shield.

During the seal evaluation, the measured interior noise levels within the fuselage were so low (40 dB or less) that microphone self-noise was the only measurable response. It is believed that no further improvement in the seal design is necessary as is shown in Section II.D.5.

2. Cabin Acoustic Response

The structure-borne noise transmission level for a unit rms input force on the wing front spar at Wing Station 96 (see Figure 19) is given in Figure 9. The SPL response in Figure 9 is from microphone P4 at Fuselage Station 26; similar response occurred throughout the cabin. As can be seen, the spectrum is quite rich in apparent resonant response which can be attributed to cabin interior acoustic resonances, fuselage structural resonances, or wing resonances. It is difficult to experimentally separate cabin acoustic resonances and fuselage structural resonances in the highly coupled system. For purposes of identifying acoustic resonances, the hardwall acoustic modes of the cabin were computed using a finite element procedure (ref. 13), and the results from the analysis are shown in Figure 10. The cabin acoustic modal density is moderately high, with 26 modes in the frequency range below 500 Hz. A plot of acoustic modal density of the cabin is given in Figure 11a.

A finite element dynamic model of the fuselage structure was also developed (ref.13) consisting of 3,492 dynamic degrees of freedom. The modal density plot for the fuselage structure is given in Figure 11b. The high number of resonant modes in the 70 Hz to 100 Hz frequency range are local cabin floor modes. The floor modes do not significantly contribute to structure-borne noise transmission due to their poor coupling with the interior acoustic modes

(ref. 13). Modal responses above 100 Hz are primarily fuselage shell modes. Local fuselage panel modes were above the 500 Hz frequency range of interest. Typical computed mode shapes for the fuselage structure are shown in Figure 12.

3. Wing Structural Response

An experimental modal analysis of the wing structure attached to the fuselage was carried out in order to provide an indication of resonant structural modes for the noise transmission path. Analysis of the overall wing structure and typical 15.75 inch x 14.25 inch panels were carried out and the results are summarized in Table 1. An in-depth finite analysis of the free-free wing structure was also carried out as reported in Reference 14. A high number of wing panel modes were found to occur below 200 Hz due to the rather large, nearly flat, un-stiffened wing panels between the wing spars and ribs.

4. Propeller Noise Source

The noise source fitted with the two-bladed propeller was run and the thrust and torque were recorded at various speeds. The torque and load cell produced repeatable results and the propeller speed could be held to within 5 rpm. The propeller performance data for an inlet flow of 70 ft/sec are shown in Figure 13. The maximum speed for the propeller source is 5700 rpm, requiring approximately 13.5 horsepower. At the lower propeller speeds (below 2700 rpm), the propeller extracted energy from the inlet air, giving rise to a negative thrust. The propeller produces a high level of airborne noise, as can be seen in the spectra shown in Figure 14a. The two-bladed propeller fundamental, at a speed of 5100 rpm, occurs at 170 Hz. The first five propeller tones, denoted as P1 through P5, are readily seen in the source spectra R1, as well as the interior cabin response at microphone P2 (see Figure 14b). Several other distinct periodic components are present in the source spectra, which can be attributed to the propeller inlet air source which operates at 1750 rpm. The axial fan has nine blades, giving rise to a 262.5 Hz fundamental, with 525 Hz and 787.5 Hz harmonics, denoted as F1 through F3 in the R1 spectrum. The periodic components near 600 and 800 Hz are attributed to the gearing of the hydraulic motor and power supply. The propeller harmonics are easily identified in the interior spectrum shown in Figure 14b. What appears to be a P1/2-propeller harmonic in the interior spectrum is not propeller-related, but rather a modal response of the cabin fundamental acoustic mode (approximately 93.5 Hz) excited by the low frequency vibratory response of the microphone traversing mechanism used to obtain the spatial average at P2. The spectra of Figure 14 were obtained with the propeller source placed at approximately Wing Station 80, with a propeller to wing leading edge spacing of approximately 22 inches.

Estimates of the propeller dynamic loading were analytically developed during the program (ref. 14). The predicted wing cyclic pressure loading developed at various times during the passage of the propeller given in Figure 15 is taken from Reference 14. It is of interest to note that the only significant loading within the first several propeller harmonics, insofar as overall induced forces to the wing, is a dynamic bending moment contribution about the propeller axis. This analytical observation was indirectly confirmed during the experimental program reported herein.

5. Apparatus Dynamic Range

To determine the dynamic range of the test apparatus for structure-borne noise control measure development and evaluation, test runs were carried out for wing-attached and wing-detached configurations. In the wing-detached configuration, the wing was placed into the acoustic shield in the normal attached position; however, support was provided by small wooden wedges placed in the acoustic seal gap. The wing front and rear spar fuselage attachment bolts were not installed, thus preventing contact between the two structures. The wooden wedges introduced less than a 5 percent blockage of the acoustic seal. The major result was to cut the wing vibration transmission path and, hence, eliminate the structure-borne noise transmission path. Data with the wing attached and detached were acquired at fixed propeller speeds of 3450, 4260, 4980, and 5700 rpm. Interior sound pressure levels were acquired at 12 interior microphone locations, P2, P3, and P4, (see Figure 7) at Fuselage Stations 5, 26, 47, and 67 (see Figure 19). Spatial average interior noise levels were then computed from the 12 interior spectra. The resulting data are presented in Table 2. As can be seen, sufficient dynamic range exists throughout the higher propeller speeds for structure-borne noise detection procedures and control measure development. It is of interest to note that the increase in acoustic seal effectiveness with increasing frequency determined previously is reflected in the general trend of increased apparatus dynamic range with increasing propeller speed.

III. INSTALLATION EFFECTS EVALUATION

A. Power Plant Placement

The effect of propeller placement on the transmission of structure-borne noise was studied by recording interior noise levels at several propeller speeds while varying the position of the propeller source relative to the wing. The cabin microphone array was continuously swept along the length of the cabin to obtain space average sound pressure levels. The propeller source was placed in the wing chord plane at Wing Station 80 and then moved forward from a wing leading edge separation distance of S = 0.25 propeller diameters (7 inches) to S = 0.5 and then to S = 0.75. The spatial average SPL recorded at the various propeller/wing separation distances are shown in Figure 16. In general, the data indicate that the strength of the propeller-induced forces contributing to wing excitation and subsequent structure-borne noise propagation decreases as the propeller-to-wing separation distance increases. With the propeller/wing separation distance fixed at S = 0.25, a similar variation in spanwise placement of the propeller source was carried out. As can be seen fro the data in Figure 17, there does not appear to be a consistent trend relating spanwise propeller placement and structure-borne noise transmission.

B. Engine/Nacelle Mass

To establish a reasonable mass to simulate the effects of an engine and nacelle installation for the structure-borne noise test apparatus, typical full scale twin engine aircraft data were obtained and scaled based on bare-wing weights and propeller diameters. The following data were obtained from a general aviation manufacturer for one of their more popular twin engine aircraft.

Bare Wing Weight (W_w)	925	lbs
Engine Weight (W_e)	850	lbs
Engine Roll Inertia (I_e)	76,747	lbs
Nacelle Weight (W_n)	430	lbs
Forward of Firewall	248	lbs
Aft of Firewall	182	lbs
Landing Gear Weight (W_{lg})	160	lbs
Nacelle Frontal Area (A_n)	7.65	sq-ft
Propeller Diameter (D_p)	105	inches

The significant structure-borne noise test apparatus specifications are:

Bare Wing Weight (w_w)	29.55	lbs
Propeller Diameter (d_p)	28	inches

When using the above data to develop a target nacelle design size, weight, and roll inertia, one must realize that the engine is dynamically supported on vibration isolators. The isolators are generally set to a support frequency at least a factor of three below the driving frequency so as to obtain a degree of isolation (isolation begins at a factor of 1.414 below the driving frequency). The effective engine mass is then reduced by the factor

$$F_m = \left| 1 - \frac{1}{1 - \left(\frac{f_s}{f}\right)^2} \right|$$

where f_s is the engine support frequency and f is the driving frequency. When $\frac{f_s}{f}$ is equal to 1/3, then $F_m = 0.125$. For the present evaluation, we will assume this ratio is representative at any propeller frequency and, thus, the effective engine weight becomes 0.125 W_e (= 106 lbs). In this manner, the effective engine weight may be added to the nacelle weight as a rigid mass attached to the wing. Thus, the total effective added wing weight (neglecting the landing gear weight) is:

$$W_t = W_n + 0.125W_e = 430 + 106 = 536lbs.$$

Normalizing this added weight with respect to the bare wing weight results in:

$$W_t' = \frac{536}{925} = 0.58.$$

The engine effective radius of gyration is:

$$\rho = \left[\frac{I_e}{W_e} \right]^{0.5} = 9.5inch,$$

and when normalized with respect to the propeller diameter:

$$\rho' = \frac{9.5}{105} = 0.09.$$

The nacelle aerodynamic blockage as a fraction of the propeller diameter is computed from an equivalent circular cross-section of diameter $D_n = 37.5$ inch, and becomes 37.5/105 = 0.36.

Thus, the estimated effective added weight to simulate an engine and nacelle for the structure-borne noise test apparatus is:

$$w_t = W'_t * w_w = 0.58 * 29.55 = 17.1 lbs.$$

The effective roll inertia from the engine is computed from the effective engine weight and radius of gyration as:

$$i_e = \left[\frac{(0.125 * W_e)}{W_w}\right] * w_w * [\rho' * d_p]^2$$

$$= \left(\frac{106}{925}\right) * 29.55 * [0.09 * 28]^2$$

$$= 21.5 lb\text{-}in^2$$

The effective inertia of the nacelle is computed based on an equivalent cylinder with an effective diameter of 0.36 * d_p. = 10.0 inch; and a nacelle weight of 13.7 lbs ([430/925]*29.55). The nacelle weight is assumed to be uniformly distributed within the 10 inch diameter which results in a nacelle inertia of:

$$i_n = weight * \frac{(diameter^2)}{8}$$

$$= \frac{[13.7 * (10)]^2}{8} = 171 lb\text{-}in^2$$

The total engine/nacelle roll inertia is then:

$$i_{en} = i_e + i_n = 21.5 + 171 = 192.5\ lb\text{-}in^2,$$

with an effective weight of 17.1 lbs. It is felt that the engine/nacelle roll inertia is more important than the effective weight since previous analytical calculations showed that propeller wake/vortex dynamic excitation is a dynamic chordwise moment with zero net vertical excitation.

The engine/nacelle for the test apparatus was constructed from a solid block of Philippine mahogany. The installed article is shown in Figure 18. The engine/nacelle is fixed to the wing via a forward clamping arrangement, bolted rear connection to the rib at Wing Station 64 and solid contact along the main spar via surface adhesives. The engine/nacelle installed weight is

17.6 lb, with a roll inertia of 183.7 lb-in squared. The roll inertia was determined using a parallel pendulum suspension with a roll excitation. The natural frequency of the excited item then determines the roll inertia (plus fixture inertia).

Propeller speed sweeps were carried out while recording the interior noise levels of the first propeller tone at four interior microphones, #4 (P2 at F.S. 26), #6 (P4 at F.S. 26), #7 (P2 at F.S. 47), and #9 (P4 at F.S. 47), as schematically shown in Figure 19. The resulting sound pressure levels were compared to clean wing levels recorded prior to the engine/nacelle installation and are shown in Figure 20. As can be seen, the addition of the simulated engine/nacelle mass resulted in bands of increased and decreased structure-borne noise transmission. In general, a decrease in structure-borne noise transmission occurred in the propeller speed range from approximately 4400 rpm to 5000 rpm and from 5400 to 5700 rpm. A small increase in structure-borne noise transmission occurred below approximately 4400 rpm, while a measurable increase was recorded in the 5000 to 5400 rpm range, with the peak increase occurring around 5200 rpm. For the two-bladed propeller, the major increase in structure-borne noise transmission occurs around 170 to 175 Hz. This change in transmission is attributed to a shift of the wing third bending mode from 191 Hz (see Table 1) to approximately 170 Hz.

C. Wing/Fuselage Attachment

Spherical bearings were originally installed at each of the three wing-to-fuselage attachment points. This allowed simplified analytical modeling as well as being a representative configuration for chordwise moment transfer for a majority of general aviation and military type aircraft. Larger commercial passenger aircraft are generally constructed with an integral wing spar which passes through the fuselage. The latter configuration is more closely represented by a solid wing/fuselage attachment. To simulate the solid wing/fuselage attachment, the spherical bearings were replaced with solid bushings which allowed moment transfer about all axes at the attachments. Propeller sweep data were recorded for the solid wing/fuselage attachment configuration and compared to the data recorded with spherical bearings at the attachments. The resulting data comparison for the bare wing configuration is shown in Figure 21. For the most part, structure-borne noise transmission was unaffected by the wing/fuselage attachment changes for propeller speeds below 5000 rpm. Above 5000 rpm, significant increases in structure-borne noise transmission occurred as is shown by microphones #4, #6, and #7.

Similar comparison of the effects of solid wing/fuselage attachment versus spherical bearings for the case when the engine/nacelle mass was installed is shown in Figure 22. Here,

the increase in structure-borne noise transmission is more broadly distributed across the 4000 to 5700 rpm sweep range. Again, microphone #9 appears to be somewhat less sensitive to changes in the wing/fuselage attachment.

One possible explanation for the increased structure-borne noise transmission for a solid wing/fuselage attachment is that the local wing panel disturbances produced by the propeller are partially transmitted into overall wing spar bending waves, which can be propagated into the fuselage via differential lateral shear at the wing/fuselage attachments. This type of transmission will take place for either type of attachment. However, the local disturbances which do not conform to global wing bending are reflected from the spherical bearing attachments as they see a highly reflective zero impedance termination. The solid attachment provides a non-zero impedance and thus some transmission is possible.

Data comparisons were also made to determine the effects of engine/nacelle insstallation for the case when the solid wing/fuselage attachments were installed. This data comparison is shown in Figure 23 and, as can be seen, the bands of increased and decreased structure-borne noise transmission appear much the same as for the spherical bearing wing/fuselage attachment data given in Figure 20.

IV. STRUCTURAL RESPONSE MODIFICATION

Various wing structural response modifications were evaluated by direct comparison of recorded interior sound pressure levels (SPL) at the fixed microphone locations denoted in Figure 24, while the propeller speed was slowly swept (30 rpm/sec) from 4000 to 5700 rpm. Comparisons were then made to identical sweeps with the wing modification installed. Repeated sweeps within a 2-3 hour period, both with increasing and decreasing propeller speed, resulted in interior SPL repeatability within ±1 dB. Nevertheless, baseline data (clean wing) were recorded as often as possible during the various test runs to eliminate long term variations. Typical long-term variation of the baseline microphone responses, taken over a four-week period, is shown in Figure 25. The effectiveness of the various control measures was evaluated relative to the baseline data acquired just after removal of the control measure.

In the sections to follow, data comparisons at specific microphone locations will be given which represent typical data trends. The only exceptions are the centerline microphones which often exhibited low SPL responses due to being near nodal lines of responding acoustic resonances and as such were insensitive to most control measures.

A. Blocking Mass/Fuel

To study the potential benefits of using wing-carried fuel as a blocking mass for structure-borne noise transmission from the propeller excitation, the two most inboard wing cavities were fitted with a liquid retaining plastic bladder. Cell #1 is in the wing leading edge area forward of the front spar and, when filled with water, contained 7.4 lb of simulated fuel. Cell #2 occupied the volume between the front and rear spars and, when filled with water, contained 17.3 lb of simulated fuel, see Figure 24. The most aft cell in the area behind the rear spar would hold, at most, 0.3 lb of simulated fuel and, therefore, was not used. Baseline, no fuel, runs were made and sound pressure level responses were recorded at several interior microphone locations. When simulated fuel was added to Cell #1, negligible reduction in interior noise levels resulted . However, when simulated fuel was then added to Cell #2, a measurable noise reduction was achieved above 4800 rpm (160 Hz for the first propeller tone), as is shown in Figure 26a. Upon removal of the simulated fuel in Cell #1, leaving Cell #2 full, the noise reduction persisted, see Figure 26b.

From this data, it appears that fuel in the wing area between the front and rear spars inboard of the propeller is an effective structure-borne noise control measure. In an attempt to discover the mechanism responsible for the reduced levels of vibration transmission into the fuselage,

solid masses with a total weight and center-of-gravity simulating the liquid in Cell #2 were attached to the wing front and rear spars in the Panel #2 area, and the noise transmission data acquisition was then repeated. A photograph of the attached solid masses is shown in Figure 27. The masses were attached to both the upper and lower wing spar flanges. As can be seen by the data given in Figures 28a and 28b, the blocking masses were quite effective in reducing structure-borne noise levels throughout the cabin.

1. Installation Effects

The effects of rigid wing-to-fuselage attachment and engine/nacelle installation on the structure-borne noise reduction effectiveness of wing fuel was also evaluated. The initial evaluation of wing fuel as structure-borne noise control measure, reported above, made use of the spherical bearing wing-to-fuselage attachment. The data presented in Figure 29 show the comparative effects of rigid wing-to-fuselage attachments (see Figure 29b) and the combined effect when adding the engine/nacelle mass (see Figure 29c). In general, we see that the use of liquid fuel in the inboard wing cell is most effective for the spherical bearing attachments. When the attachments are replaced with rigid connections, the effectiveness of the control measure is reduced; however, when the engine/nacelle is installed, the control measure effectiveness nearly disappears. It is believed that the wing fuel acts as a blocking mass to wing global bending motion, however, it is not effective on local wing panel disturbances which do not conform to global wing bending motion. Thus, the rigid wing-to-fuselage attachment reduces the blocking mass effects. When the large engine/nacelle mass is added to the wing, the reflective effects of the inboard fuel blocking mass completely disappears since the reflective path is blocked by the outboard mass.

B. Damping Treatments

1. Wing Panels

The effect of applying damping material to the surface of Panel #2 (see Figure 24) was also carried out. A commercially available self-adhesive, low-weight, 0.16 lb/ft^2 constrained layer damping material of thickness 0.016 inch was used in the study. The 0.040 inch thick aluminum wing skin exhibited an increase in structural loss factor from 0.018 to 0.080 upon application of a single layer of the damping material. The damping measurements were made using a single degree-of-freedom circle fit technique in the frequency range from 155 to 169 Hz at a nominal test temperature of 70°F. The fundamental panel frequency increased upon application of the damping material, reflecting a constrained layer configuration (ref. 17). Typical reduction in structure-borne noise transmission is shown by the data in Figure 30. As

can be seen, the effect of the added damping treatment was negligible in comparison to the effect of blocking mass or simulated wing fuel. It is concluded that the mechanism responsible for the structure-borne noise control effectiveness of the simulated wing fuel is its blocking mass effect. As with most liquids, only a portion of the liquid in Cell #2 acted as an effective mass, thus accounting for the reduced structure-borne noise effectiveness when compared to the solid equivalent masses.

Damping material was also systematically applied to various panels and panel combinations along the entire wing span in both upper and lower surfaces, as is shown in Figure 31. The use of surface damping treatment was, for the most part, ineffective, except on the center panel areas of Wing Panels 3 and 4, which were directly in the wake of the propeller. The most effective use of panel damping occurred when it was used in conjunction with the blocking masses, as is seen in Figure 32, with comparison made to Figure 28. Here, we can see the damping treatment improves the structure-borne noise transmission losses of the system below 5100 rpm and somewhat degrade the reduction at the higher speeds. Note that the center panel first mode frequency occurred around 169 Hz (5070 rpm for first propeller tone). One might view the propeller-induced wing vibrations as traveling waves being dissipated by the damping material and then reflected by the blocking masses on the wing spar. The waves are again damped upon passing through the propeller source region.

2. Wing Leading-Edge

Treatment of the wing leading edge in an attempt to reduce the impact forces of the propeller wake was also evaluated using wing leading-edge damping/isolation material. Several types of damping material and/or foam products were used to shield the wing leading edge, up to 5 inches aft, along the span of the propeller. No measurable reduction in structure-borne noise transmission occurred at any of the monitored microphone locations. This was the first experimental indication that the propeller source was not highly confined to the wing leading edge. To verify that the primary loading is more uniformly distributed, as was predicted analytically (ref. 14), a piece of 6 inch diameter rigid PVC pipe was cut lengthwise and used as a non-contacting wing leading-edge shield. The leading-edge shield showed little or no measurable effect on structure-borne noise transmission. Thus, it is concluded that the propeller wake as a noise source is not confined to the wing leading-edge, but is a more uniformly distributed spatial source within the propeller wake.

C. Tuned Mechanical Damper

In the frequency range from 133 to 190 Hz, which contains the dominant first propeller harmonic, the design and implementation of low-damped, high amplification, tuned dampers

were found to be quite difficult. Such dampers, which rely solely on structural damping of the tuned beam material, exhibit extremely narrow half-power bandwidths (around 1 Hz or less). Coupled with a relatively compliant wing mounting base (the main spar), the performance of such a bench-proven damper design fell considerably short of expectation when excited by the propeller source.

However, the use of an elastomerically damped tuned resonator appears to be a viable structure-borne noise transmission control measure. The highly damped design with increased system half-power bandwidth (approximately 16 Hz) provides adequate tuning design margin and propeller speed variation compensation. Such a system exhibited 10 to 15 dB interior noise reduction.

Figure 33 shows a photograph of the highly damped (5% critical) elastomeric damper design evaluated for structure-borne noise transmission control. The damper configuration consists of a base elastomeric (natural rubber) "sandwich mount," 1.5 inch diameter x 1.0 inch tall, rated as 350 lb/inch in shear at 50 lb load, and 2800 lb/inch in compression at 420 lb load. The sandwich mount weighing 0.11 lb supports a 2.15 lb weight with a mass center approximately 3.5 inch above the base of the mount. The high mass center allows damper response to various base input excitation. Base and support mass mounted accelerometers were used to obtain a measure of the frequency response characteristics of the damper. As shown in Figure 34, identical dampers were mounted on the upper and lower flanges of the wing front spar at Wing Station 41.0. The external mounting of the damper facilitated mounting and monitoring of the damper's response. The propeller airstream did not impinge on the damper.

An electrodynamic shaker attached to the wing front spar at Wing Station 48.0 was used to obtain damper design installation effects and primarily provide for quick-look screening of candidate damper designs. The mechanical damper in Figure 33 shows a mass-to-base vertical resonant response of around 160 Hz, using the shaker as a source of excitation. The damper vertical excitation resonant response decreased to 150 Hz under propeller excitation. Typical structure-borne noise transmission reduction obtained with the mechanical damper is shown in Figure 35. A resonant response in the frequency range of 150 to 160 Hz would not normally be expected for an oscillatory spring rate of 2800 lb/inch and mass of 2.15 lb. However, recall that elastomeric materials are preload sensitive and, under dynamic loading, increase in stiffness by a factor of as much as 2 or 3 (ref. 18). This being the case, a shift from an expected 110 Hz, based on static properties, to 155 Hz (ref. 4650 rpm on Figures 35 and 36), under dynamic excitation, appears reasonable.

To verify that energy extraction was the principal mechanism of the tuned damper, a dummy sandwich mount was constructed from a cylindrical section of aluminum, duplicating the outside diameter, height, and weight of the elastomeric mount. This rigid damper was also tested, and the results are given in Figure 36. As can be seen, the rigid damper provided only a small amount of blocking mass and, thus, dissipation is the primary mechanism for reduced structure-borne noise transmission from the elastomeric damper.

It is of interest to note that for a bare wing weight of 29.55 lb, an added total damper weight of 4.52 lb produced 10 to 15 dB of interior noise reduction in a broad range of propeller speeds, while 17.3 lb of liquid fuel mass in the same wing area produced approximately 6 dB noise reduction over a much more limited propeller speed range. Thus, tuned mechanical dampers appears to be an efficient noise control measure for propeller wake induced structure-borne noise transmission.

1. Installation Effects

The effects of rigid wing-to-fuselage attachment and engine/nacelle installation on structure-borne noise reduction of the tuned mechanical damper was also evaluated. The data presented in Figure 37 show the comparative effects (see Figure 37a for spherical bearing attachments) of rigid wing-to-fuselage attachments (see Figure 37b), and the combined effect when adding the engine/nacelle mass (see Figure 37c). As can be seen in Figure 37b, the tuned damper effectiveness was decreased in the propeller speed range below 5100 rpm and somewhat increased at the higher propeller speeds. When the engine/nacelle mass was added increased effectiveness of the damper was realized except at the highest of propeller speeds. In general, tuned mechanical dampers appear to work very well for most installations and it is believed that one could obtain increased structure-borne noise control with additional tuning for a particular installation and propeller speed combination.

D. Active Vibration/Noise Control

The development of dual shakers for simulation of the wing propeller wake/vortex excitation is reported in Section VI and reference is made to the discussions and data reported therein for justification of their use for this particular task. In Section VI, it is shown that structure-borne interior noise levels equivalent to those produced by the propeller wake/vortex impingement could be easily produced with a low level of dual shaker excitation when the shakers were driven out-of-phase, thus producing a dynamic moment excitation. This led to the belief that one could possibly actively control the transmission of structure-borne noise into the aircraft interior using a dynamic excitator attached to the wing structure. The dual shaker arrangement shown in Figure 38 was employed to evaluate this possibility. As denoted in Figure

39, the dual shakers were attached at Wing Stations 48 and 80, which lie outside the propeller wake. In this manner, the shaker force struts would not be influenced by the propeller wake. The shakers were driven 180 degrees out-of-phase and the force level at the wing attach points were controlled to desired levels.

Initially, the effects of the shaker attachment on interior noise was evaluated by sweeping the propeller in the speed range from 4500 to 5400 rpm while recording the sound pressure level of the first propeller tone at microphone #7 for the case of the shakers detached and for the case of the shakers attached without power to the shaker amplifiers. The resulting difference in recorded sound pressure level is shown in Figure 40 as a noise control level for the blocking mass effect of the dual shakers. As can be seen, there is a low level of noise reduction due to the shaker attachment.

Initially, an open loop control circuit was developed to determine the optimum shaker amplitude and phase, relative to a given control signal, for minimum interior noise transmission. Several control signals were used to pick up the frequency of the first propeller tone, such as wing root strain or acceleration; however, it was found that when a high level of control was achieved the control signal was also reduced to such an extent that the control feedback was eliminated. This resulted in a beating control which was not acceptable. It was found that an external microphone, receiving the propeller direct airborne noise was an appropriate control signal for keeping the shakers in synchronization with the propeller wake excitation.

Optimum interior noise control was achieved by adjusting the shaker amplitude and phase relative to the external microphone signal. It was found that a peak reduction of structure-borne noise transmission, on the order of 18 dB, could be achieved at a propeller speed of 5100 rpm. The optimum control noise reduction obtainable at discrete propeller speeds is shown in Figure 40. Here we see that optimum control ranged from 1.8 dB to 18 dB. In general, the optimum control level was reached when the interior tone level was reduced to the background noise level. The required phase between the reference external microphone and the shaker drive signal ranged from -20 degrees to +20 degrees with weak sensitivity. The shaker amplitude was the most sensitive control parameter ranging from 0.27 to 1.55 lbs rms. A propeller sweep was run from 4500 to 5400 rpm with a fixed shaker amplitude of 0.43 lbs rms, and a fixed phase of 18 degrees. This data, also given in Figure 40, shows a moderate level of interior noise control (14 dB maximum) was achieved. In general, a high level of structure-borne noise control can be achieved in the propeller speed range from say 5000 to 5400 rpm with reduced effectiveness below 5000 rpm.

The data presented in Figure 40 are results of control monitoring at microphone #7. The spatial extent of the achievable structure-borne noise control using shaker excitation was evaluated by tuning the shakers for optimum control at microphone #7 and monitoring the control level at several other interior microphone locations. The results obtained at a propeller speed of 5100 rpm are as follows.

Microphone Location	Noise Reduction dB
#4	13.
#6	18.
#7	18.
#9	16.

Thus, global noise reduction was achieved as one would expect since the source was effectively reduced as seen by the cabin structure.

From this limited evaluation, it is concluded that active structure-borne noise control can be achieved on a global basis via wing structural excitation. The question of implementation of a wing self-contained device to provide the required excitation along with electronic control was beyond the scope of the present effort. However, it is believed that a counter-rotating eccentric mass shaker producing approximately 16 to 32 in-lbs rms dynamic moment could be developed for this purpose.

V. IN-FLIGHT STRUCTURE-BORNE NOISE DETECTION

The detection of structure-borne noise transmission due to propeller wake/vortex impingement on the wing structure (or due to engine/propeller vibration via the aircraft engine mounts) in the presence of equal or higher direct airborne sidewall transmitted noise is a major problem area for developing efficient noise control measures for propeller driven aircraft. In fact, the lack of structure-borne noise detection techniques may be the major reason for interior noise levels of propeller aircraft being much higher than acceptable levels of present-day turbofan aircraft. It is believed that the majority of propeller aircraft noise control efforts have been directed towards sidewall treatment while in fact structure-borne noise may be the major contributor. Since the airborne and structure-borne propeller noise sources are fully correlated, conventional signal analysis/detection techniques do not apply (ref. 19) and a more case specific data analysis approach is needed. In the sections to follow, the procedures developed to detect in-flight structure-borne noise transmission due to propeller wake/vortex excitation are described, along with data analysis procedures. As will be seen, extension to other structure-borne noise sources appears to be straight forward.

A. Test Procedure

The test procedure for detection of in-flight propeller-induced structure-borne noise is most easily described with reference to the schematic of Figure 41. The structural path, being the wing structure, is excited with simulated forces F_i at N locations in the area of the propeller wake and S structural response measurements X_k are acquired, along with P interior microphone responses P_j. During ground test measurements, the pressure response to input force,

$$HPF(\omega)_{ji} = P(\omega)_j / F(\omega)_i$$

frequency response functions (FRF's) are computed along with structural response to input force FRF's.

$$HXF(\omega)_{ki} = X(\omega)_k / F(\omega)_i$$

The pressure response to structural response FRF's are then computed as

$$HPX(\omega)_{ijk} = HPF(\omega)_{ji} / HXF(\omega)_{ki}$$

During flight test, the structural responses $\overline{X}(\omega)_k$ are acquired and estimates of interior structure-borne noise levels are computed from the ground-based FRF's as

$$\overline{P}(\omega)_{ijk} = HPX(\omega)_{ijk} * \overline{X}(\omega)_k$$

A variation in the computed interior levels occurs from the multiple simulated excitation, multiple structural response measurements, and multiple microphone locations within the receiving cabin.

This procedure appears straightforward; however, upon application several questions arise: 1) which structural response parameters, acceleration, strain, etc., should be utilized; 2) at what structural locations for optimum results; and 3) what type of simulated force excitation should be used in the FRF acquisition? The propeller-induced, structure-borne noise test apparatus was utilized to answer several of these questions. The apparatus was employed, as shown in the frontispiece, to record frequency response function data and propeller-induced structure-borne noise level data. The fuselage structure was then removed from the acoustic shield and propeller excitation was used to simulate in-flight conditions wherein both structure-borne and direct propeller airborne noise excitation of the fuselage occurs, as shown in Figure 42.

B. Data Acquisition and Analysis

Hammer impulse excitation was chosen for the simulated ground test frequency response function acquisition. The impulse technique produces a broadband input and, within five to seven sample averages, produces highly repeatable results. While the signal-to-noise ratios were not as high as would be possible with single-frequency sinusoidal excitation, they nevertheless appeared adequate for the initial evaluation. Six excitation locations were used on the wing hard structure in the propeller wake area. The wing front and rear spars, near the root were instrumented with accelerometers and strain gages as is schematically shown in Figure 43. Strain gages were used to record lateral strain in the front spar upper and lower flanges and the rear spar center web areas. Lateral response accelerometers were also used in the same areas, along with a set of vertical response accelerometers. In addition to these nine structural response parameters denoted, respectively, as 21-29, two vertical response accelerometers were used in the cabin to record floor motion on a hard structure point (30) and at a panel center (31). Twelve microphone locations were used to record interior sound pressure level responses.

Frequency response function spectra were obtained in a frequency range of 0-750 Hz, with an analysis bandwidth of 1.875 Hz. The frequency range of primary interest was 115-590 Hz, which covers the first through third propeller tones in the propeller speed range of 3450-5700 rpm. The acoustic shield was installed during these tests.

The 23 channels of response data were also recorded on an FM magnetic tape recorder during propeller excitation of the wing surface at set speeds of 3450, 4260, 4980, and 5700 rpm for both structure-borne noise transmission only and simulated in-flight excitation (fuselage exposed to propeller acoustic field).

Values of the response ratios HPF and HXF were chosen from the hammer impact frequency response function data at frequencies corresponding to the first three propeller tones at the four set propeller speeds. Typical spatial average response parameter sensitivities, i.e., the HPX ratio, are given in Table 3 for the first propeller tone. The standard deviation of the response parameter sensitivity is derived from the variation of response due to the 6 independent hammer excitations and the average of the 12 interior microphone responses making up the spatial average response. It is of interest to note that the sensitivities are rather uniform across groups of response parameters and even across the frequency spectrum. However, direct comparison of a strain parameter response in decibels per micro-strain and an accelerometer response in decibels per unit gravity does not lend itself to useful interpretation. Recalling the definition of the response parameter ratio HPX, it is seen that a more sensitive structural response parameter corresponds to the smaller values listed in Table 3. The magnetically recorded propeller-running data were sample averaged and the spectral responses were recorded at peaks corresponding to the first three propeller tones for the structural and interior microphone responses. Data for the structure-borne only and in-flight simulation configurations were recorded. The structural responses and the response parameter ratios were then combined to predict the level of expected structure-borne noise for the two propeller-running configurations.

C. Typical Results

A measure of the validity of the proposed procedures is a direct comparison of the spatial average interior noise levels predicted from the simulated FRF ground test data and the measured structural response during propeller excitation with the actual measured structure-borne noise levels. Typical correlation plots of such data are given in Figure 44 for the wing front spar lateral strain and acceleration response parameters. The measured (or target) levels are plotted as the mean value $\pm 1\sigma$ (arising from a spatial average) as horizontal bars and the predicted levels plotted with $\pm 1\sigma$ as small circles. Only data for the first two propeller tones were employed in the data analysis, since the third propeller tone was generally near or into the apparatus noise floor. As can be seen by the data given in Figure 44, the higher interior noise levels were well predicted using the proposed procedures.

A more quantitative interpretation of the accuracy of the predicted noise levels among the various structural response parameters is given by the standard deviation of the residual error between the measured mean and predicted mean structure-borne noise level. Results of such analysis are given in Table 4, wherein the values listed under R40 consist of all data with measured interior levels above 40 dB, under R50 all data above 50 dB, etc. As can be seen, the front spar lateral strain and acceleration response parameters (Nos. 21, 22, 24, and 25) yield the best estimates of the "target" levels.

A similar analysis was carried out for the structural response data recorded during simulated in-flight operations. Predicted and measured structure-borne noise levels were compared and the standard deviation of the residual computed for each of the response parameters. Results of the analysis are given in Table 5. When comparing these results with those in Table 4, it can be seen that the wing front spar lateral strain response parameters (21 and 22) were much less affected by the introduction of a high level of airborne noise radiation from the propeller than the acceleration response parameters (24 through 31), which showed both degradation and fortuitous improvement.

The significance of the accuracy obtained using the proposed procedures for predicting structure-borne noise levels during flight operations is best reviewed relative to the measured interior noise levels. A comparison of spatial average structure-borne and the in-flight simulation (acoustic shield removed) interior noise levels recorded during the evaluation are given in Table 6 for the first two propeller tones. As can be seen the in-flight simulation interior noise levels are measurably higher than the structure-borne only ones. Depending on the relative phase, at a value of 3.0 to 6.0 for ΔdB, the airborne noise transmission is equal to the structure-borne transmission; this is the case for the first propeller tone at 4980 rpm. With the standard deviation of residuals (see Table 5) being a good estimate of the expected accuracy of the procedures, then, relative to the interior recorded noise levels (see Table 6), the proposed procedures appear to be sufficiently accurate to indicate whether a structure-borne noise problem exists. If a structure-borne noise problem exists, the proposed procedures can also be used to evaluate the effectiveness of imposed control measures.

D. Improved Procedures: Dual Shaker Excitation

The object of this task was to evaluate dual shaker moment producing excitation for the generation of ground-based frequency response functions for in-flight structure-borne noise transmission detection by direct comparison to data generated using a single shaker producing vertical force excitation. Analytical evaluations of the propeller wake induced vortex has shown the pressure field on the wing surface results in span-wise dynamic bending moments with no

resultant net vertical excitation. It was therefore of great interest to compare these two types of wing excitation for the generation of ground-based frequency response function data used to predict in-flight structure-borne noise transmission. The development of the dual shaker as an appropriate propeller excitation source is reported in Section VI.

In the present evaluation a limited set of response sensors are employed along with reduced number of interior microphone locations. As shown in the schematic of the test setup given in Figure 45, rigid wing to fuselage attachments were used in this evaluation along with four interior microphone locations (#4, #6, #7 and #9) and four structural response sensors; two lateral response strain gages and two lateral response accelerometers attached respectively to the upper and lower flanges of the wing front spar. The propeller source was located at Wing Station (W.S.) 64 and the dual shakers were attached at the wing front spar at W.S. 58 and W.S. 70. The shaker attachment at W.S. 70 was used for the single shaker excitation.

Frequency response function data were recorded using distinct tone harmonic excitation simulating the first propeller tone at propeller speeds of 4500, 4650, 4800, 4950, 5100, 5250, 5400, and 5550 rpm. This expanded data set was chosen to span the expected cabin interior sound pressure level responses (see Figure 40). Equivalent first blade passage excitation frequencies range from 150 to 185 Hz. The shaker excitation level was set at 3 pounds rms. which was found to be an appropriate level for good interior response similar to that produced by direct propeller excitation. A summary of the predicted structure-borne noise transmission levels by microphone location and propeller speed is given in Table 7. The data listed shows the error in predicted structure-borne noise level at each microphone from that measured via direct propeller excitation and the statistics of mean, maximum minus minimum levels, and the unbiased standard deviation (ref. 19) of the structure-borne noise levels predicted from the four sensors. As can be seen, errors exceeding 22 dB can occur and therefore some form of data screening would appear necessary to improve confidence in the predictions using either dual or single shaker excitation techniques. It is to be noted however, that the dual shaker predictions on an average appear to be more accurate than the single shaker generated data.

In Figure 46 the predicted microphone response error is plotted against the microphone mean sound pressure level and against the unbiased standard deviation of the predicted levels from the four structural response sensors. This data shows that one possible error indicator is the mean response level, i.e.. possible dynamic range problems or noise floor problems which could be corrected by eliminating predicted responses 20 dB below the maximum predicted levels, thus responses below 75 dB. It appears that a second indicator of prediction error is a large standard

deviation among the predicted responses from different structural sensors. By eliminating response predictions with standard deviations greater than approximately 4 dB would also appear to improve the prediction accuracy.

Correlation of overall spatial average structure-borne noise transmission for the four interior microphones to the measured levels is shown in Figures 47 and 48 for dual shaker and single shaker FRF generation, respectively. In general the correlation is good at the higher propeller speeds, which are also the higher response levels. It is of interest to note that the 4950 rpm case is poorly predicted using dual shaker excitation, while the 4500 rpm case is very poorly predicted using single shaker excitation. While each are improved by a change in excitation type neither improves to truly acceptable levels. We also see that in general strain gage sensors appear to perform somewhat better than the accelerometer sensors. This conclusion is more clearly seen by the data summary given in Table 8 where the average error, average rms. error, and error standard deviation is given for the overall spatial level predictions.

Correlation of predicted and measured overall spatial average structure-borne noise transmission for predictions for all sensors combined are also given in Table 8 along with the same data after filtering the predicted responses using a 75 dB minimum overall level and a 4.1 dB maximum standard deviation. Corresponding correlation plots are given in Figures 49 and 50, respectively, for dual and single shaker excitation results. As can be seen, the data filtering based on the predicted results show marked improvement in both the dual and single shaker excitation data. The average error for the dual shaker data dropped from 1.88 dB to 0.4 dB with a corresponding drop from 4.34 dB to 2.53 dB in the error standard deviation. The single shaker data showed similar trends with a drop from 2.32 dB to 0.38 dB in average error and a drop from 7.04 dB to 3.17 dB in the error standard deviation.

Based on this limited, yet through, evaluation it is concluded that the dual shaker method of excitation for developing ground-based transfer functions for in-flight structure-borne noise transmission detection will yield superior results as compared to those developed using single shaker excitation. It is further believed that selective filtering of the predicted data based on individual microphone level response and standard deviation from multi-sensor predictions will yield considerably improved estimates of the true structure-borne noise transmission levels.

VI. PROPELLER SOURCE SIMULATION

The objective of this task is to evaluate the use of dual shakers to simulate propeller wake/vortex excitation. The dual shaker arrangement could provide excitation for improved ground based development of structure-borne noise control measures. The evaluation of the use of dual shakers is based on comparisons with single shaker excitation data for control measures development. In-flight structure-borne noise detection improvement using dual shaker excitation is reported in Section V.D.

A. Dual Shaker System

A schematic of the test apparatus used during the dual shaker development is shown in Figure 45 and the photographs of Figure 38 reflect the general arrangement of the test apparatus. The physical arrangement consists of rigid wing to fuselage attachments and installed engine/nacelle mass. Interior microphones #6 and #7 were used as representative structure-borne noise level indicators. The dual shakers were placed at Wing Stations (W.S.) 58 and 70 and attached directly to the wing main spar. With the propeller source at W.S. 64, the shakers were placed symmetrically about the propeller axis with a moment arm of 12 inches. Single shaker excitation was accomplished by removing the shaker at W.S. 58 and driving the shaker at W.S. 70.

The instrumentation used to drive the dual shakers is shown in Figure 51. Two 50 lb modal (current driven) shakers were used for excitation. The modal shakers and amplifiers were factory matched and can be driven out of phase via a front panel switch. Initially, the control of a single shaker with feed back from the load cell produced adequate load control for the one shaker, however, due to differences in driving impedance seen by the two shakers, the second shaker did not maintain the desired force level to produce pure moment excitation. When a second controller was employed and phase coupled to the first controller an acceptable level of control was achieved as is shown in Figure 52. In Figure 52, the amplitude ratio of the two load cells is plotted in dB level and their phase difference in degrees. Here we see that in the frequency range of interest for the first propeller tone (133 to 190 Hz) the shakers remain close to 180 degrees out of phase, thus producing a dynamic moment with little vertical excitation. However, in the frequency range of the second propeller tone (266 to 380 Hz) the 180 degrees out of phase condition did not persist. Due to the poor phase control for the second propeller tone, it was decided that efforts would be directed toward evaluation of responses in the frequency range of importance to the first propeller tone.

The predicted propeller induced wing loads for the test apparatus are given in Figure 15. Here we see that predicted excitations for the first propeller tone, over the propeller speed range of interest (4000 to 5700 rpm), range from 24 to 84 in-lb rms. This translates as 2 to 7 lb rms excitation for the 12 inch moment arm. It is also to be noted that the predicted loading resulted in a pure dynamic moment with no vertical resultant, which places emphasis on phase control between the two shakers.

Data acquisition during this evaluation consisted of direct spectrum analysis of the input loads and microphone responses. Data were generated either by a slow propeller sweep in the speed range from 4000 to 5700 rpm or a shaker sweep in the frequency range form 133 to 190 Hz. A spectrum analyzer was used in the "peak hold" mode to capture the peak spectral response during the sweeps. Sweep rates of 0.5 Hz/sec or approximately 15 rpm/sec were found to be adequate to capture character of the transmitted noise. A 1.25 Hz bandwidth of analysis was used during the spectral analyses. Structure-borne noise transmission from propeller excitation of the wing is shown in Figure 53 for microphones #6 and #7. As can be seen by this data, similar structure-borne noise levels are developed at these two microphone locations and from previous evaluations similar responses are expected throughout the fuselage cabin.

To determine the level of shaker excitation required to produce the propeller induced structure-borne noise levels, a single shaker was placed Wing Station 70 and a controlled sweep at a 3.0 lb rms level was executed. The required single shaker excitation levels were determined from the recorded frequency response function data (microphone response to shaker level) and the previously recorded propeller running microphone response levels. The single shaker force levels required to produce the propeller induced structure-borne noise levels are shown in Figure 54. The required force levels are very consistent for the two microphone response locations. The high level of required force around 4500 rpm is somewhat strange in that it occurs prior to the peak structure-borne noise transmission in the same frequency region for propeller excitation.

Similar data were generated for dual shaker excitation at the 3.0 lb rms excitation level. The corresponding shaker required force levels are given in Figure 55. The dual shaker force requirements appear to be somewhat more reasonable relative to the 2 to 7 lb rms predicted levels. It is also of interest to note that a moment like excitation is a much more efficient excitation for structure-borne noise transmission in the 4200 to 4700 rpm range and 5000 to 5500 rpm range than single shaker excitation. Peak structure-borne noise transmission occurred in these two propeller speed ranges for propeller excitation (see Figure 53).

From the above data it is concluded that dual shaker excitation, with proper control of phasing is a much preferred method of excitation. If active control were the objective, the much reduced levels of excitation would appear to warrant the complexity of a dual excitator arrangement.

B. Control Measure Evaluation

All three types of wing excitation, propeller, single shaker, and dual shakers, were employed to evaluate the noise control measure effectiveness of the tuned mechanical damper applied to the wing at Wing Station 41, as reported in Section IV.C. The results of the evaluation are shown in Figures 56 and 57, respectively, for microphones #6 and #7. In general, the spectral distribution in the predicted noise reduction was much better for dual shaker excitation than for the single shaker as compared to that recorded for the propeller excitation. Likewise, the level of noise reduction for the dual shakers, especially at microphone #7, was also closer to the propeller excited case. While the dual shaker arrangement generally over predicted the expected noise reduction, it was more consistent between the two microphone locations than that of the single shaker.

VII. CONCLUSIONS AND RECOMMENDATIONS

A laboratory based test apparatus was developed that would allow the study of structure-borne noise transmission due to propeller induced wake/vortex excitation of in-wake structural appendages. The test apparatus was employed to evaluate aircraft installation effects, evaluate structural response modifications for structure-borne noise control, develop in-flight structure-borne noise detection techniques, and develop propeller simulation techniques for improved ground based testing. The following conclusions and recommendations are drawn from this study:

1) Due to the spatial extent of the propeller excitation of the wing surface, structure-borne noise transmission is a weak function of power plant placement.

2) The installation of an engine/nacelle mass results in bands of increased and decreased structure-borne noise transmission with measurable increases for the higher propeller speeds.

3) The method of attachment of the wing-to-fuselage can significantly influence the structure-borne noise transmission. Restricting local moment transfer at the attachments via the use of spherical bearings reduces the level of structure-borne noise transmission at the higher propeller speeds (above 5000 rpm).

4) The use of inboard wing fuel appears to be an effective structure-borne noise control measure for spherical bearing wing-to-fuselage attachments. The fuel acts principally as a blocking mass, reflecting energy back into the wing structure. The effective solid blocking mass is less than the total fuel mass. However, the structure-borne noise control benefits are noticeable reduced when rigid wing-to-fuselage attachments are employed and becomes negligible when the effects of the engine/nacelle mass are included.

5) The use of damping material on the wing panels in the area of the propeller wake is a somewhat effective structure-borne noise control measure. However, the use of damping material in the propeller wake area in combination with inboard fuel, is a more effective structure-borne noise control measure.

6) Wing leading-edge treatments do not reduce the impact of the propeller impingement and therefore are not effective structure-borne noise control measures.

7) The use of inboard wing spar mounted tuned mechanical absorbers of highly damped design was found to be an effective structure-borne noise control measure which was only modestly influenced by installation effects.

8) Active vibration/noise control can be applied to the wing structure via dynamic moment excitation which will produce cabin global structure-borne noise transmission control.

9) Through the use of a test procedure employing ground based frequency response functions and in-flight structural response measurements, propeller induced structure-borne noise levels can be predicted in the presence of high levels of airborne noise, such as expected in flight.

10) Selective filtering of the predicted in-flight structure-borne noise transmission levels based on individual microphone level response and standard deviation from multi-sensor predictions will yield considerably improved estimates of the true structure-borne noise transmission levels.

11) Dual shaker excitation of the wing, with proper control of phasing to produce dynamic moment excitation, is the most efficient simulation of propeller wake/vortex impingement loading. The use of dual shaker excitation wing loading simulation leads to:

    a) Improved structure-borne noise control measure development.

    b) Improved prediction of in-flight structure-borne noise transmission.

    c) Potential for developing spatially global active structure-borne noise control.

While the test apparatus used during this evaluation employed components typical of aircraft construction, the extent to which the technology gained in this program can be directly applied to a given full-scale aircraft is unknown. However, the analysis procedures developed were scale independent and therefor should be valid for a wide variety of structure-borne noise transmission problems. It is highly recommended that the in-flight structure-borne noise detection procedures be applied to a full scale aircraft such as the NASA Propfan Test Assessment Aircraft.

REFERENCES

1. Mixson, J.S.; Barton, C.K.; and Valcaitis, R.: "Investigation of Interior Noise in a Twin-Engine Light Aircraft," Journal of Aircraft, Vol. 15, No. 4, April 1978, pp. 227-233.

2. Barton, C.K.; and Mixson, J.S.: "Noise Transmission and Control for a Light, Twin-Engine Aircraft," Paper No. 80-1036, AIAA 6th Aeroacoustics Conference, Hartford, Connecticut, June 4-6, 1980.

3. Rennison, D.C.; Wilby, J.F.; Marsh, A.H.; and Wilby, E.G.: "Interior Noise Control Prediction Study for High-Speed Propeller Driven Aircraft," NASA CR-159200, Bolt, Beranek and Newman, Inc., September 1979.

4. Revell, J.D.; Balena, F.J.; and Koval, L.R.: "Analytical Study of Interior Noise Control by Fuselage Design Techniques on High Speed, Propeller Driven Aircraft," NASA CR-159222, Lockheed California Company, July 1978.

5. Dugan, J.F.; Miller, B.A.; Grabber, E.J.; and Sagersen, D.A.: "The NASA High Speed Turboprop Program," NASA TM-81561, [1980].

6. Valcaitis, R.; and Mixson, J.S.: "Theoretical Design of Acoustic Treatment for Noise Control in a Turboprop Aircraft," Journal of Aircraft, Vol. 22, No. 4, April 1985, pp. 303 310.

7. Stefko, G.L.; Bober, L.J.; and Neumann, H.E.: "New Test Techniques and Analytical Procedures for Understanding the Behavior of Advanced Propellers," Paper 830729, Society of Automotive Engineers Business Aircraft Meeting & Exposition, Wichita, Kansas, April 12-15, 1983.

8. Unruh, J.F.; Scheidt, D.C.; and Pomerening, D.J.: "Engine Induced Structure Borne Noise in a General Aviation Aircraft," NASA CR-159099, August 1979.

9. Unruh, J.F.; and Scheidt, D.C.: "Engine Isolation for Structural-Borne Interior Noise Reduction in a General Aviation Aircraft," NASA CR-3427, May 1981.

10. Unruh, J.F.; and Scheidt, D.C.: "Design and Test of Aircraft Engine Isolators for Reduced Interior Noise," NASA CR-166021, December 1982.

11. Miller, B.A.; Dittmar, J.H.; and Jerachi, R.J.: "The Propeller Tip Vortex -- A Possible Contributor to Aircraft Cabin Noise," NASA TM-81768, April 1981.

12. Metcalf, V.L.; and Mayes, W.H.: "Structure-borne Contribution to Interior Noise of Propeller Aircraft," Paper 830735, Society of Automotive Engineers Business Aircraft Meeting & Exposition, Wichita, Kansas, April 12-15, 1983.

13. Unruh, J.F.; and Dobosz, S.A.: "Fuselage Structural-Acoustic Modeling for Structure-Borne Interior Noise Transmission," Transactions of the ASME, Journal of Vibration, Stress, and Reliability in Design, Vol. 110, April 1988, pp. 226-233.

14. Unruh, J.F.: "Prediction of Aircraft-Propeller-Induced, Structure-Borne Interior Noise," AIAA Journal of Aircraft, Vol. 25, No. 8, August 1988, pp. 758-764.

15. Pope, L.D.; Wilby, E.G.; and Wilby, J.F.: "Propeller Aircraft Interior Noise Model," NASA CR-3813, 1984.

16. Pope, L.D.: "Propeller Aircraft Interior Noise Model: Utilization Study and Validation," NASA CR-172428, September, 1984.

17. Soovre, J.; and Drake, M.L.: "Aerospace Structures Technology Damping Design Guide, Volume 1 - Technology Review," Air Force Wright Aeronautical Labs, TR-84-3089, December 1985.

18. Snowdon, J.C.: Handbook of Vibration and Noise Control, Applied Research Laboratory, The Pennsylvania State University, Report TM 79-75, April 1979.

19. Bendat, J.S.; and Piersol, A.G.: Engineering Applications of Correlation and Spectral Analysis, John Wiley & Sons Inc., New York, 1980.

TABLE 1. MEASURED WING STRUCTURAL RESONANCES

Mode No.	Freq. Hz	Description	Mode No.	Freq. Hz	Description
1	15.	1B + S	7	191.	3B
2	21.	1T + S	8	278.	P
3	50.	2B	9	306.	P
4	86.	P	10	382.	P
5	126.	P	11	435.	P
6	148.	P	12	477.	P

B - bending, T - torsion, S - support, P - panel

TABLE 2. TEST APPARATUS DYNAMIC RANGE

	Spatial average noise level, dB			
Configuration	3450 rpm	4260 rpm	4980 rpm	5700 rpm
1st propeller tone				
Wing attached	54.3	62.9	82.1	91.7
Wing detached	41.9	55.8	65.6	63.5
ΔdB	12.4	7.1	16.5	28.2
2nd propeller tone				
Wing attached	57.9	45.4	59.4	69.9
Wing detached	49.1	44.0	40.8	48.5
ΔdB	8.8	1.4	18.6	21.4

TABLE 3. IN-FLIGHT STRUCTURE-BORNE NOISE DETECTION RESPONSE PARAMETER SENSITIVITY, FIRST PROPELLER TONE

		Sensitivity dB/unit response							
		3450 rpm, 115 Hz		4260 rpm, 142 Hz		4980 rpm, 166 Hz		5700 rpm, 190 Hz	
Response Parameter	Location	Mean	σ	Mean	σ	Mean	σ	Mean	σ
Lat. strain/wing root,									
Fwd. spar, lower flange	21	69.7	1.3	72.4	2.5	84.8	3.1	87.3	2.9
Fwd. spar, upper flange	22	70.1	1.3	72.8	2.5	85.2	3.1	87.8	2.9
Rear spar, web center	23	68.0	1.3	70.7	2.5	83.1	3.1	85.7	2.9
Lat. accel./wing root									
Fwd. spar, lower flange	24	105.3	1.7	100.0	4.6	100.8	3.3	104.1	4.5
Fwd. spar, upper flange	25	102.8	2.6	98.0	4.6	100.1	3.5	104.7	4.9
Rear spar, web center	26	106.1	2.4	98.7	4.5	101.3	3.3	104.6	5.8
Vert. accel./wing root,									
Fwd. spar, lower flange	27	68.5	1.4	64.7	5.3	75.9	4.2	74.9	5.5
Fwd. spar, upper flange	28	67.8	1.3	64.3	5.3	76.0	4.1	74.8	5.3
Rear spar, web center	29	66.9	2.0	72.7	5.3	79.1	4.8	65.2	7.4
Vert. accel./cabin floor,									
Hard structure	30	95.2	1.4	102.0	2.2	101.7	2.1	112.4	2.9
Panel structure	31	101.2	1.4	108.0	2.2	107.7	2.1	118.4	2.9

TABLE 4. CORRELATION OF PREDICTED vs MEASURED STRUCTURE-BORNE NOISE, STRUCTURE-BORNE EXCITATION ONLY

	Standard deviation of residuals σ_{AvgSPL}, dB		
Response Parameter No.	R40	R50	R60
21	1.76	2.01	1.70
22	1.30	1.39	1.64
23	4.61	5.09	6.97
24	1.38	1.42	1.73
25	2.79	2.76	1.22
26	2.54	2.53	3.03
27	8.37	9.47	13.31
28	6.87	7.81	9.93
29	7.50	8.41	11.59
30	3.53	4.01	5.96
31	3.10	3.40	4.78

TABLE 5. CORRELATION OF PREDICTED vs MEASURED STRUCTURE-BORNE NOISE, IN-FLIGHT SIMULATION

	Standard deviation of residuals σ_{AvgSPL}, dB		
Response Parameter No.	R40	R50	R60
21	1.93	0.97	1.48
22	2.18	1.72	2.20
23	3.03	3.18	3.17
24	3.77	3.45	4.17
25	4.08	2.83	4.02
26	3.96	3.68	3.75
27	4.29	4.86	6.44
28	5.21	5.90	7.95
29	4.05	4.63	7.12
30	3.99	4.13	6.00
31	5.73	4.43	6.09

TABLE 6. COMPARISON OF IN-FLIGHT AND STRUCTURE-BORNE SPATIAL AVERAGE INTERIOR NOISE LEVELS

	Response, dB							
	3450 rpm		4260 rpm		4980 rpm		5700 rpm	
Configuration	Mean	σ	Mean	σ	Mean	σ	Mean	σ
First propeller tone								
Structure-borne only	54.3	5.5	62.9	8.5	82.1	3.8	91.7	4.4
In-flight simulation	67.1	5.7	74.0	5.8	88.0	3.1	94.8	4.9
ΔdB	12.8		11.1		5.9		3.1	
Second propeller tone								
Structure-borne only	57.9	5.9	45.4	9.7	59.4	3.1	69.9	3.4
In-flight simulation	65.7	4.7	73.7	5.4	75.7	3.9	85.3	5.2
ΔdB	7.8		28.3		16.3		15.4	

TABLE 7. SUMMARY OF PREDICTED STRUCTURE-BORNE NOISE TRANSMISSION BY MICROPHONE LOCATION AND PROPELLER SPEED

INFLIGHT STRUCTURE-BORNE NOISE DETECTION EVALUATION									
		DUAL SHAKERS				SINGLE SHAKER			
RPM	MIC#	Error	Mean	Max-Min	StdDev	Error	Mean	Max-Min	StdDev
4500	4	4.56	83.06	6.36	2.76	18.02	69.60	8.91	4.11
	6	3.13	79.85	7.79	3.52	14.05	68.93	7.48	3.37
	7	5.57	79.70	5.94	2.55	22.15	63.13	9.68	4.52
	9	2.00	82.33	7.03	3.11	16.63	67.70	11.18	5.34
4650	4	2.59	81.61	8.81	3.81	3.87	80.33	12.33	5.19
	6	0.99	83.12	7.45	3.20	0.40	83.72	8.43	3.55
	7	7.15	92.04	6.24	2.74	2.99	87.88	6.52	3.05
	9	0.00	85.81	13.07	5.99	6.89	78.93	6.09	2.90
4800	4	0.48	78.46	3.44	1.94	0.84	78.82	9.45	4.09
	6	8.86	77.77	4.53	2.05	12.86	81.77	9.46	4.06
	7	3.91	81.57	4.63	2.07	5.84	83.50	9.46	4.35
	9	2.72	73.58	9.85	4.22	5.52	81.81	9.46	4.41
4950	4	5.50	73.64	11.94	5.04	2.44	76.69	14.00	6.24
	6	11.32	73.34	13.46	6.24	7.88	76.78	12.31	5.79
	7	0.40	82.78	11.94	4.95	2.12	84.50	12.60	5.90
	9	22.49	62.56	13.99	6.43	6.52	78.52	12.31	5.78
5100	4	0.94	94.75	4.96	2.13	3.41	92.28	7.80	3.40
	6	4.06	89.55	9.68	4.73	2.11	91.50	6.39	2.88
	7	1.69	94.62	5.45	2.39	1.33	94.26	6.50	2.92
	9	6.61	83.43	11.71	5.88	1.26	88.78	5.93	2.75
5250	4	0.69	86.44	8.98	3.69	2.83	88.58	10.82	4.84
	6	0.16	91.35	13.84	5.88	1.66	93.17	7.86	3.26
	7	4.51	93.18	9.86	4.02	2.80	91.47	7.86	3.29
	9	2.53	87.86	10.01	4.09	1.92	92.31	9.38	4.26
5400	4	13.38	72.04	6.97	3.36	0.55	76.86	3.35	1.70
	6	2.40	88.82	7.55	3.49	3.79	87.43	3.39	1.97
	7	1.84	88.61	6.97	3.28	0.87	89.58	4.15	1.89
	9	4.05	83.61	8.38	3.68	0.46	88.12	3.39	1.79
5550	4	4.78	88.75	6.67	3.48	3.69	87.66	5.92	2.87
	6	4.08	92.51	8.62	4.59	2.26	90.69	12.18	5.11
	7	0.03	90.98	6.26	3.24	5.29	85.72	10.96	4.54
	9	0.73	88.21	6.05	3.12	3.23	90.71	12.46	5.24
Average		4.19		8.39	3.80	5.20		8.69	3.92
Maximum		22.49	94.75	13.99	6.43	22.15	94.26	14.00	6.24
Minimum		0.00	62.56	3.44	1.94	0.40	63.13	3.35	1.70

TABLE 8. SUMMARY OF STRUCTURE-BORNE NOISE PREDICTION ERROR, OVERALL SPATIAL SPL

	Average Error (dB)	Average RMS Error (dB)	Standard Deviation Error (dB)
Dual Shakers - Unfiltered			
Strain Gages	-0.06	1.53	4.62
Accelerometers	-3.71	1.96	4.41
All Sensors	-1.88	1.58	4.34
Dual Shakers - Filtered*			
All Sensors	+0.40	0.90	2.53
Single Shaker - Unfiltered			
Strain Gages	-1.79	2.08	5.98
Accelerometers	-2.86	2.95	8.40
All Sensors	-2.32	2.47	7.04
Single Shaker - Filtered*			
All Sensors	+0.38	1.19	3.17

* All responses above 75 dB and below 4.1 dB standard deviation

FIGURE 2. WING TO FUSELAGE FRONT AND REAR CARRYTHROUGH ATTACHMENTS.

FIGURE 1. WING ATTACHMENT FITTINGS.

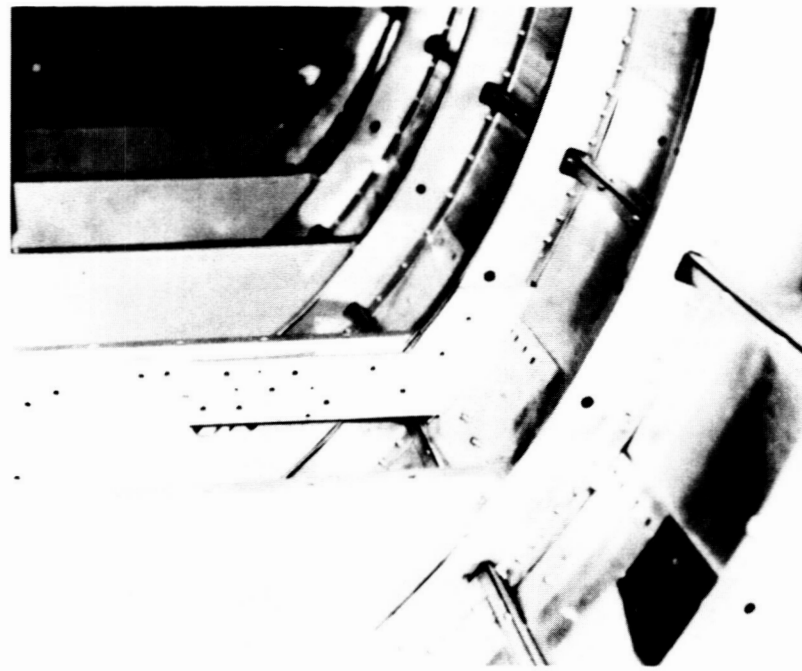

FIGURE 3. WING FRONT SPAR ATTACHMENT STRUCTURE.

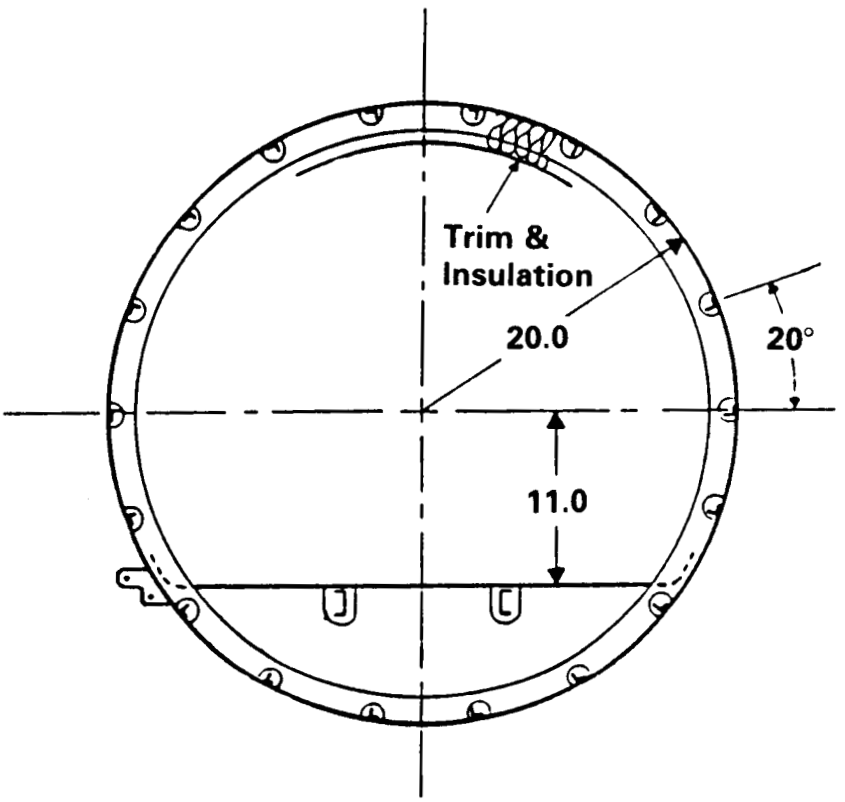

FIGURE 4. FUSELAGE STRUCTURAL DETAILS.

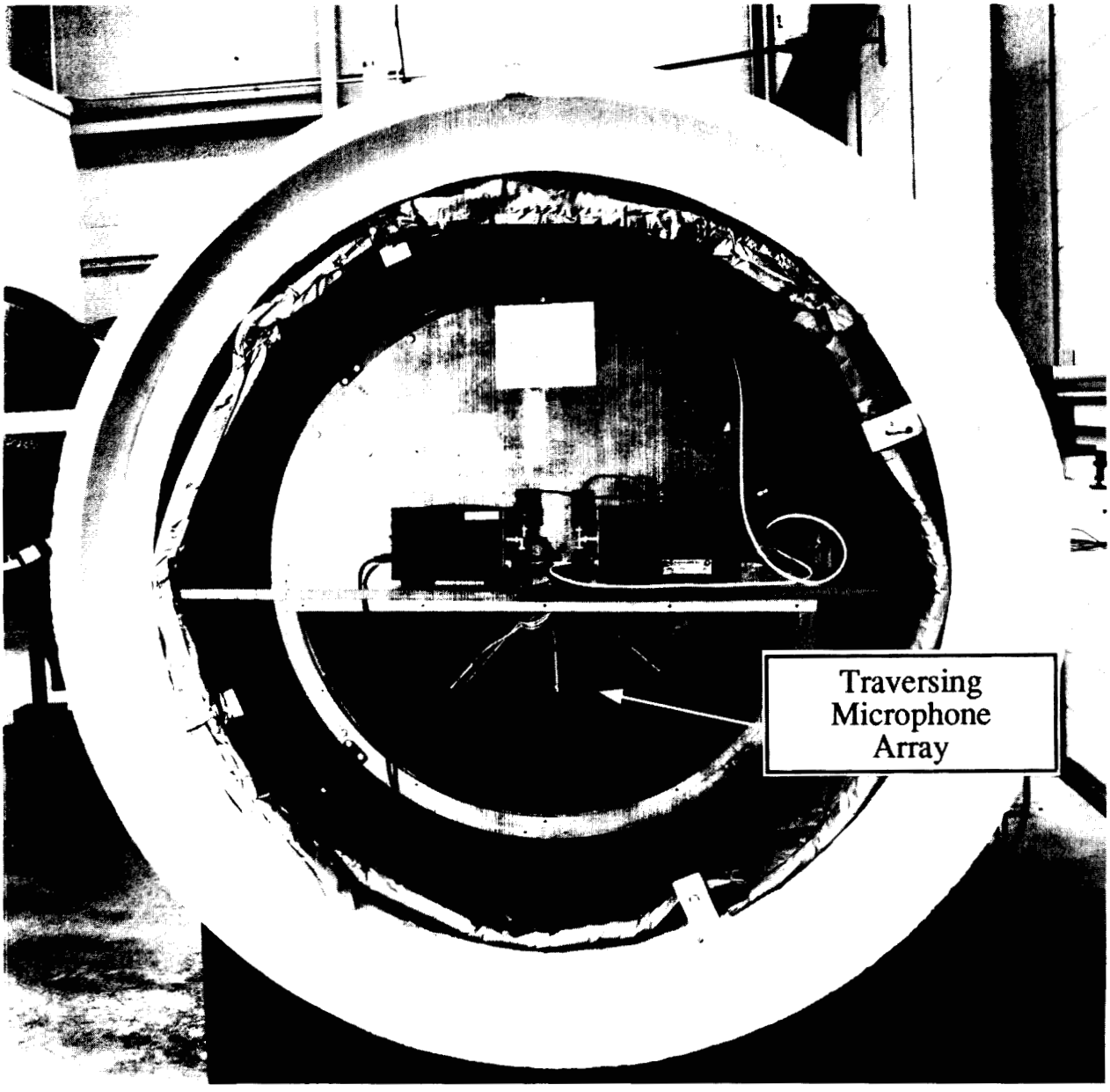

FIGURE 5. FUSELAGE INSTALLED IN ACOUSTIC SHIELD.

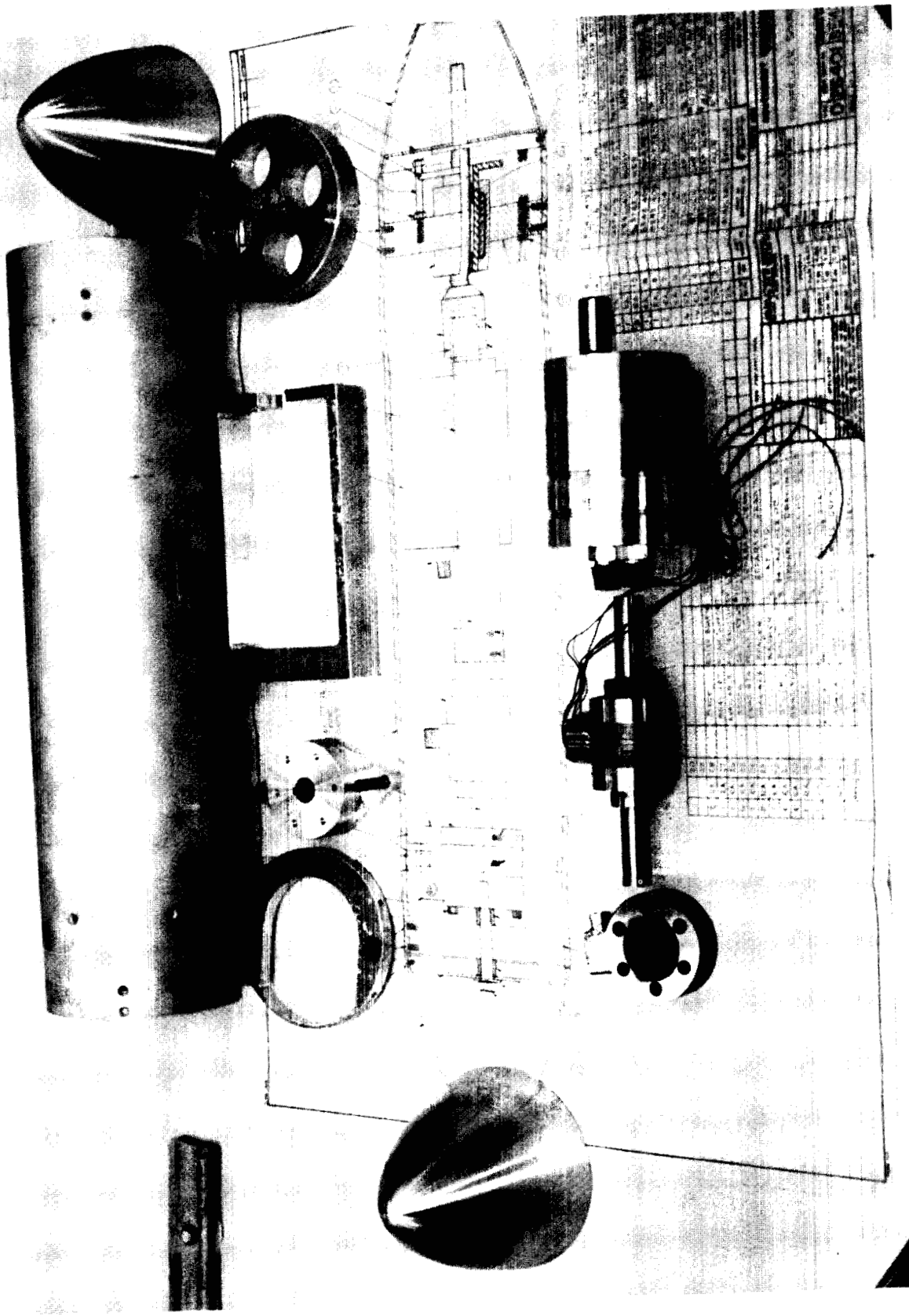

FIGURE 6. PROPELLER THRUST AND TORQUE MECHANISM.

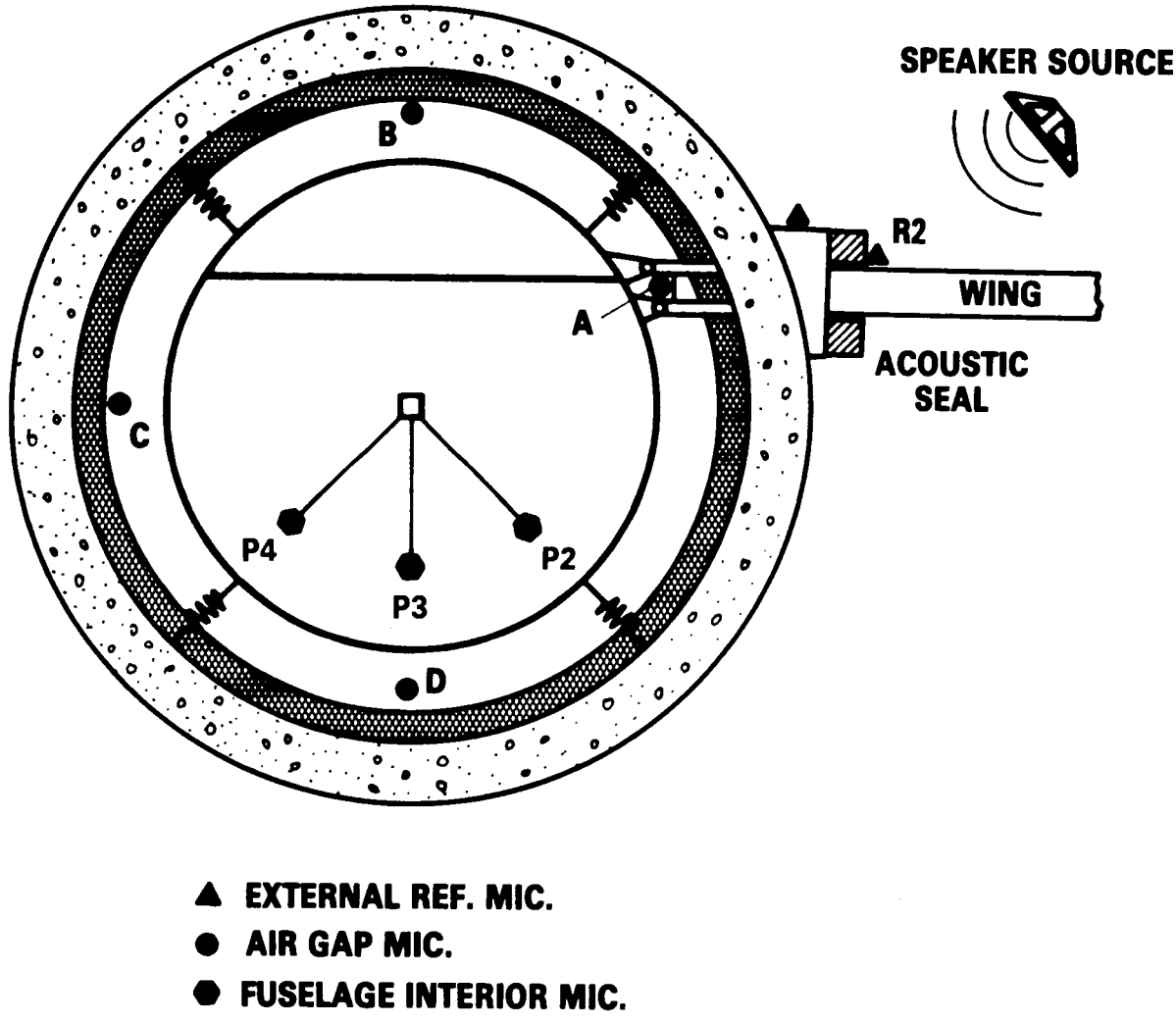

FIGURE 7. MICROPHONE LOCATIONS.

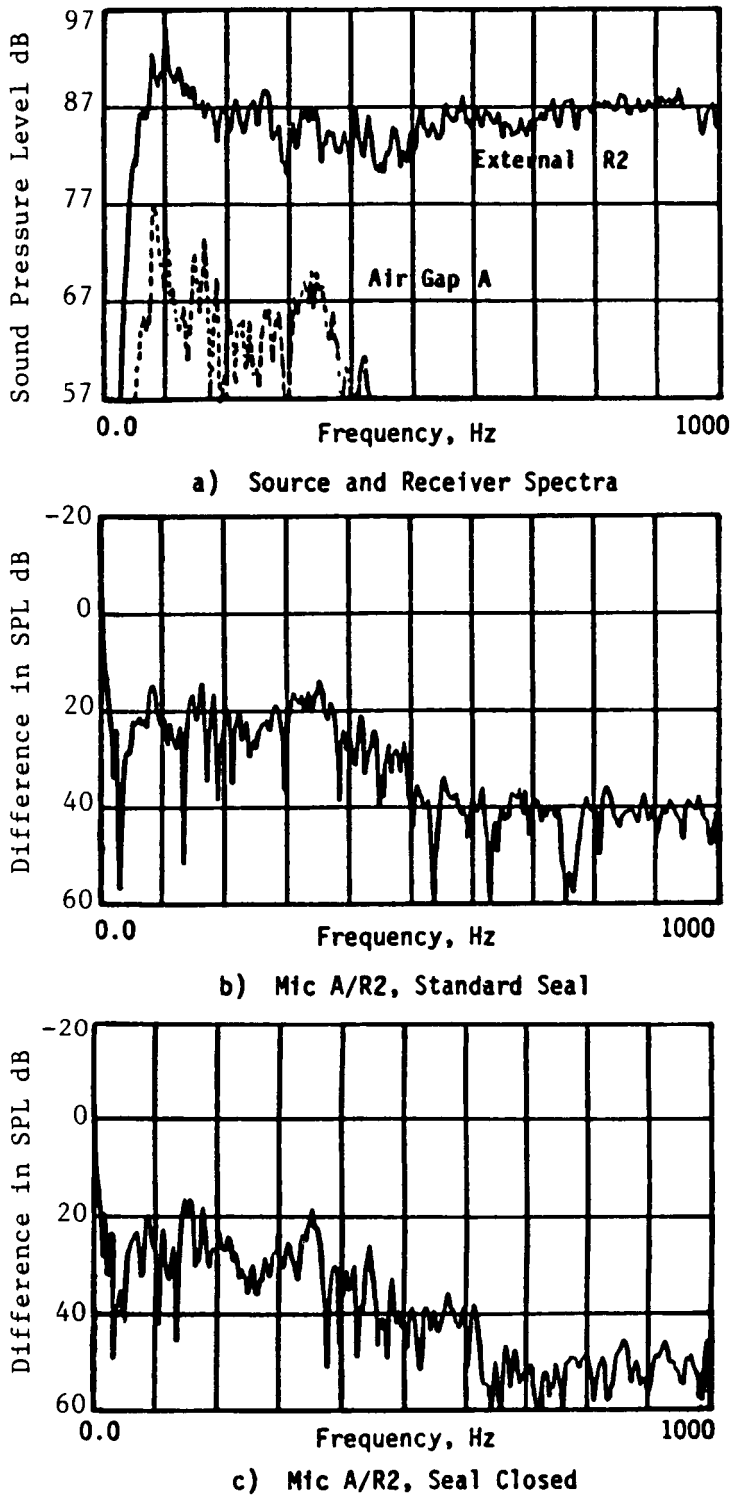

FIGURE 8. ACOUSTIC SEAL PERFORMANCE.

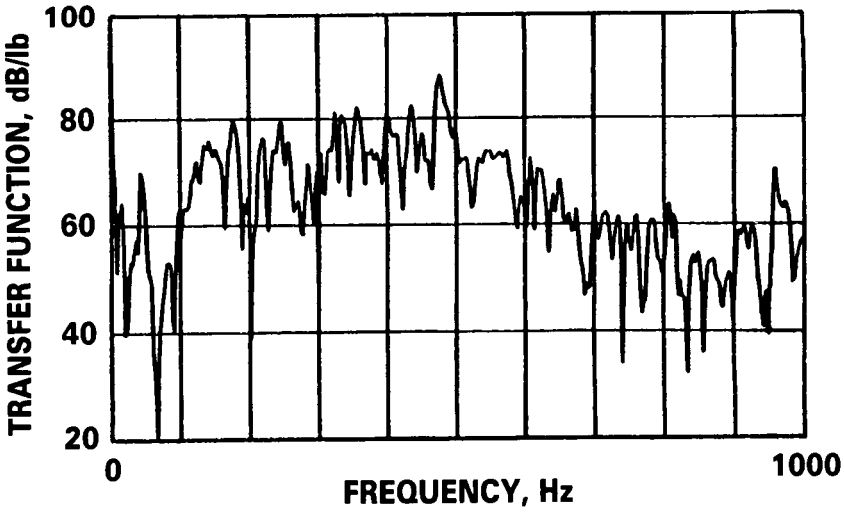

FIGURE 9. SOUND PRESSURE LEVEL RESPONSE AT P4 TO A UNIT FORCE AT WING STATION 96.

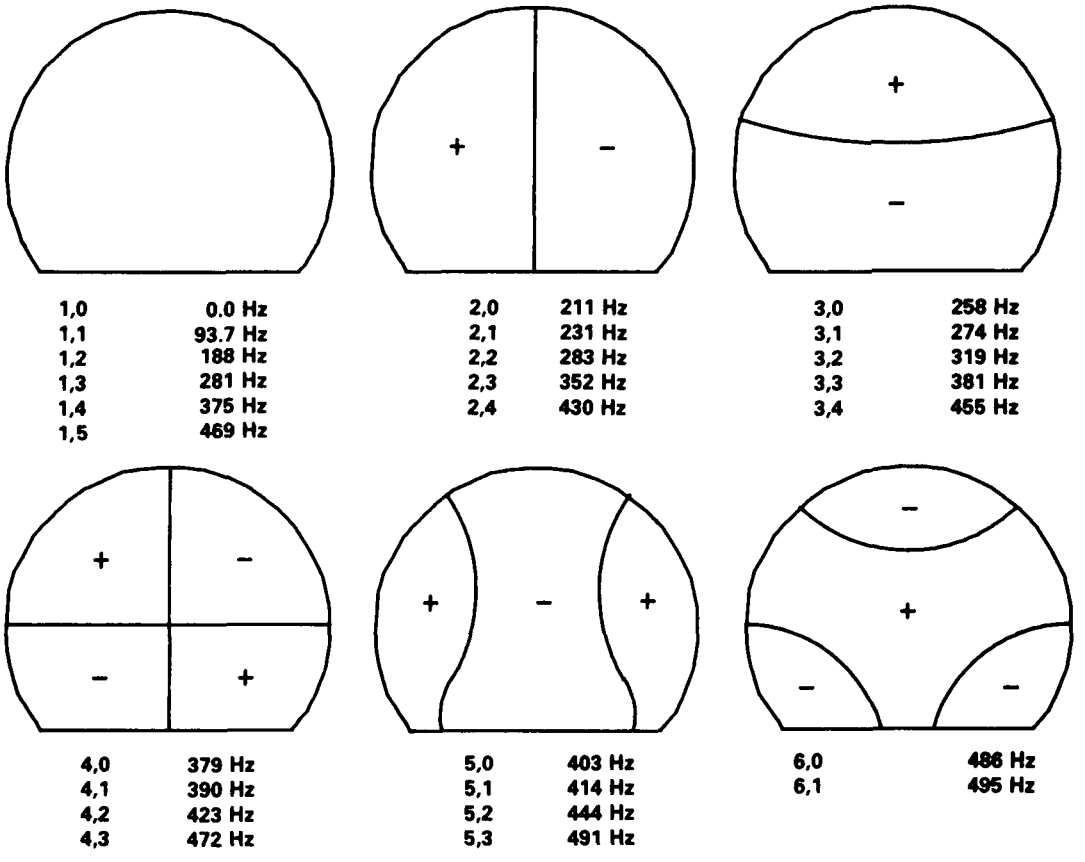

FIGURE 10. CABIN ACOUSTIC HARDWALL MODE SHAPES.

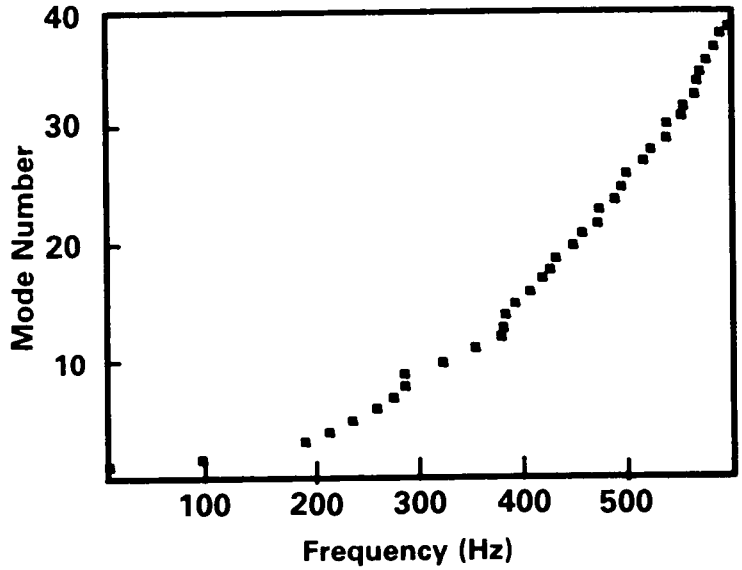

a) Cabin Acoustic

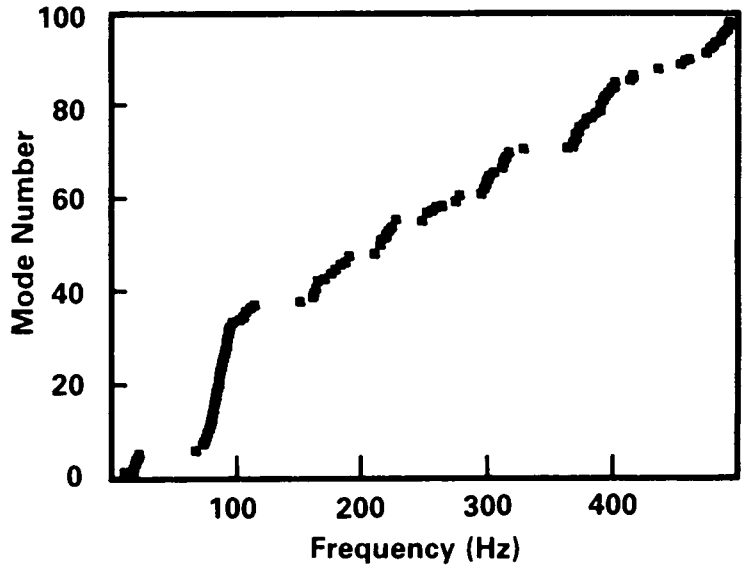

b) Fuselage Structural

FIGURE 11. CABIN ACOUSTIC AND FUSELAGE STRUCTURAL MODAL DENSITIES.

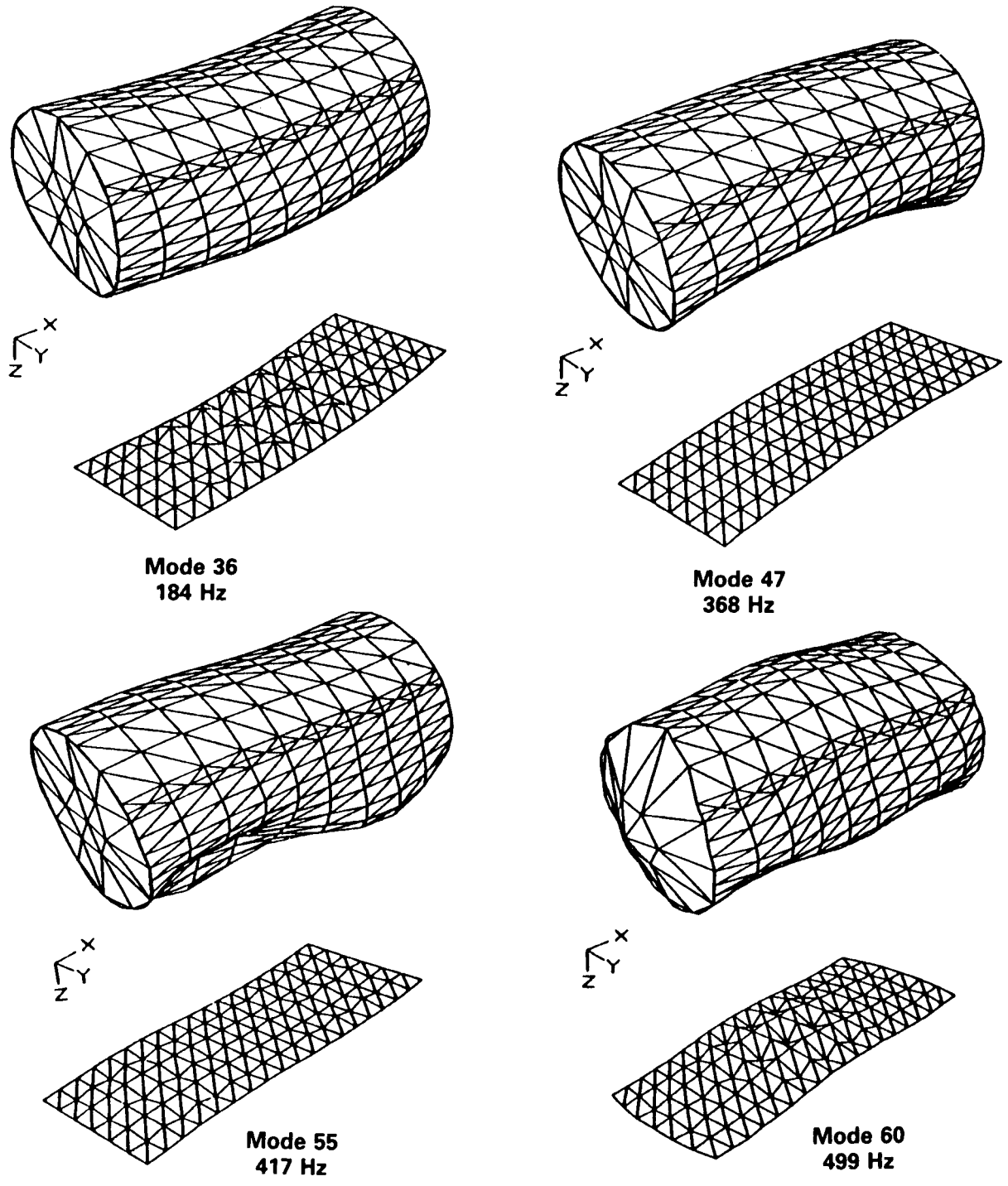

FIGURE 12. TYPICAL FUSELAGE AND CABIN FLOOR STRUCTURAL MODE SHAPES.

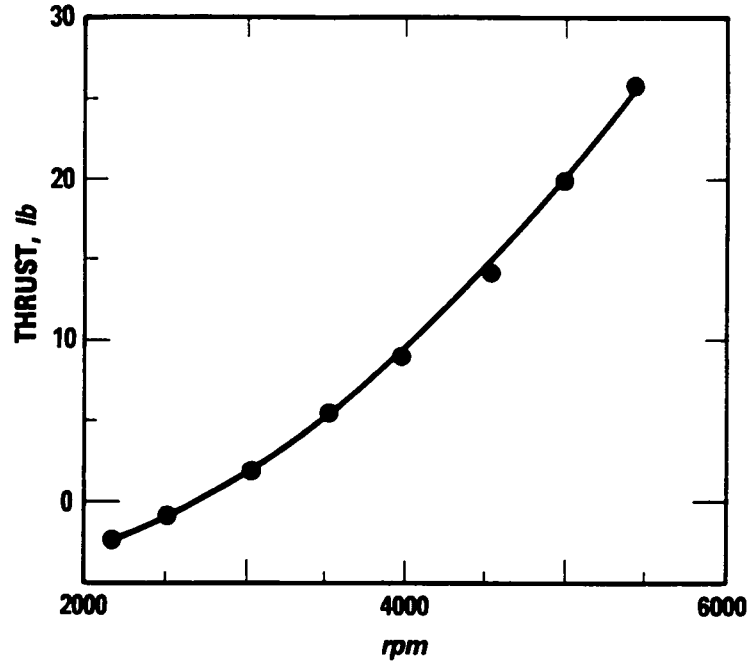

a) Propeller Thrust

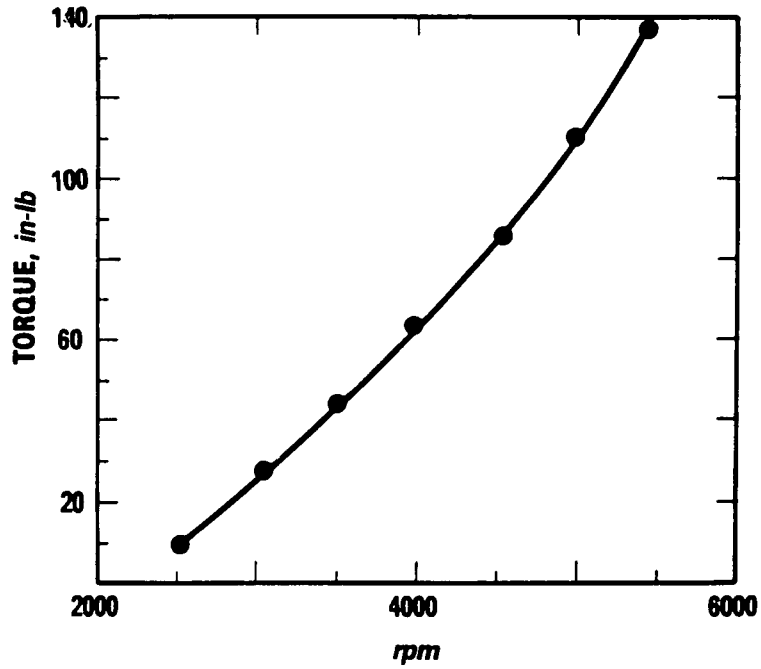

b) Propeller Torque

FIGURE 13. PROPELLER CALIBRATION.

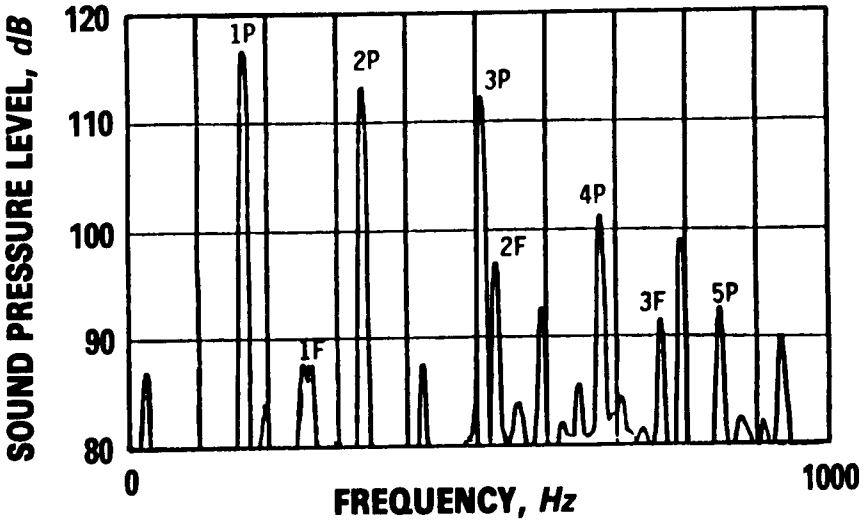

a) External R1

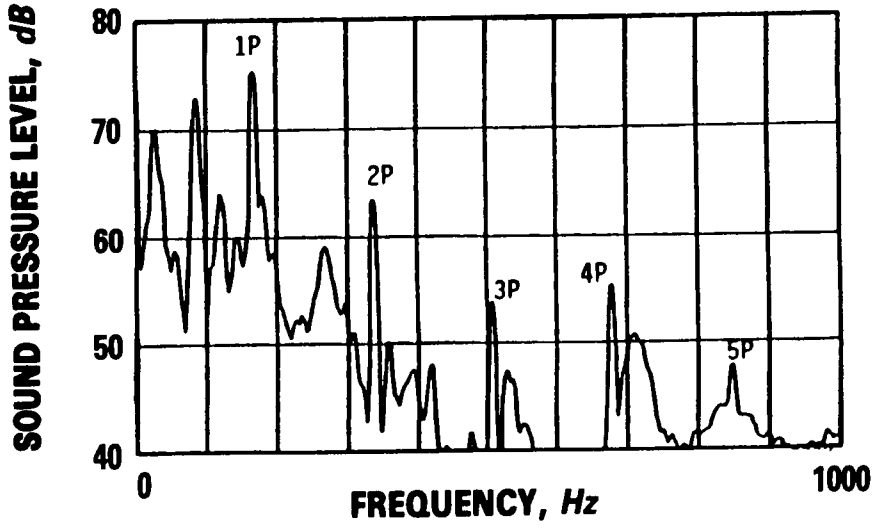

b) Interior P2

FIGURE 14. TYPICAL PROPELLER INDUCED SPECTRA AT 5100 RPM.

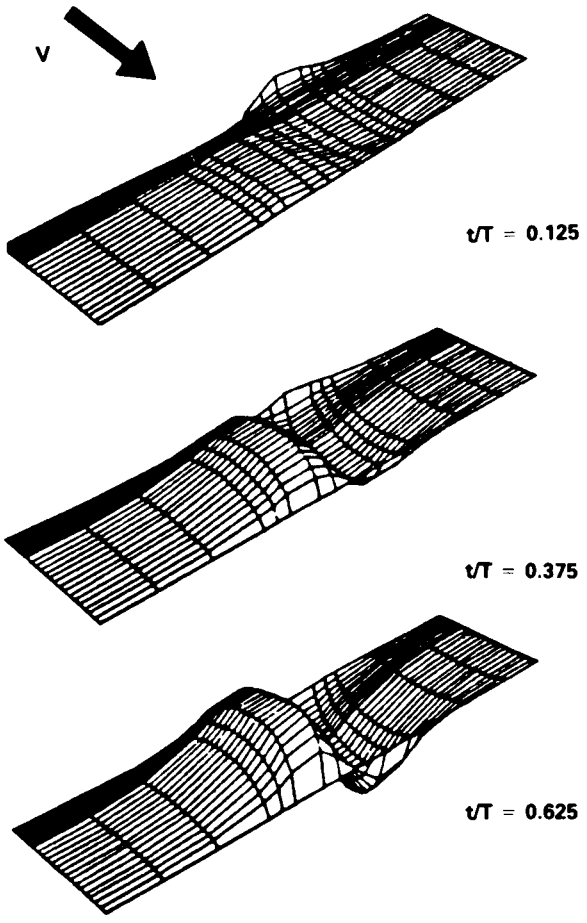

a) Surface Pressures, 4980 rpm

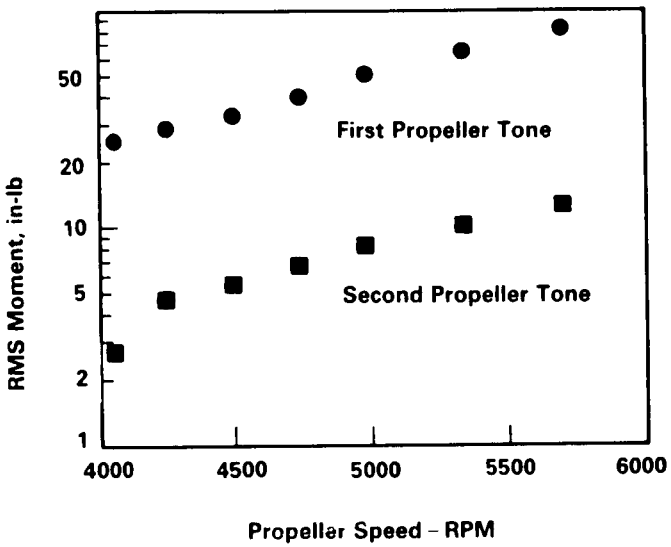

b) Spanwise Bending Moments

FIGURE 15. WING CYCLIC PRESSURE LOADING.

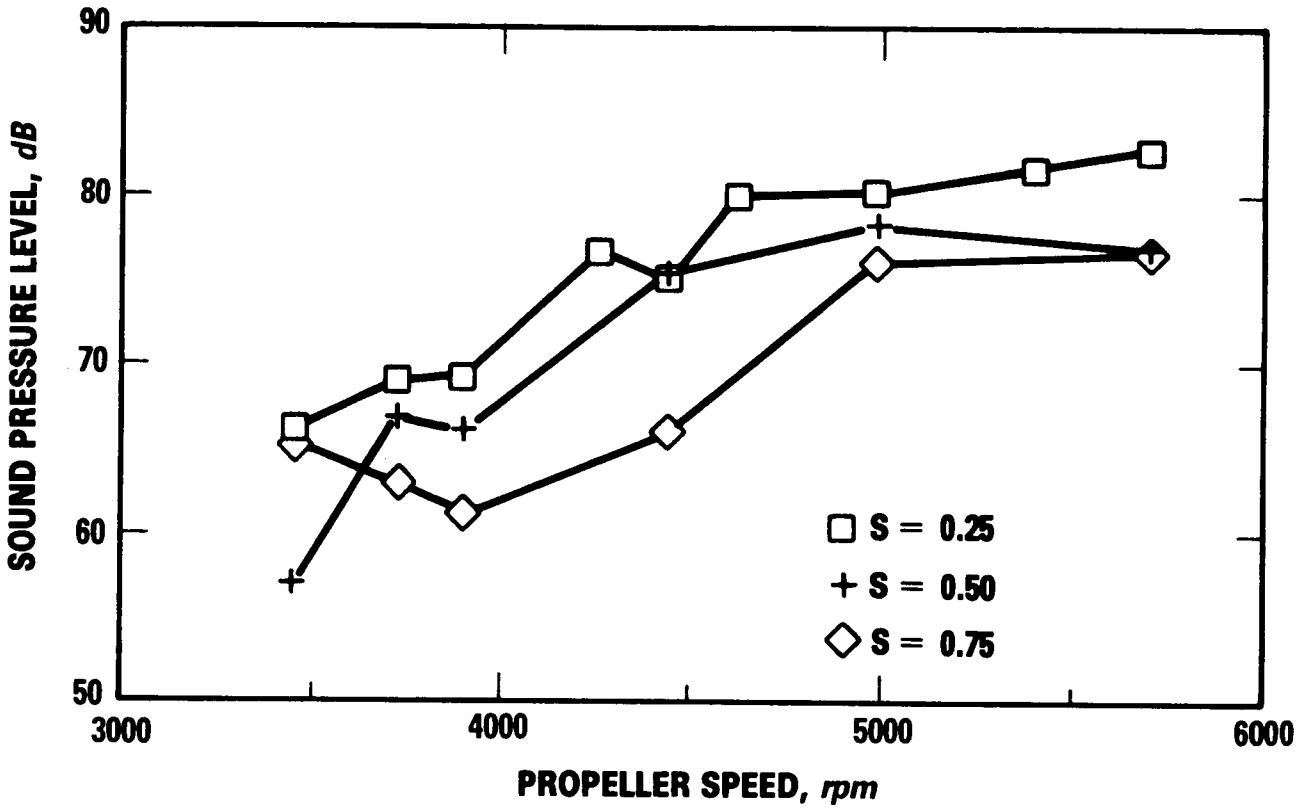

FIGURE 16. EFFECT OF PROPELLER/WING SEPARATION ON STRUCTURE-BORNE NOISE TRANSMISSION, WING STATION 80.

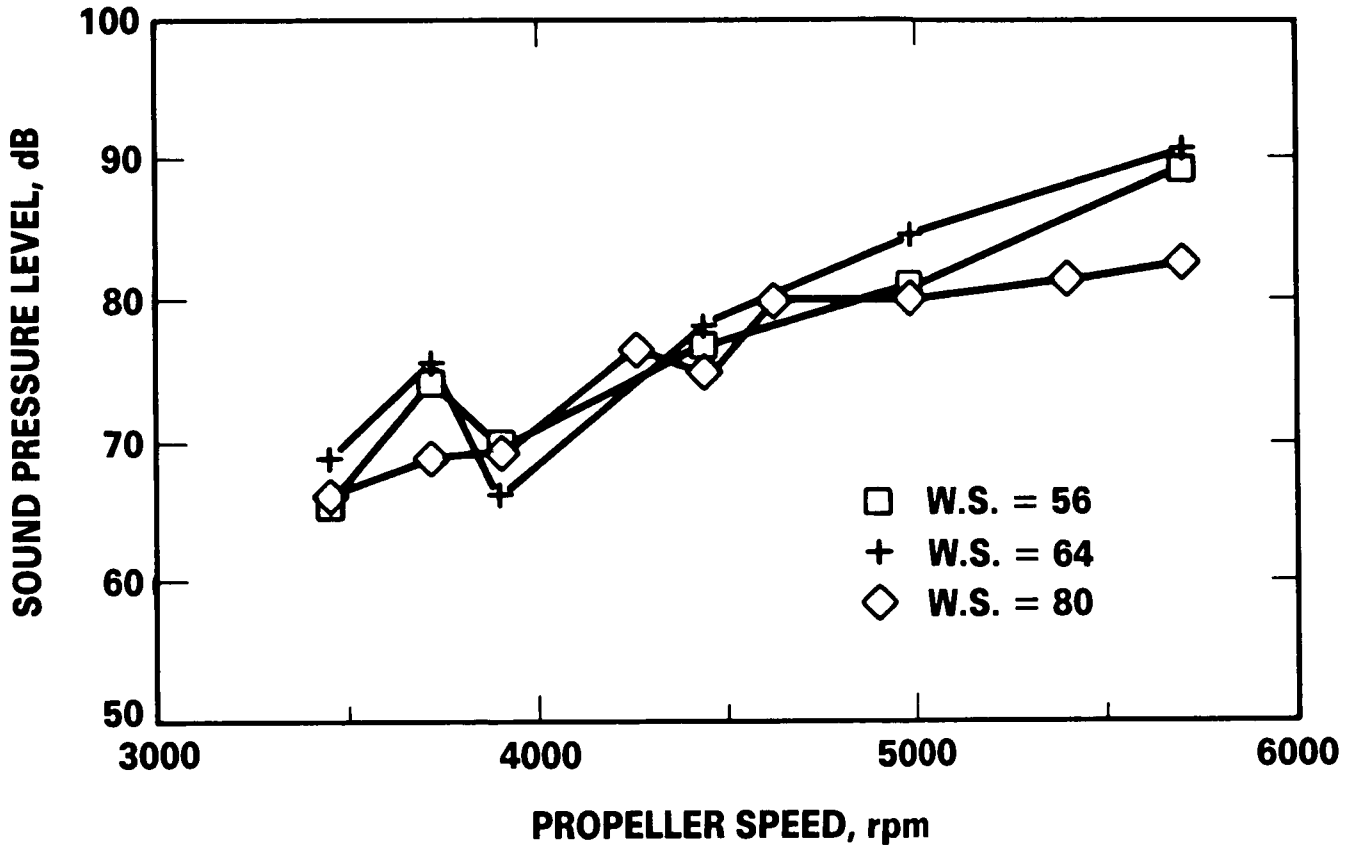

FIGURE 17. EFFECT OF PROPELLER SPANWISE PLACEMENT ON STRUCTURE-BORNE NOISE TRANSMISSION, S = 0.25.

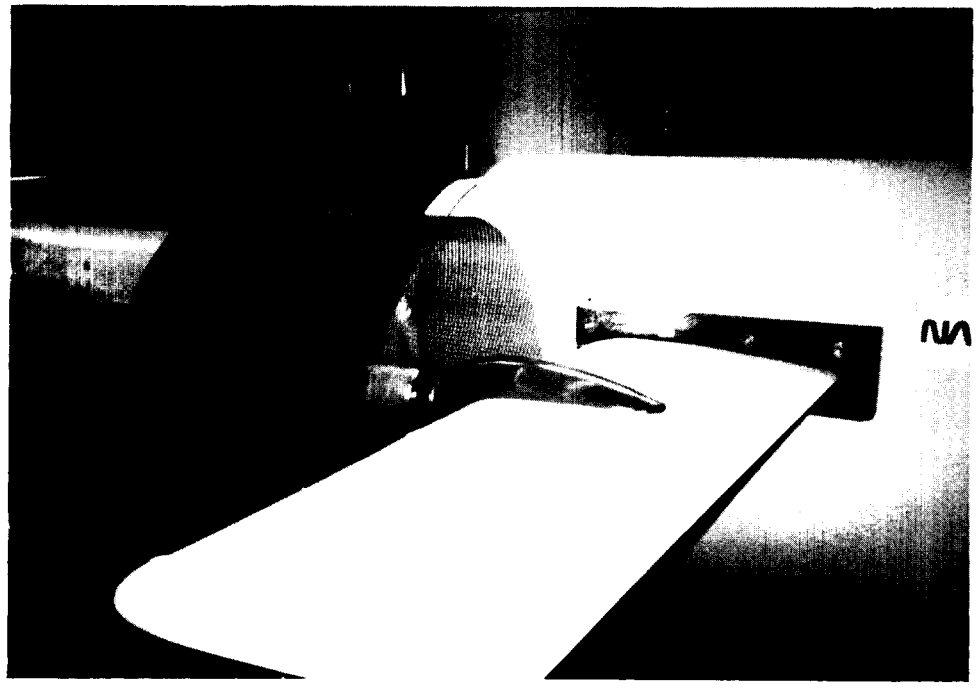

a) Overall

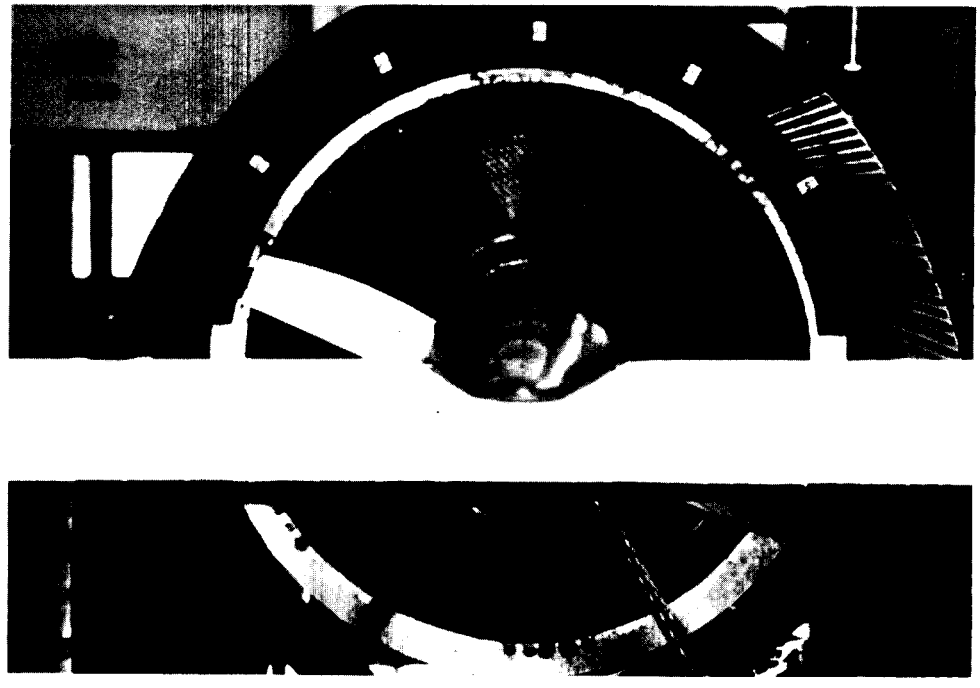

b) Rear View

FIGURE 18. INSTALLED ENGINE/NACELLE MASS.

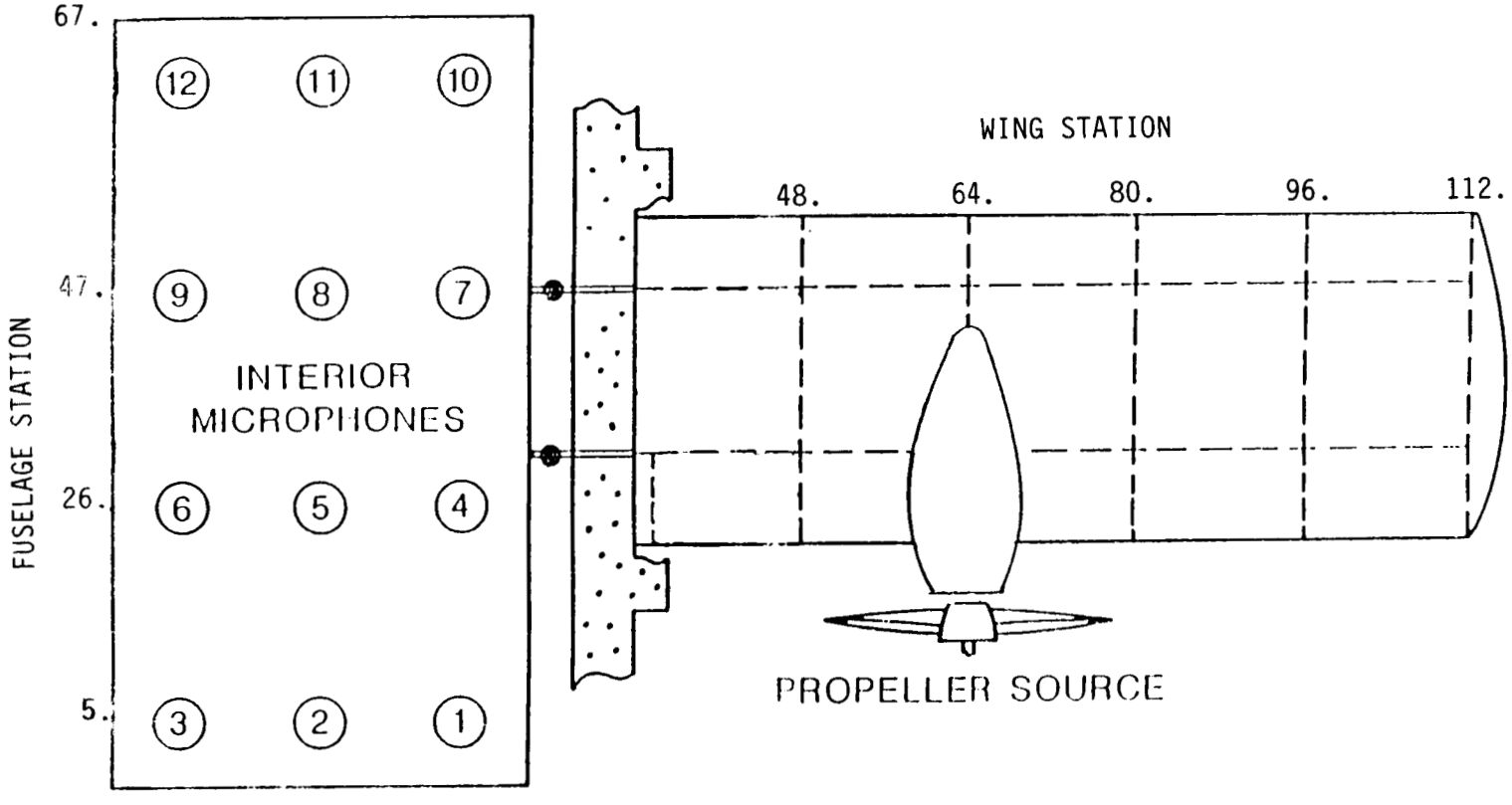

FIGURE 19. SCHEMATIC OF TEST APPARATUS.

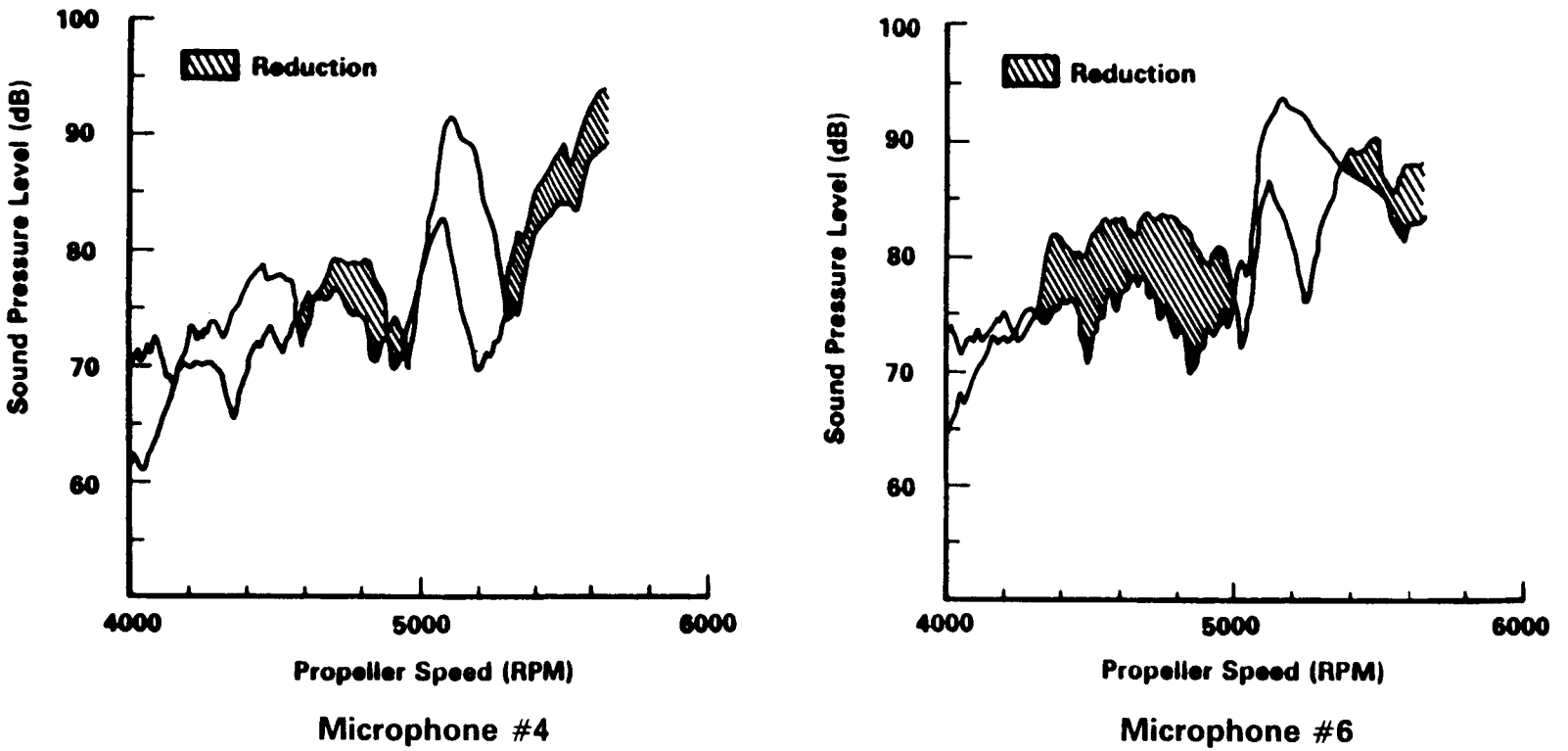

FIGURE 20. STRUCTURE-BORNE NOISE TRANSMISSION, EFFECT OF ENGINE/NACELLE INSTALLATION, SPHERICAL BEARINGS.

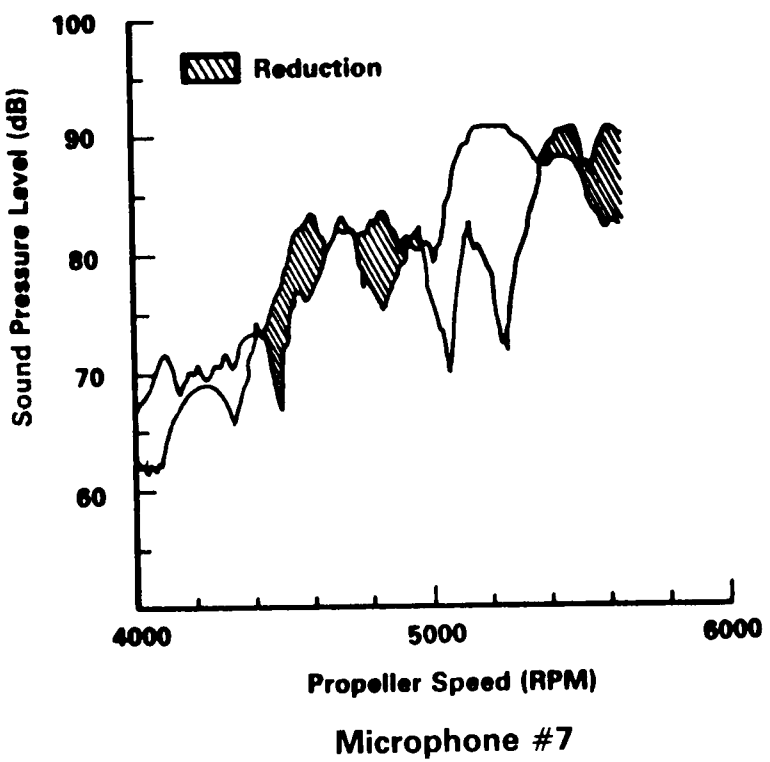

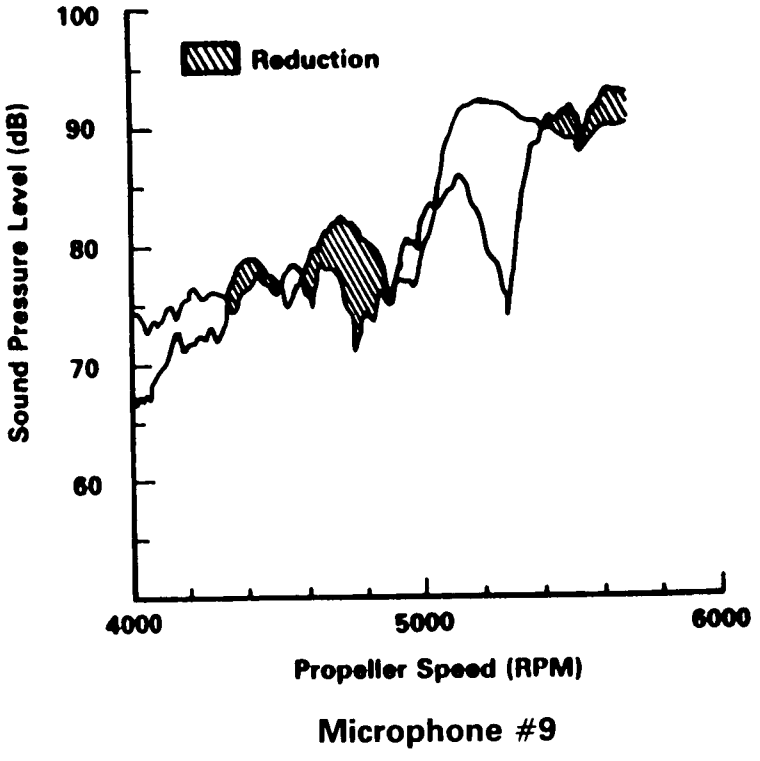

FIGURE 20 (Continued). STRUCTURE-BORNE NOISE TRANSMISSION, EFFECT OF ENGINE/NACELLE INSTALLATION, SPHERICAL BEARINGS.

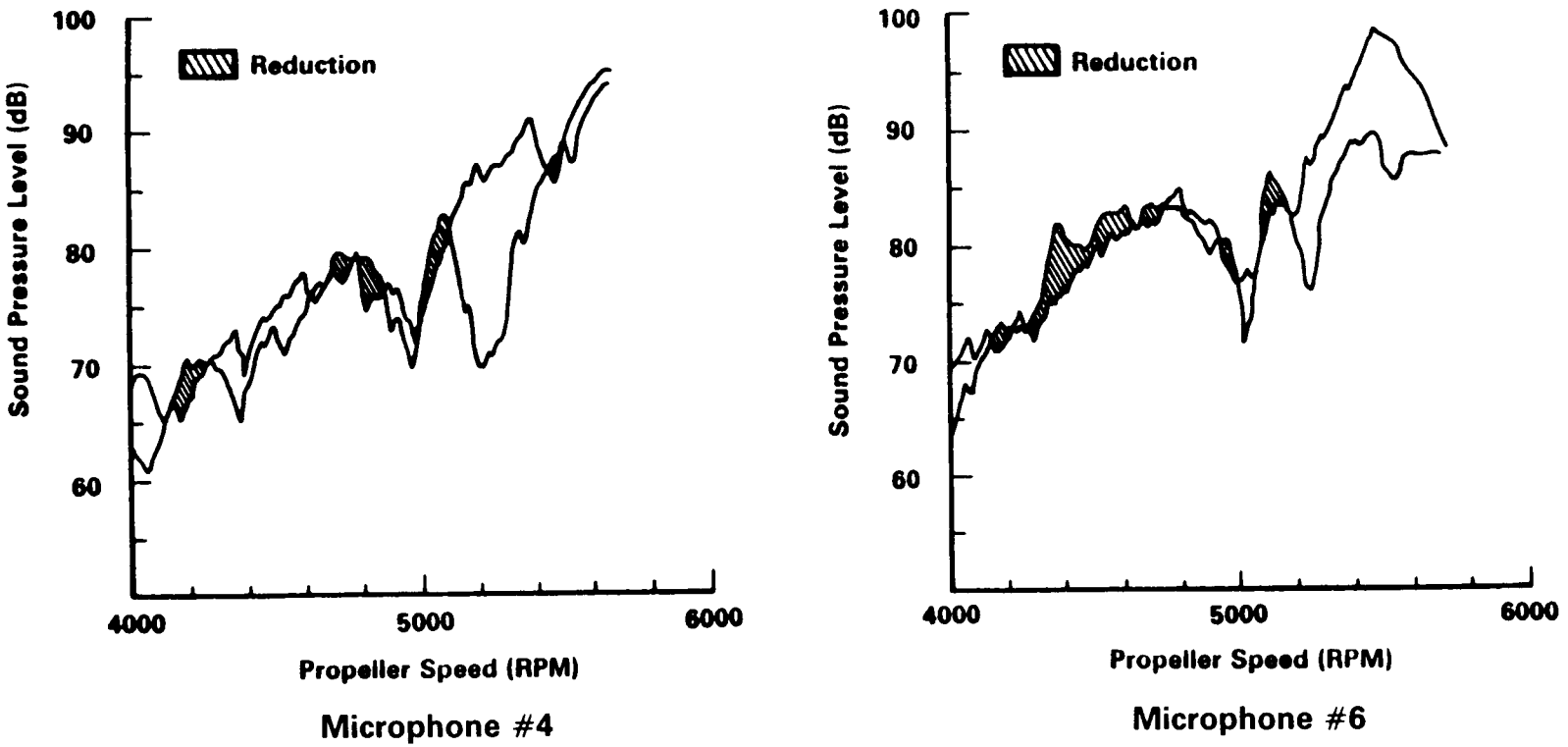

FIGURE 21. STRUCTURE-BORNE NOISE TRANSMISSION, SOLID WING/FUSELAGE ATTACHMENT VERSUS SPHERICAL BEARINGS, BARE WING.

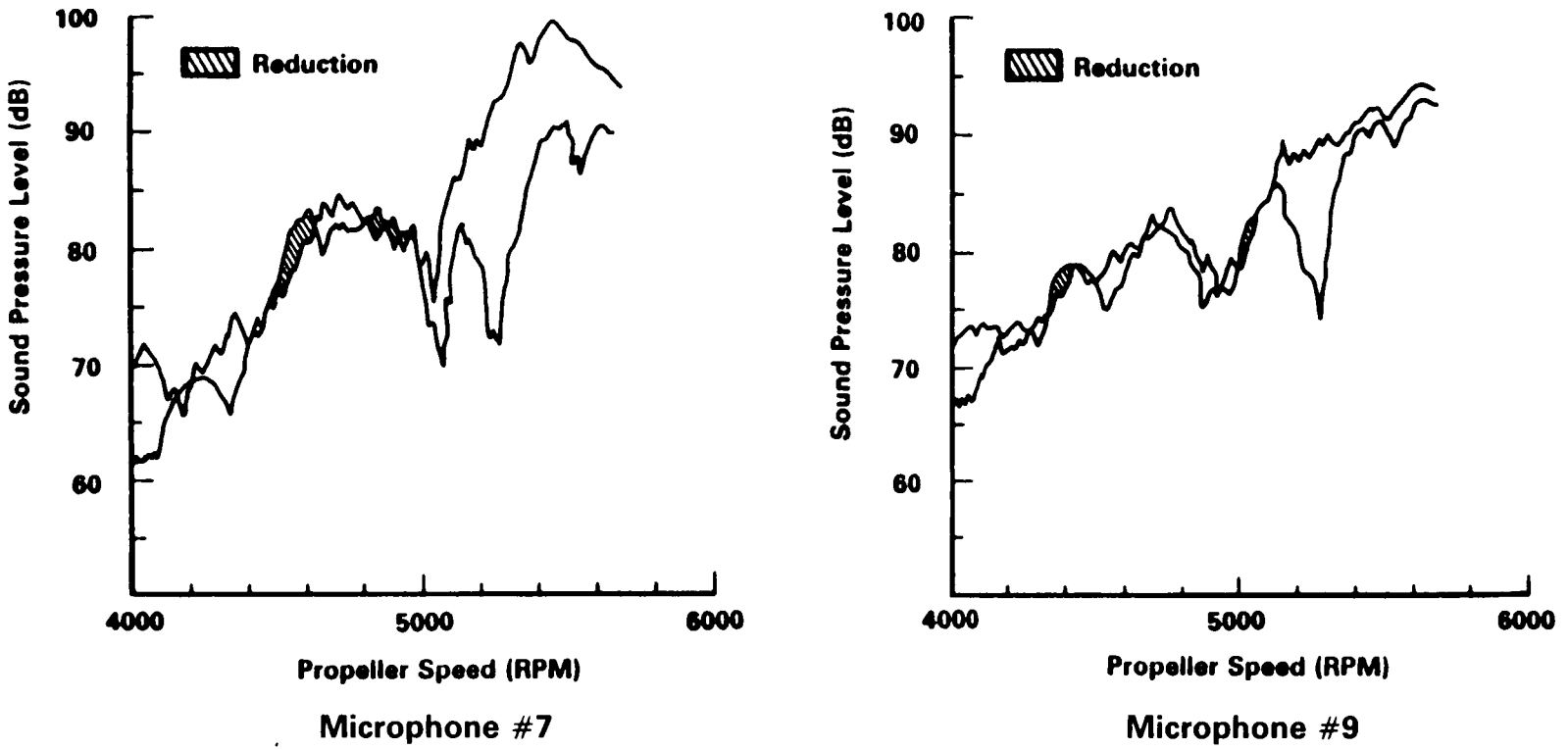

FIGURE 21 (Continued). STRUCTURE-BORNE NOISE TRANSMISSION, SOLID WING/FUSELAGE ATTACHMENT VERSUS SPHERICAL BEARINGS, BARE WING.

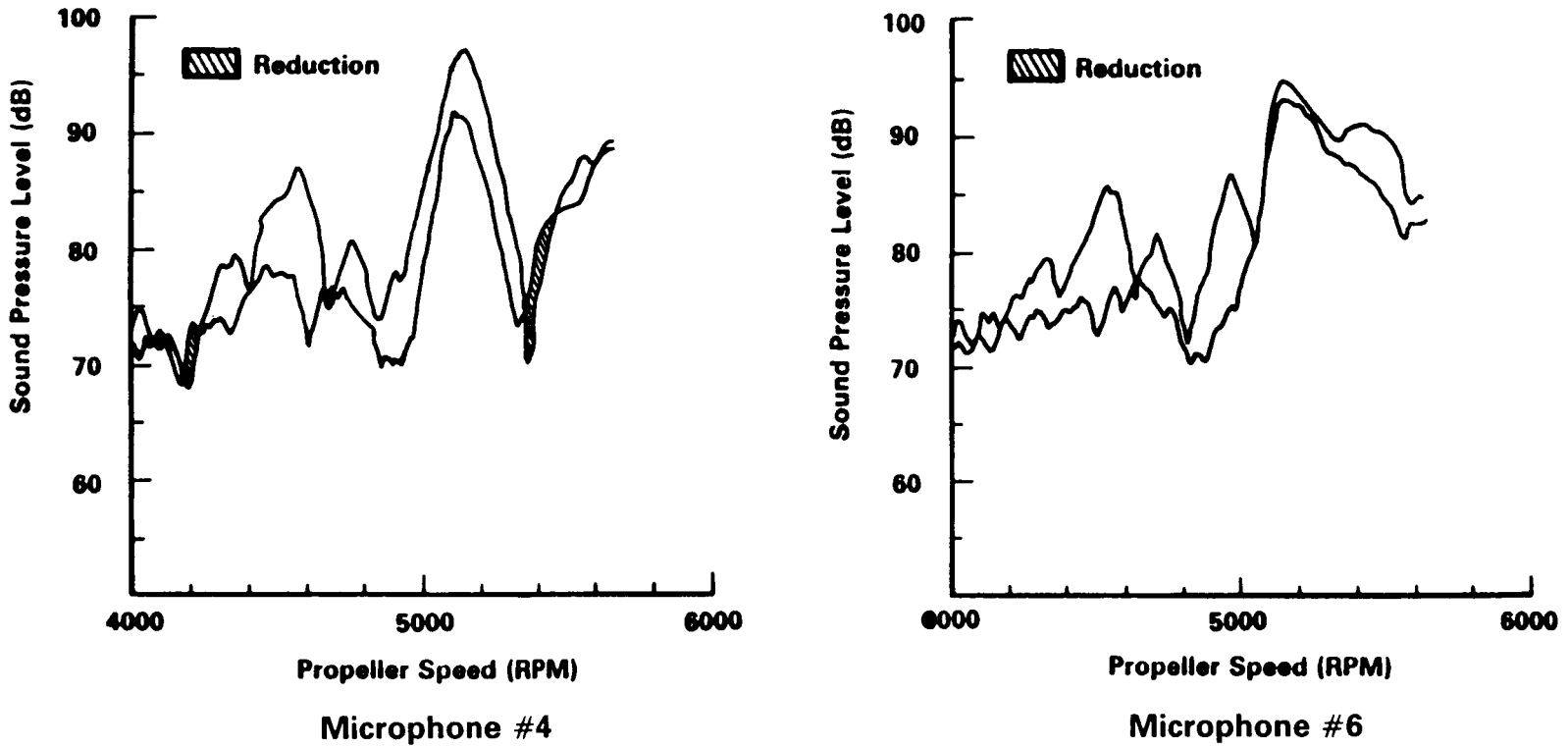

FIGURE 22. STRUCTURE-BORNE NOISE TRANSMISSION, SOLID WING/FUSELAGE ATTACHMENT VERSUS SPHERICAL BEARINGS, ENGINE/NACELLE INSTALLED.

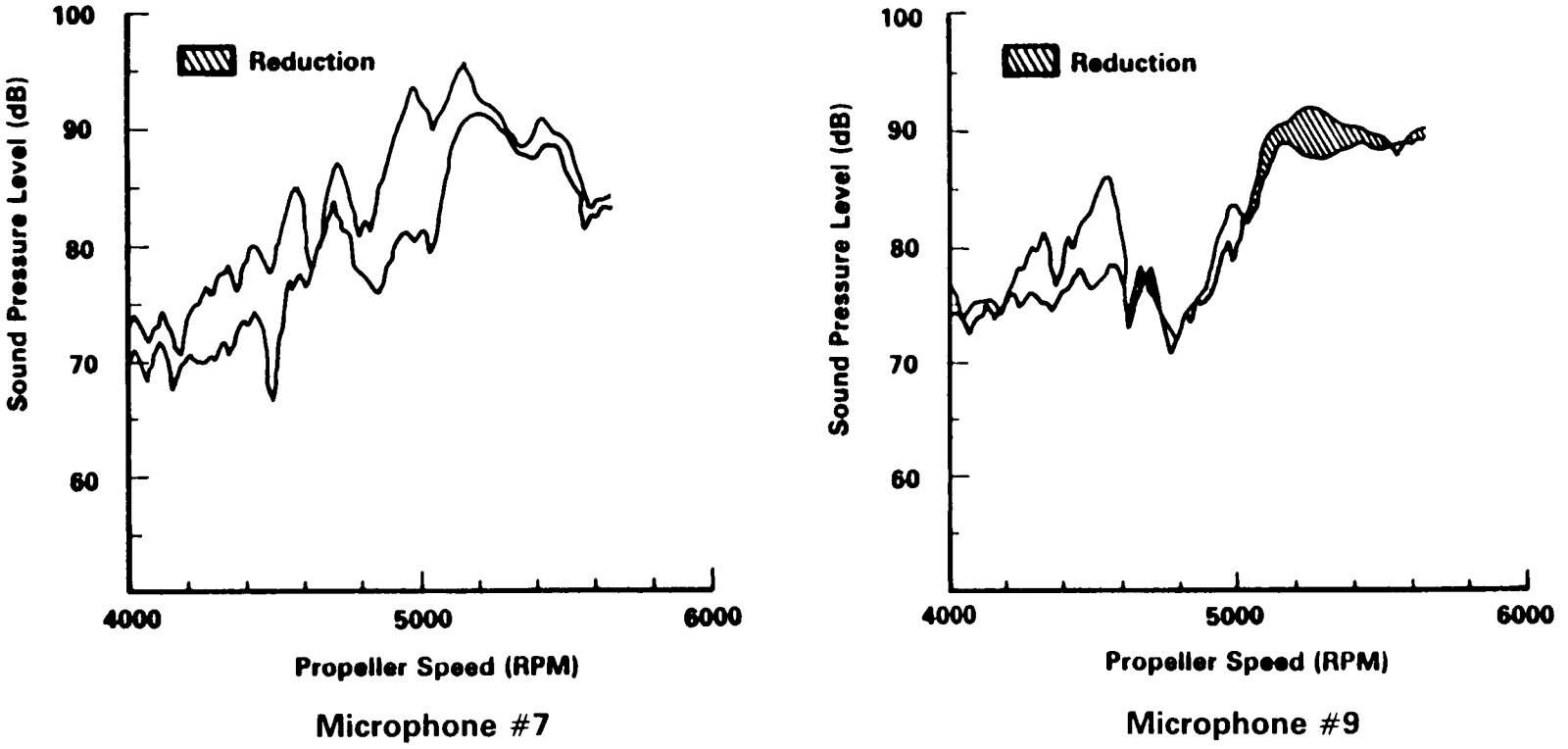

FIGURE 22 (Continued). STRUCTURE-BORNE NOISE TRANSMISSION, SOLID WING/FUSELAGE ATTACHMENT VERSUS SPHERICAL BEARINGS, ENGINE/NACELLE INSTALLED.

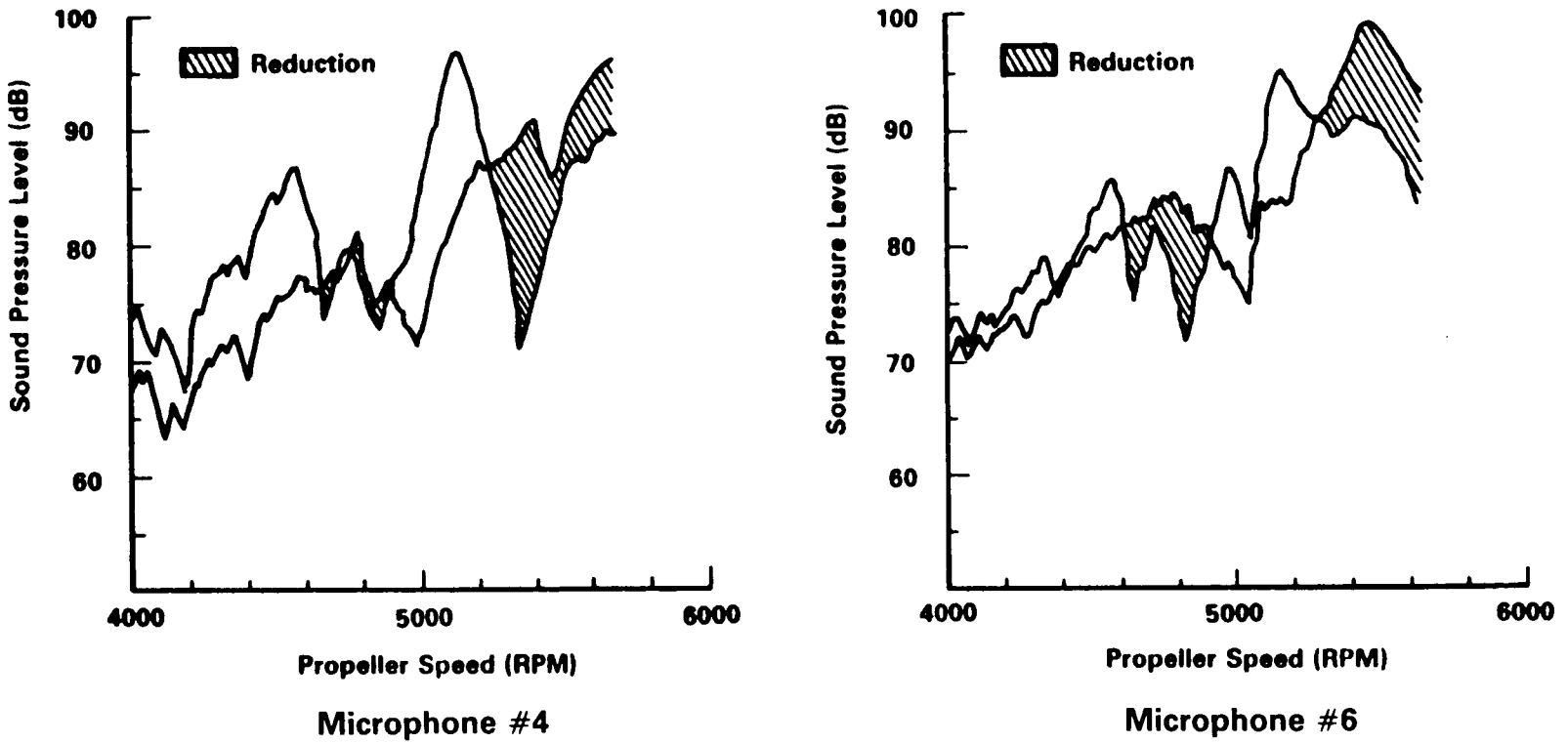

FIGURE 23. STRUCTURE-BORNE NOISE TRANSMISSION, EFFECT OF ENGINE/NACELLE INSTALLATION, SOLID WING/FUSELAGE ATTACHMENT.

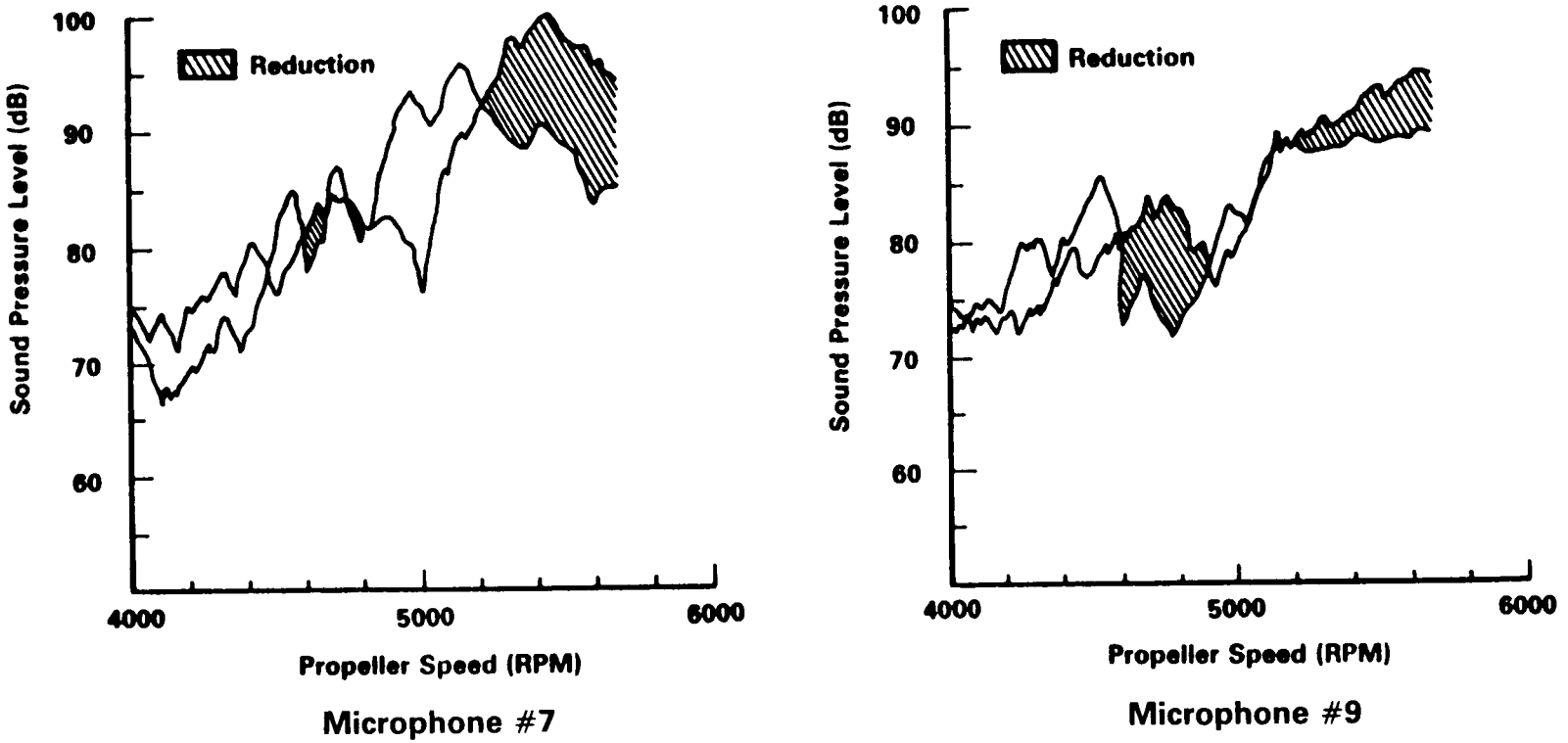

FIGURE 23 (Continued). STRUCTURE-BORNE NOISE TRANSMISSION, EFFECT OF ENGINE/NACELLE INSTALLATION, SOLID WING/FUSELAGE ATTACHMENT.

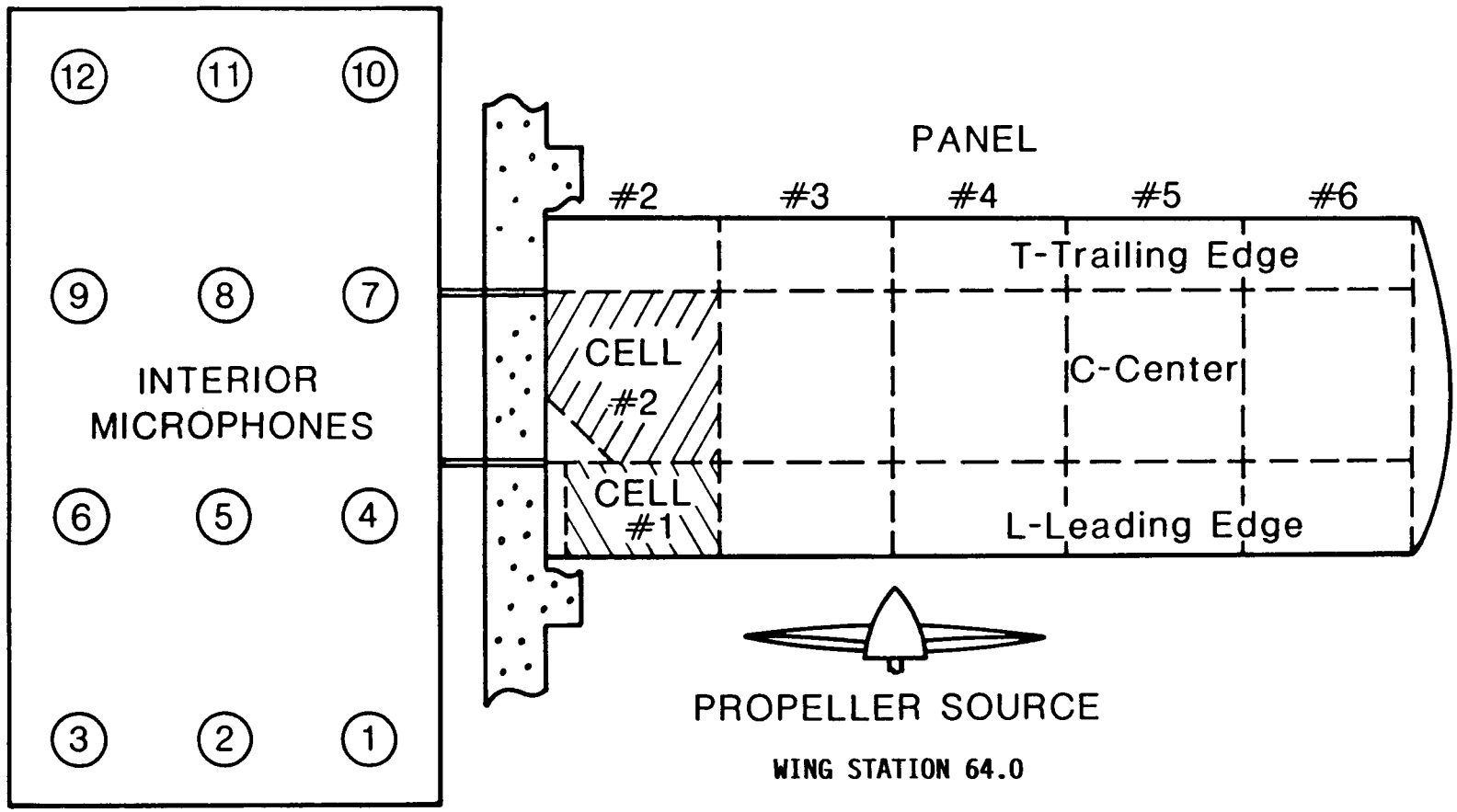

FIGURE 24. SCHEMATIC OF TEST APPARATUS AND PANEL/CELL NOMENCLATURE.

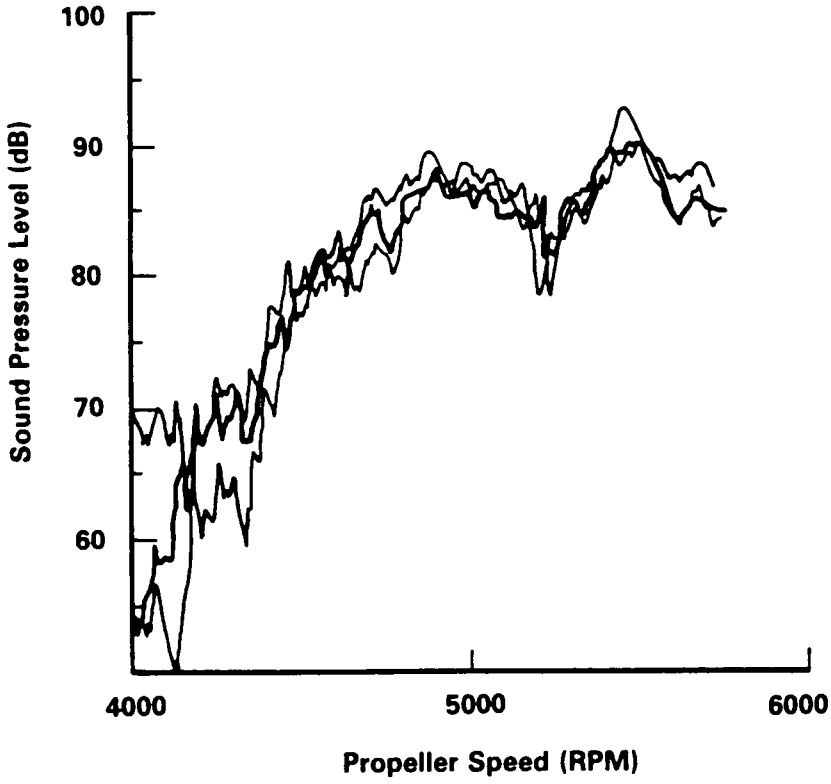

FIGURE 25. TYPICAL BASELINE REPEATABILITY, FOUR-WEEK PERIOD.

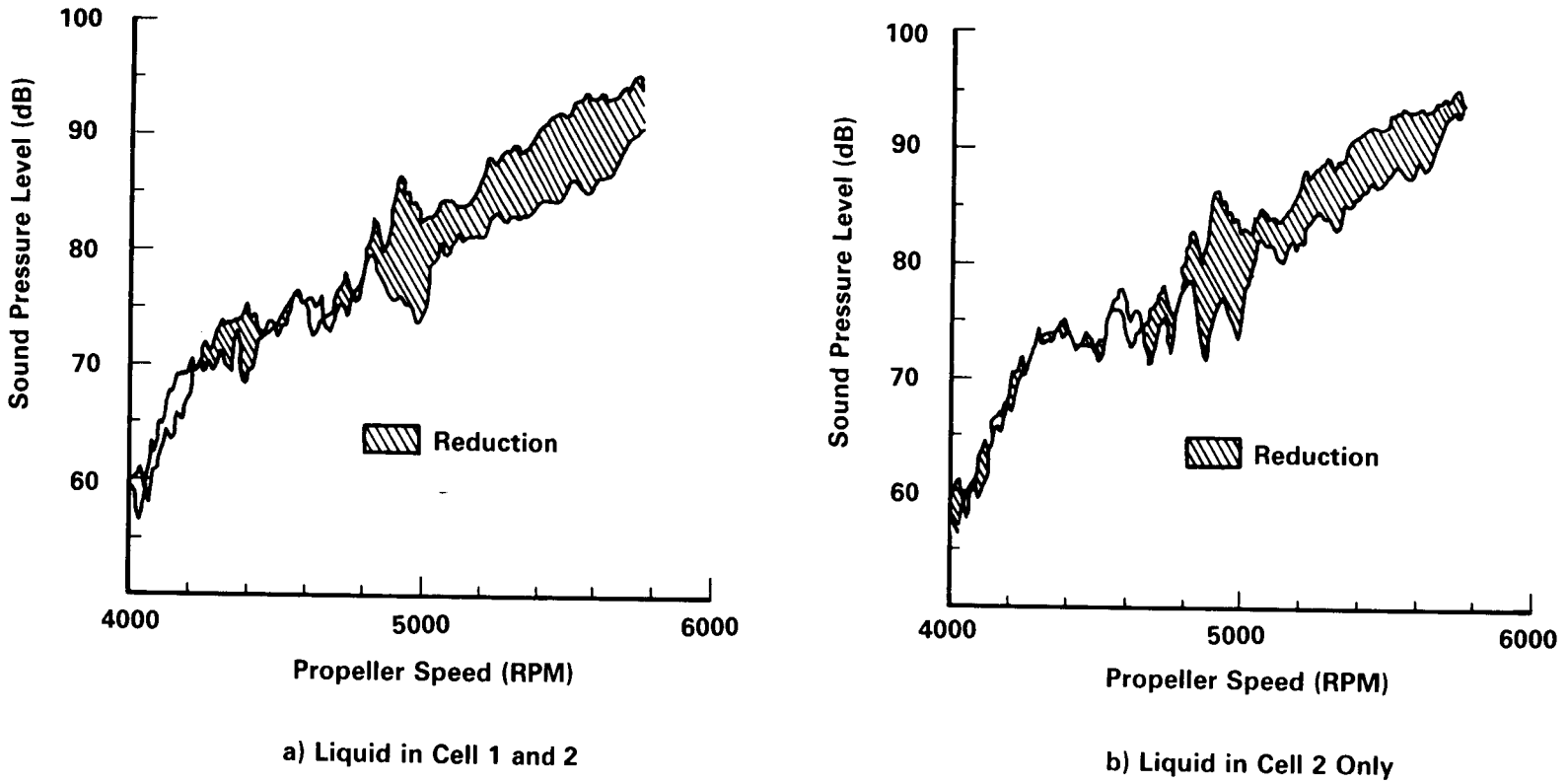

FIGURE 26. EFFECT OF SIMULATED WING FUEL ON STRUCTURE-BORNE NOISE TRANSMISSION.

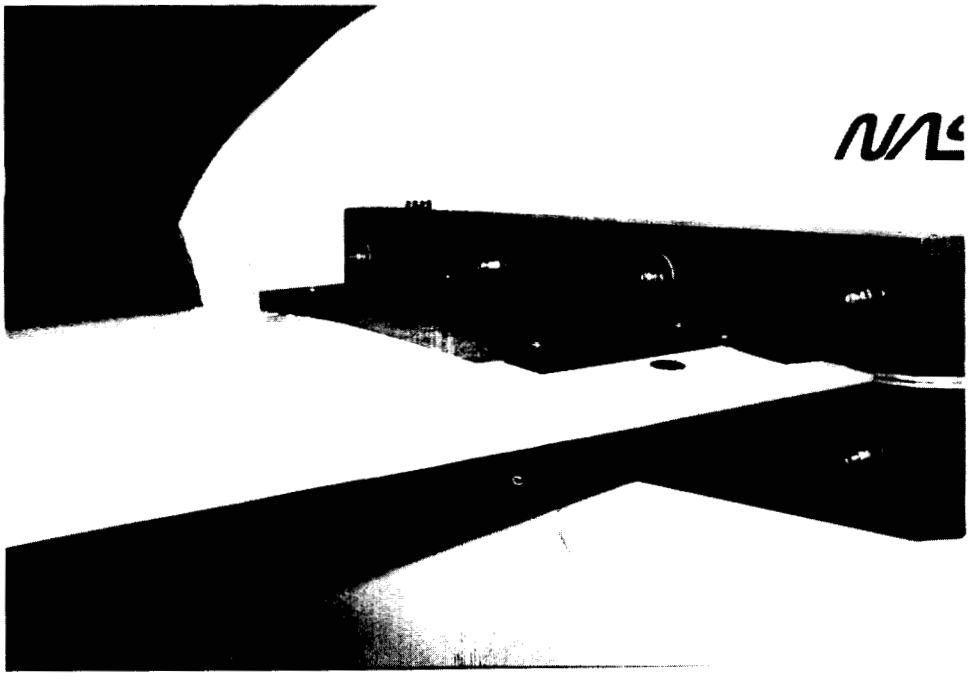

FIGURE 27. WING BLOCKING MASSES.

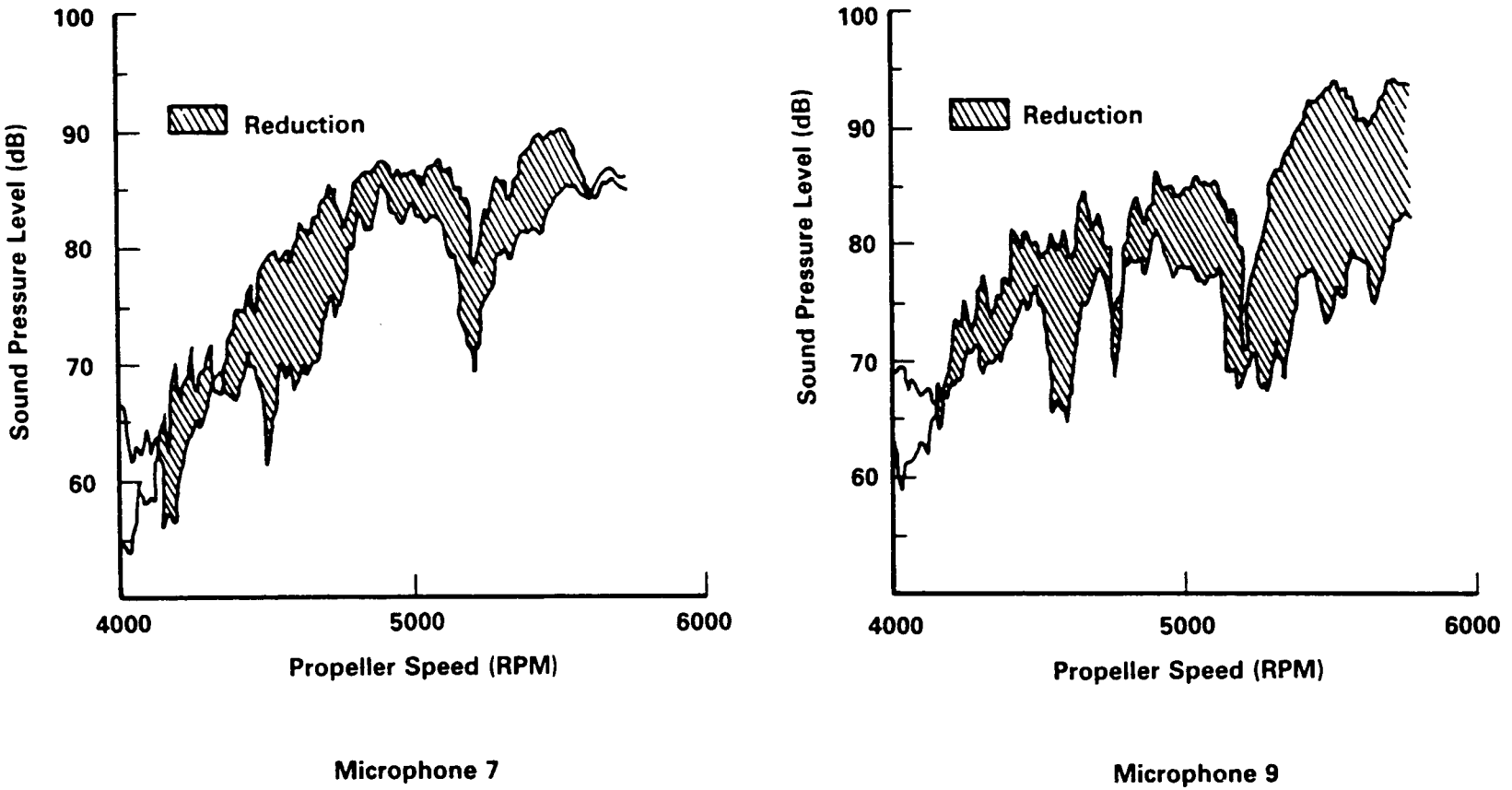

FIGURE 28. EFFECT OF SOLID MASSES ON STRUCTURE-BORNE NOISE TRANSMISSION, SPHERICAL BEARINGS.

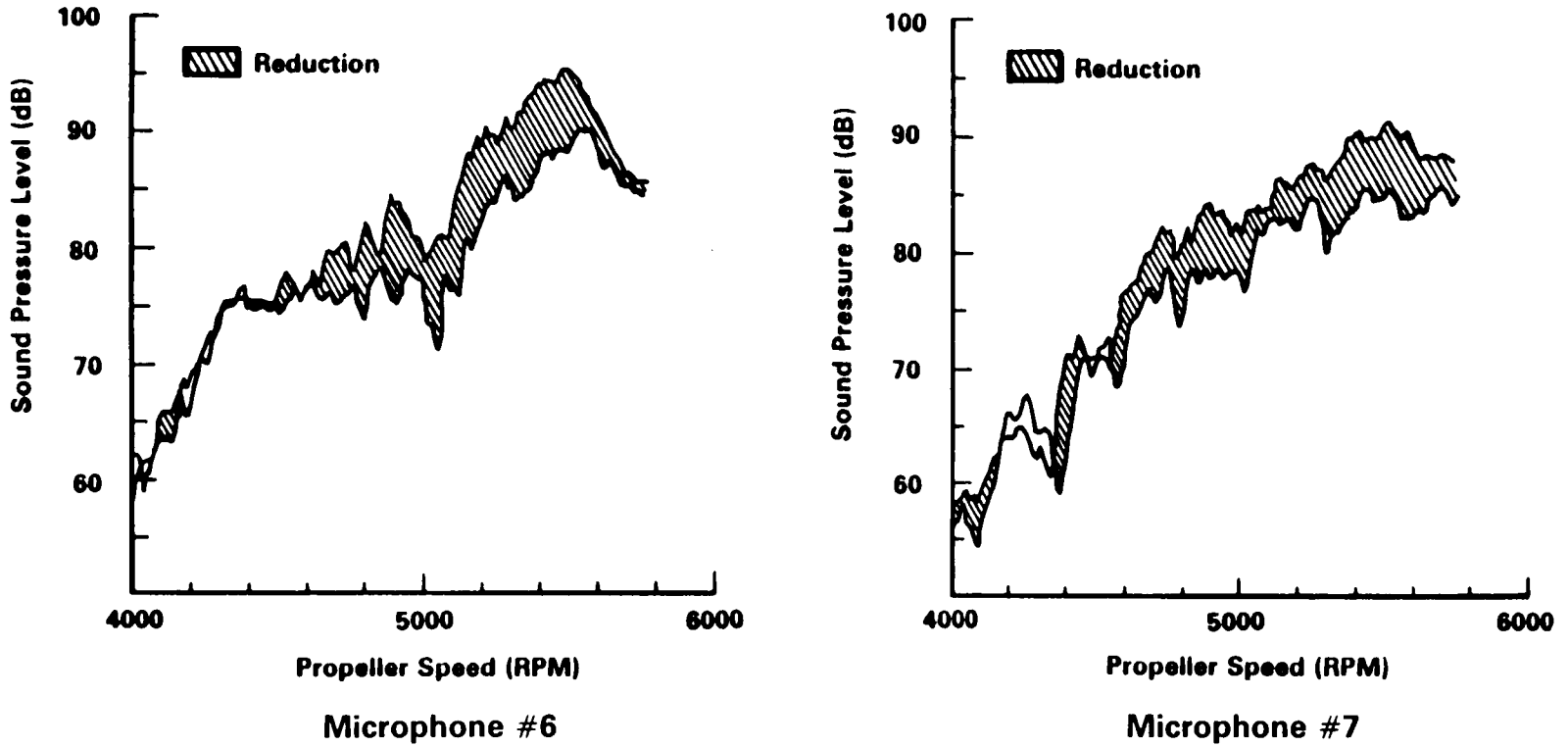

a) Spherical Bearings at Wing-to-Fuselage Attachments

FIGURE 29. INSTALLATION EFFECTS ON STRUCTURE-BORNE NOISE TRANSMISSION EFFECTIVENESS OF SIMULATED FUEL IN WING CELL #2.

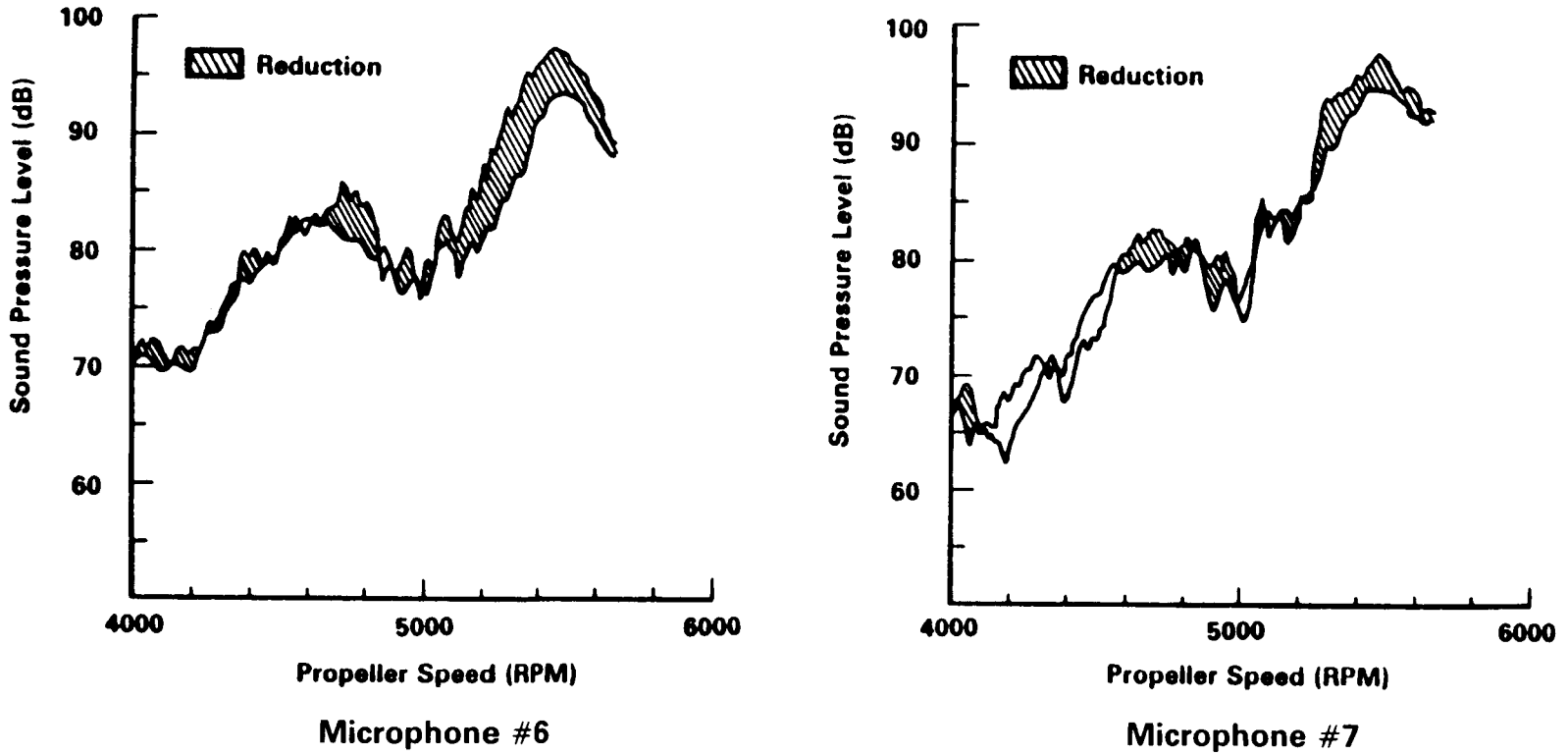

b) Rigid Wing-to-Fuselage Attachments

FIGURE 29 (Continued). INSTALLATION EFFECTS ON STRUCTURE-BORNE NOISE TRANSMISSION EFFECTIVENESS OF SIMULATED FUEL IN WING CELL #2.

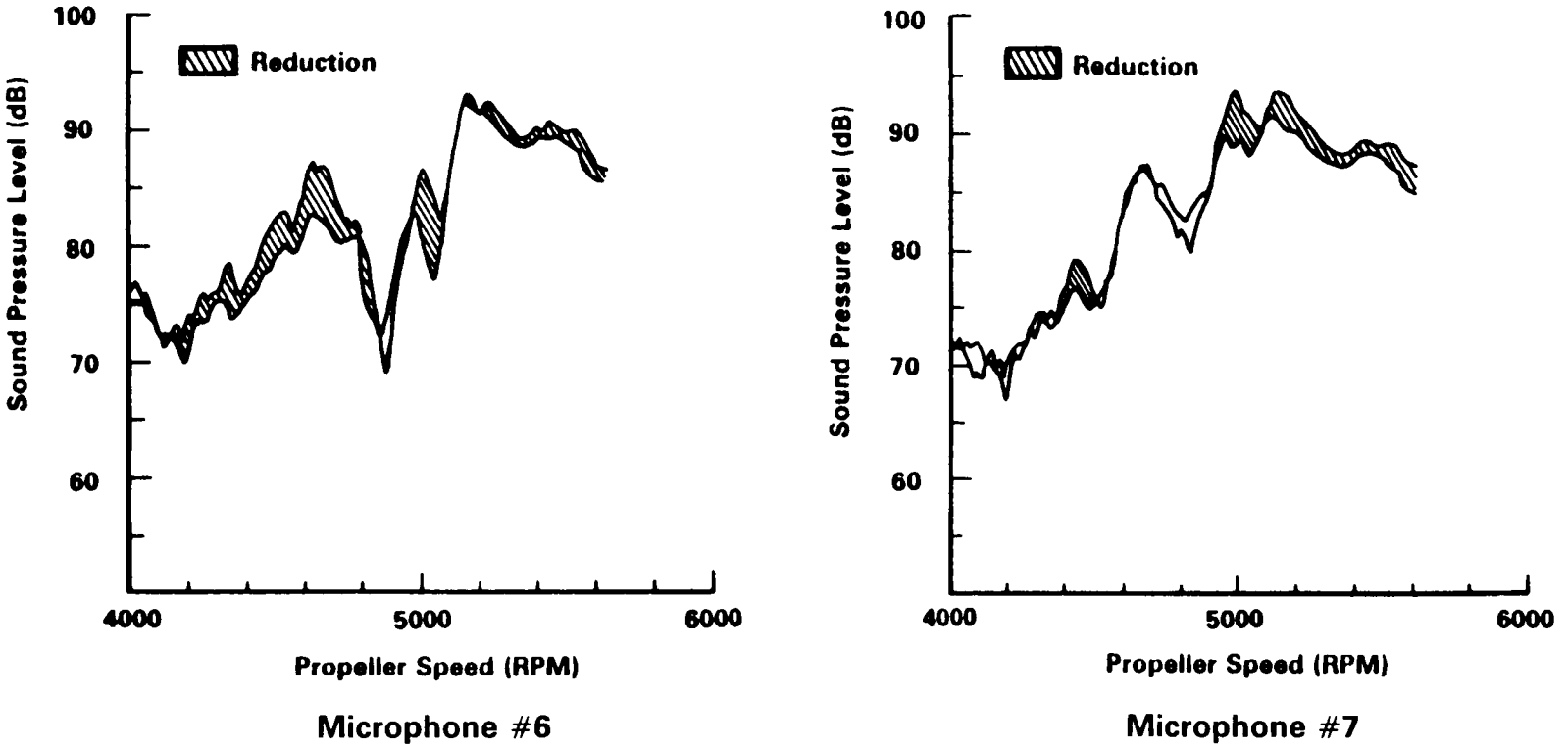

c) Engine/Nacelle Mass Installed

FIGURE 29 (Concluded). INSTALLATION EFFECTS ON STRUCTURE-BORNE TRANSMISSION EFFECTIVENESS OF SIMULATED FUEL IN WING CELL #2.

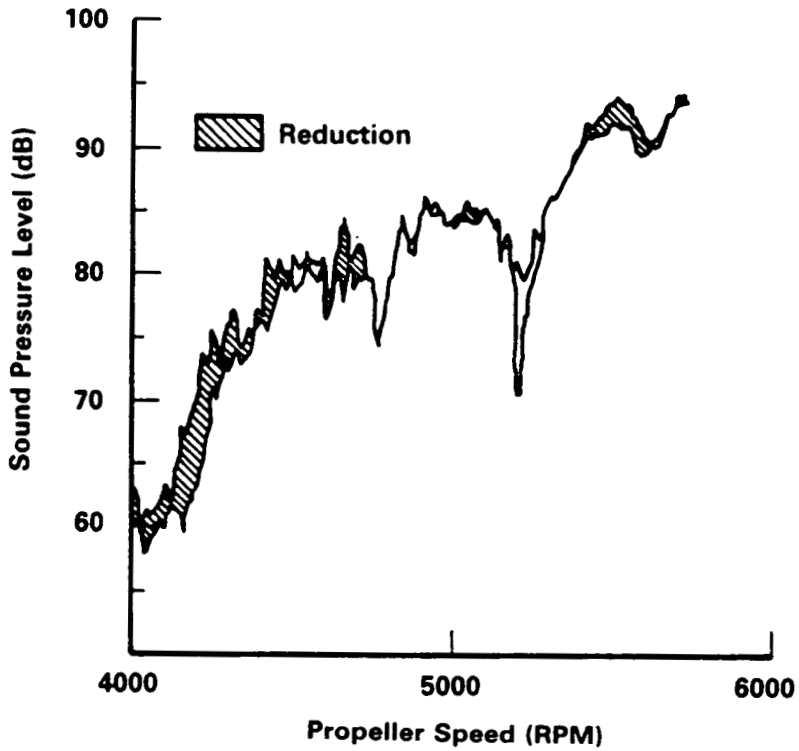

FIGURE 30. EFFECT OF DAMPING MATERIAL ON STRUCTURE-BORNE NOISE TRANSMISSION, WING CENTER PANEL #2, MICROPHONE #9.

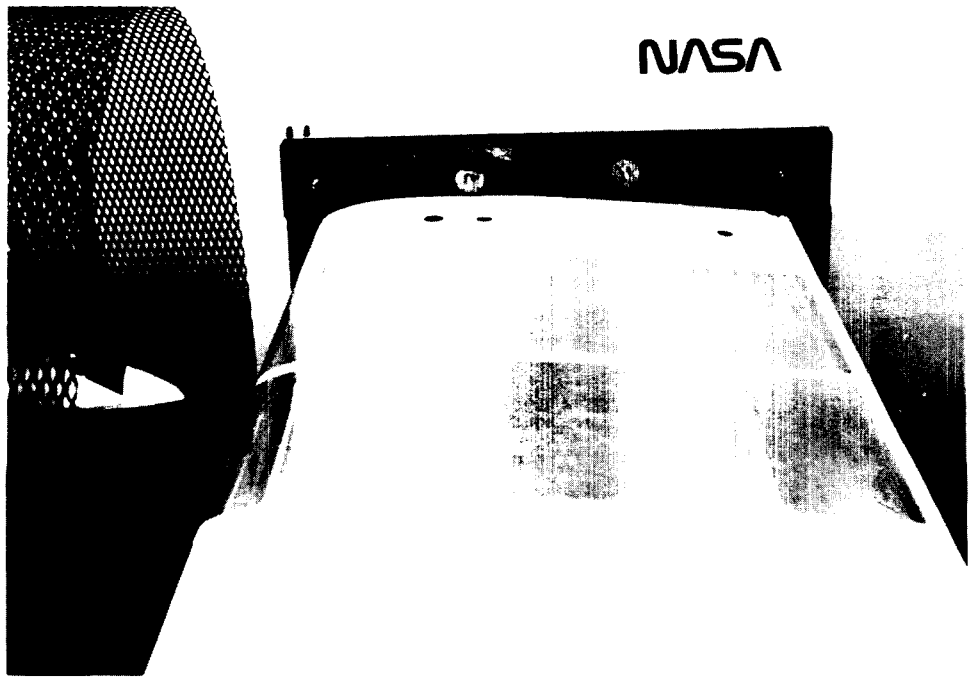

FIGURE 31. TYPICAL PANEL DAMPING TREATMENT.

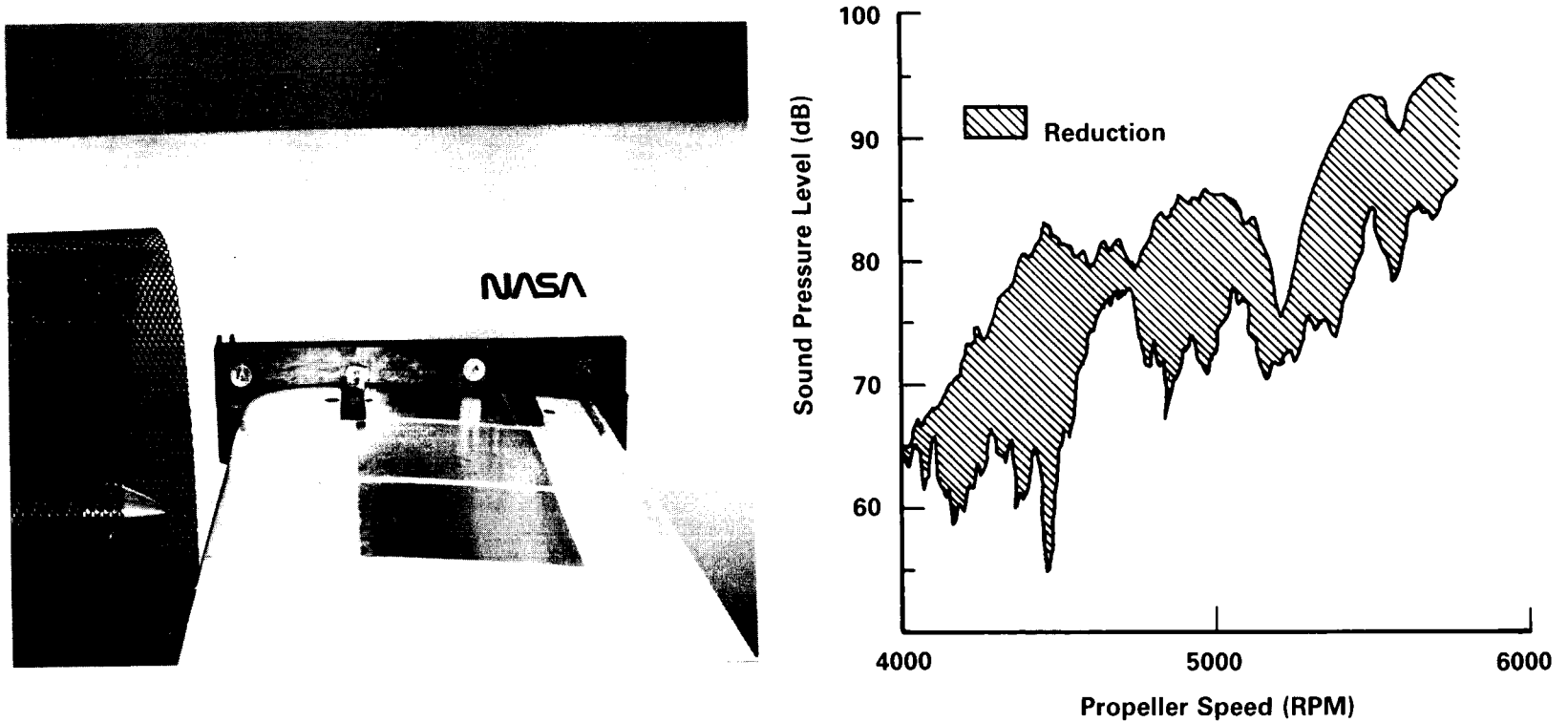

ORIGINAL PAGE
BLACK AND WHITE PHOTOGRAPH

FIGURE 32. COMBINED EFFECT OF BLOCKING MASS AND PANEL DAMPING TREATMENT ON STRUCTURE-BORNE NOISE TRANSMISSION, MICROPHONE #9.

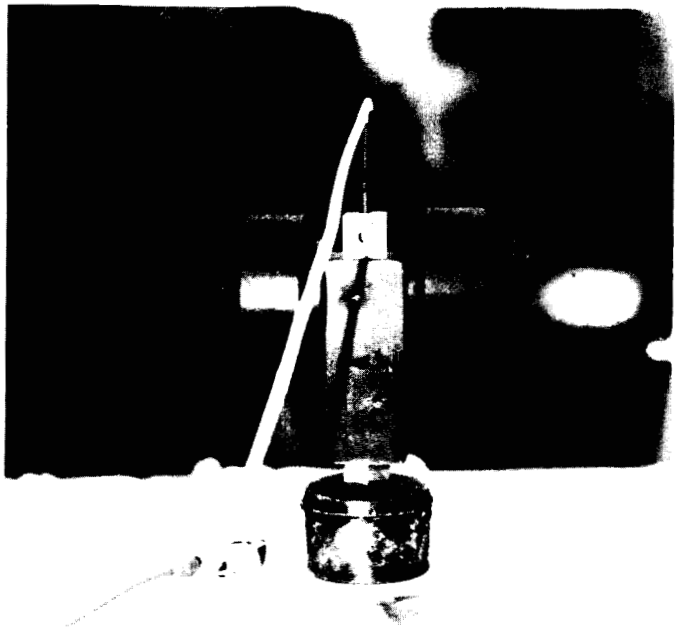

FIGURE 33. TUNED MECHANICAL DAMPER.

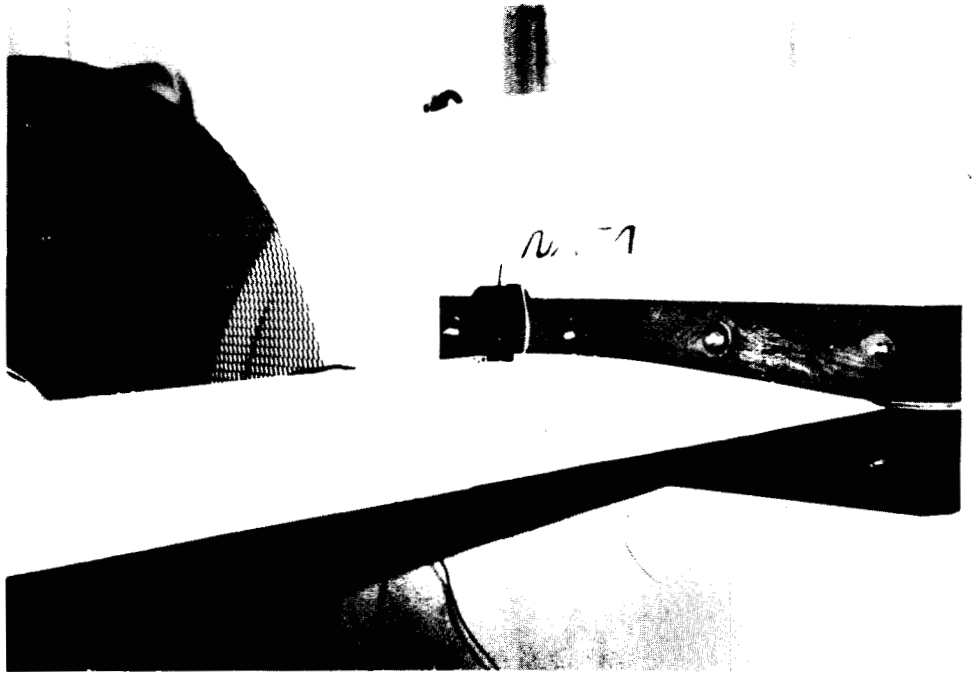

FIGURE 34. TUNED DAMPER INSTALLATION.

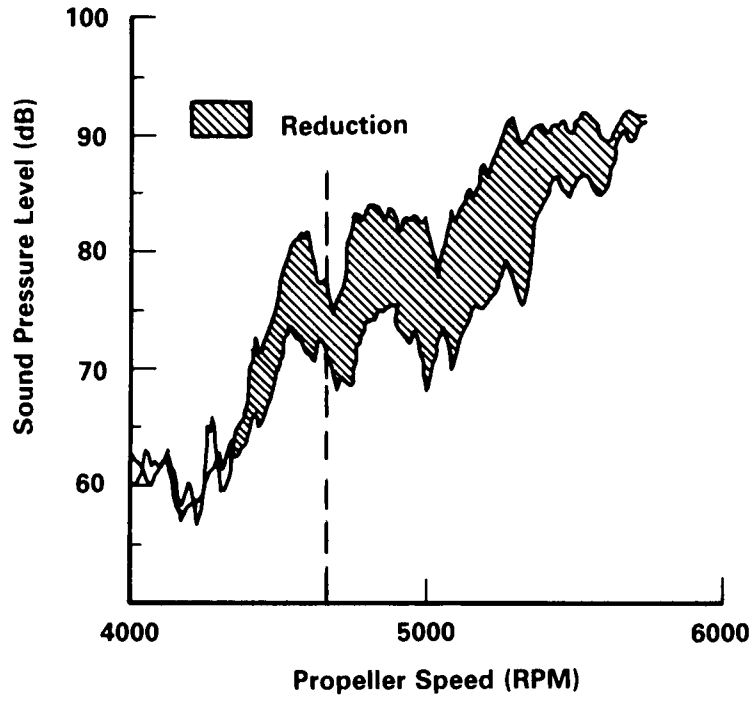

FIGURE 35. EFFECT OF TUNED DAMPER ON STRUCTURE-BORNE TRANSMISSION, MICROPHONE #7.

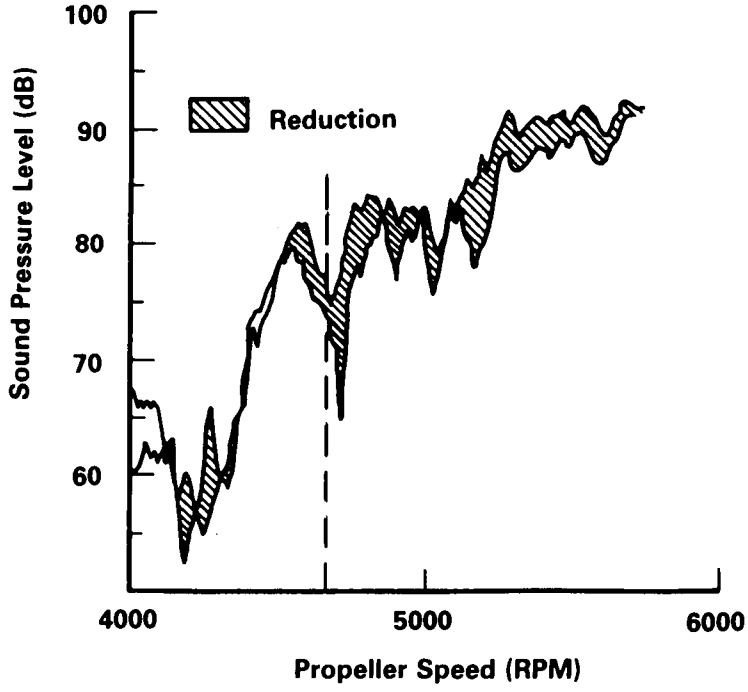

FIGURE 36. EFFECT OF RIGID DAMPER ON STRUCTURE-BORNE TRANSMISSION, MICROPHONE #7.

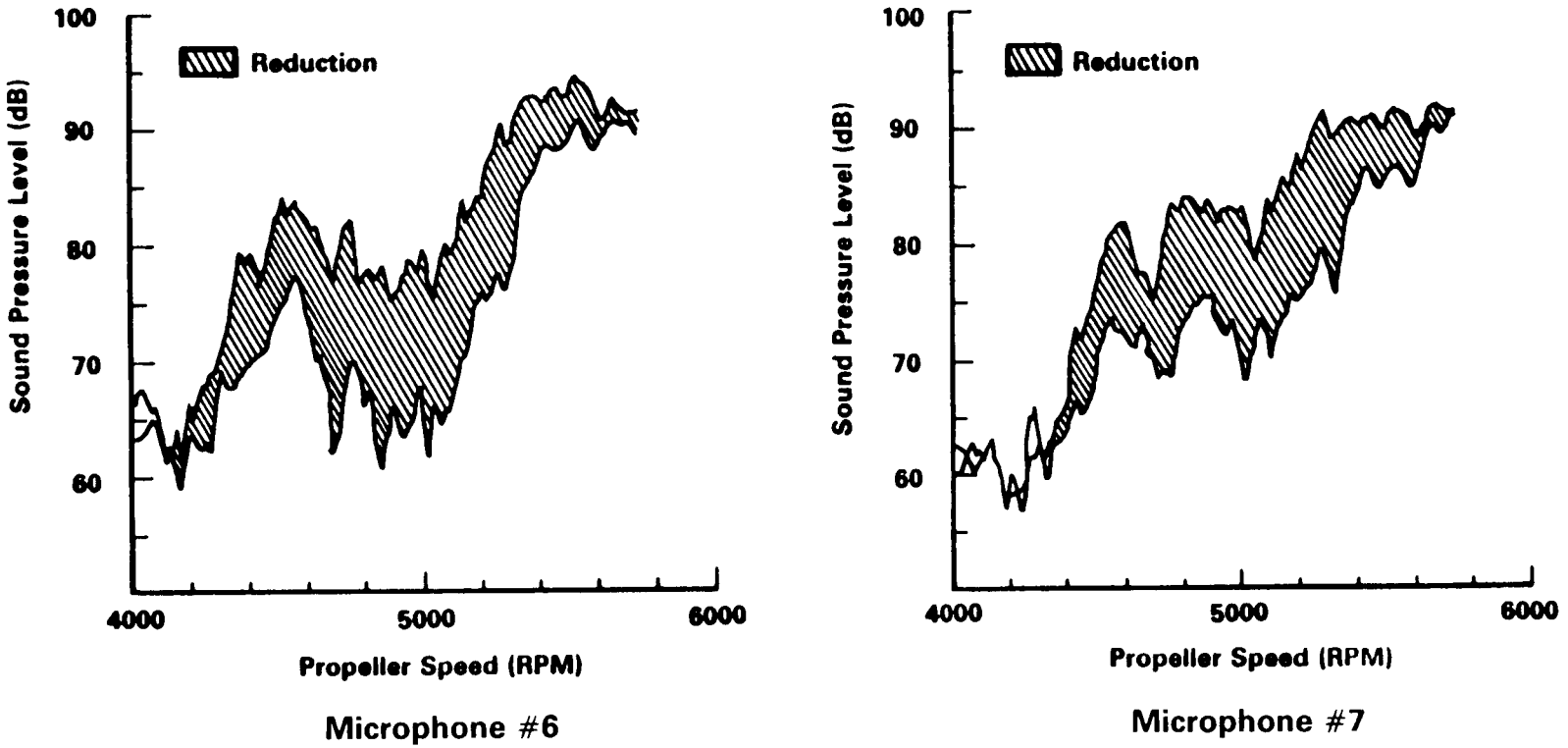

a) Spherical Bearings at Wing-to-Fuselage Attachments

FIGURE 37. INSTALLATION EFFECTS ON STRUCTURE-BORNE TRANSMISSION EFFECTIVENESS OF TUNED DAMPERS AT WING STATION 41.

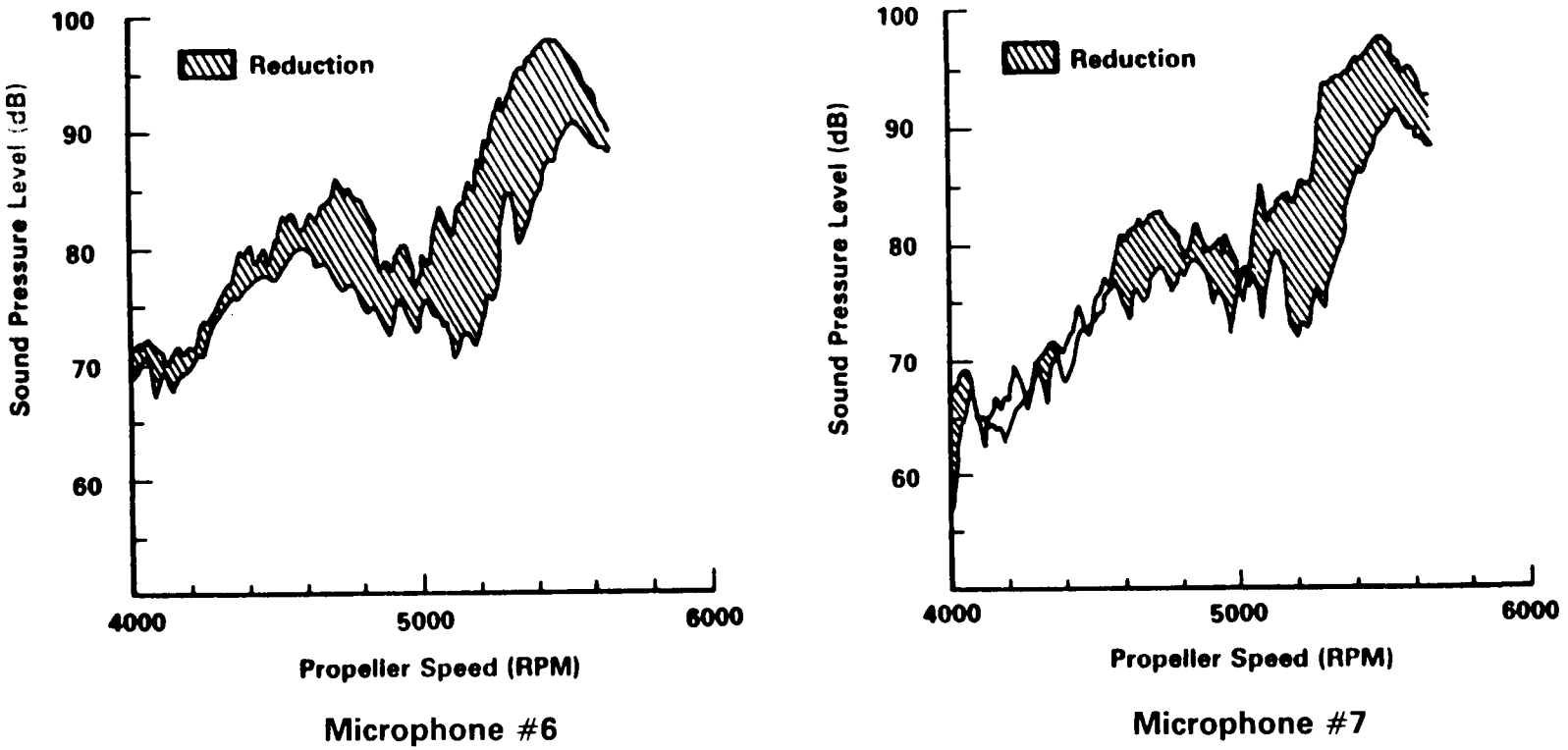

b) Rigid Wing-to-Fuselage Attachments

FIGURE 37 (Continued). INSTALLATION EFFECTS ON STRUCTURE-BORNE TRANSMISSION EFFECTIVENESS OF TUNED DAMPERS AT WING STATION 41.

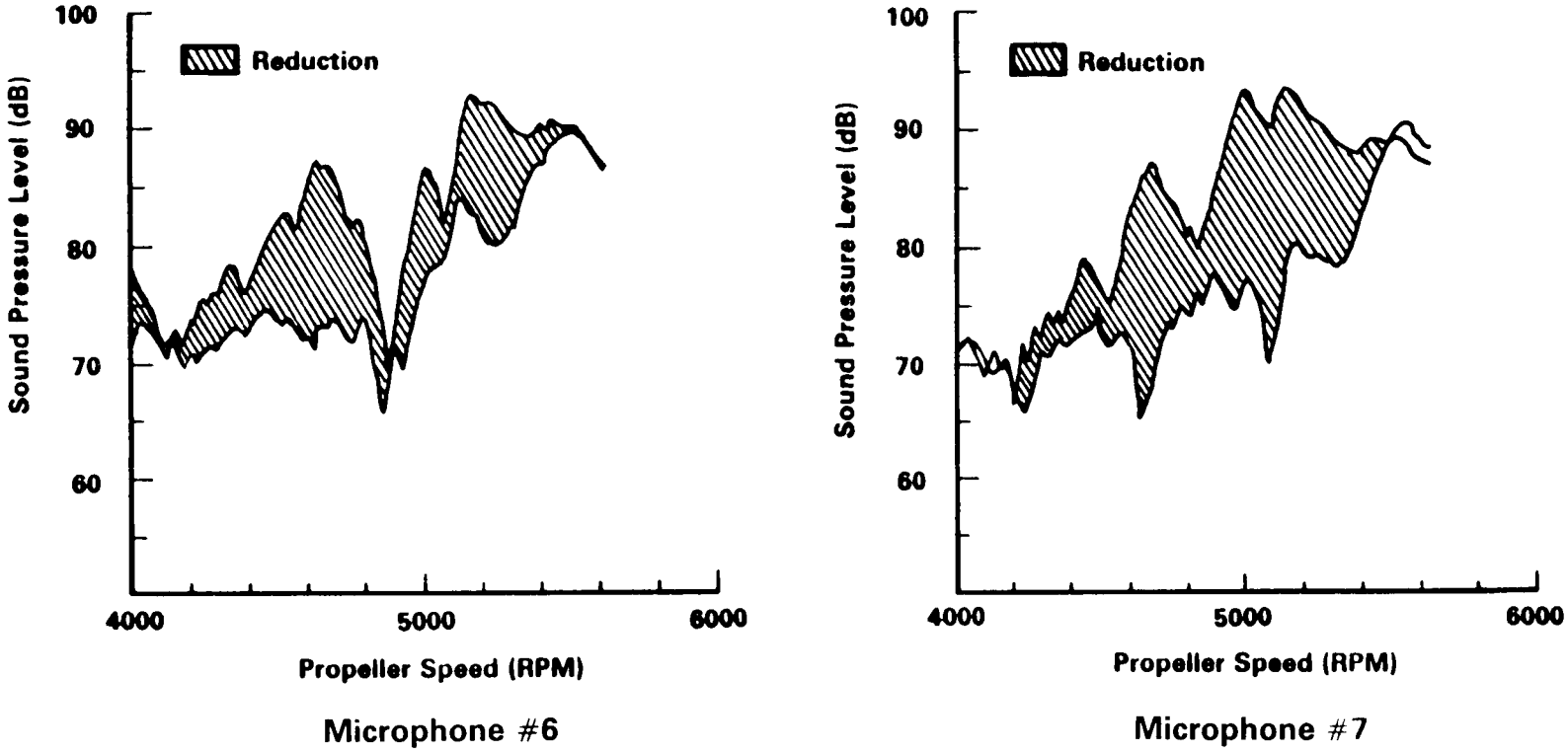

c) Engine/Nacelle Mass Installed

FIGURE 37 (Concluded). INSTALLATION EFFECTS ON STRUCTURE-BORNE TRANSMISSION EFFECTIVENESS OF TUNED DAMPERS AT WING STATION 41.

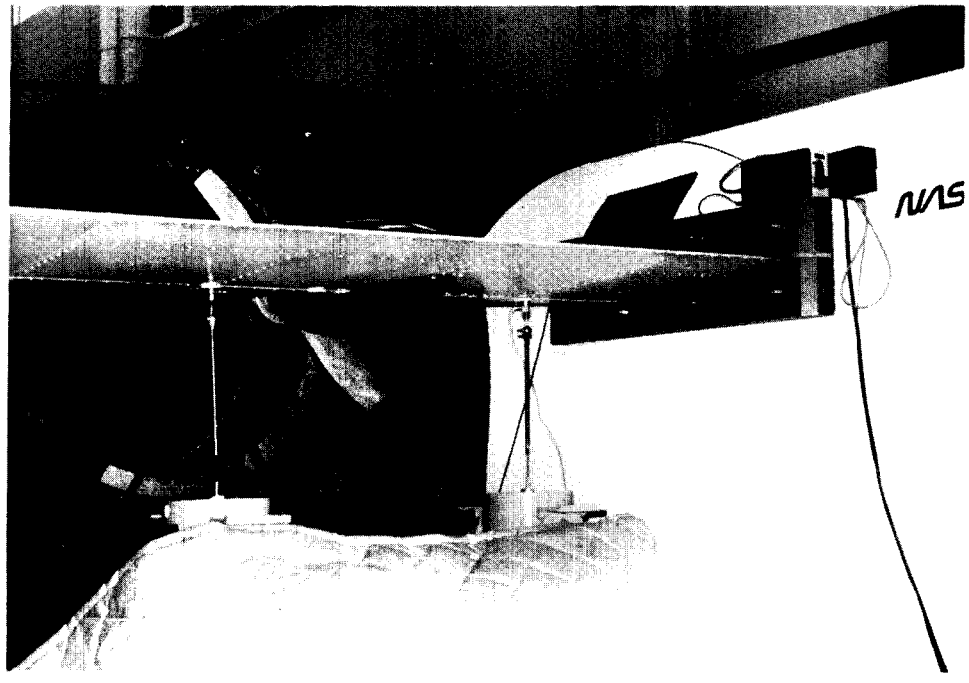

a) Overall

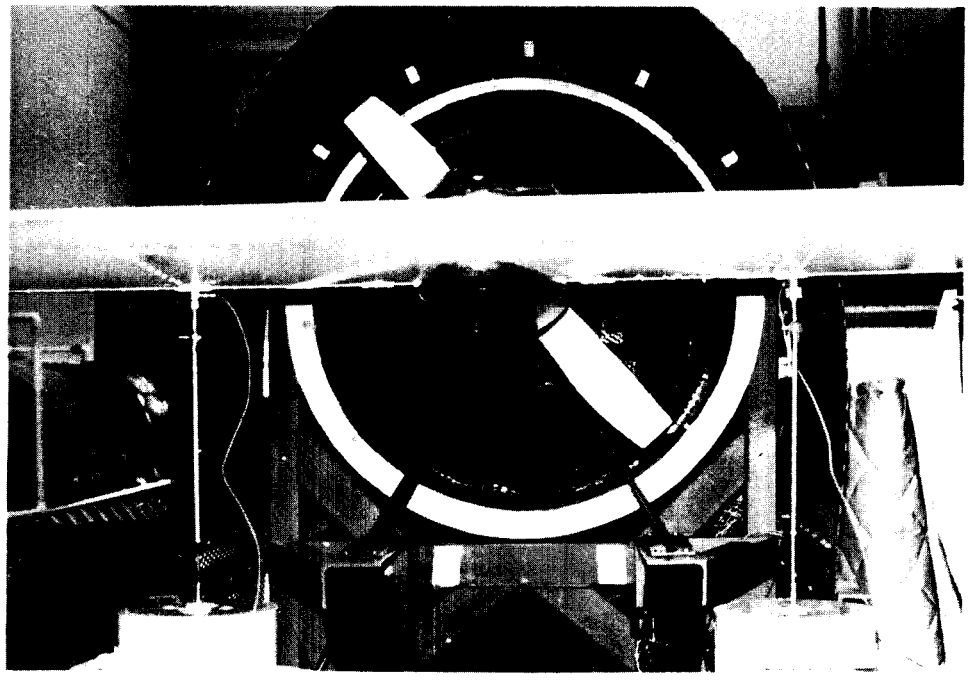

b) Closeup

FIGURE 38. PHOTOGRAPHS OF DUAL SHAKER SETUP FOR ACTIVE VIBRATION/NOISE CONTROL EVALUATION.

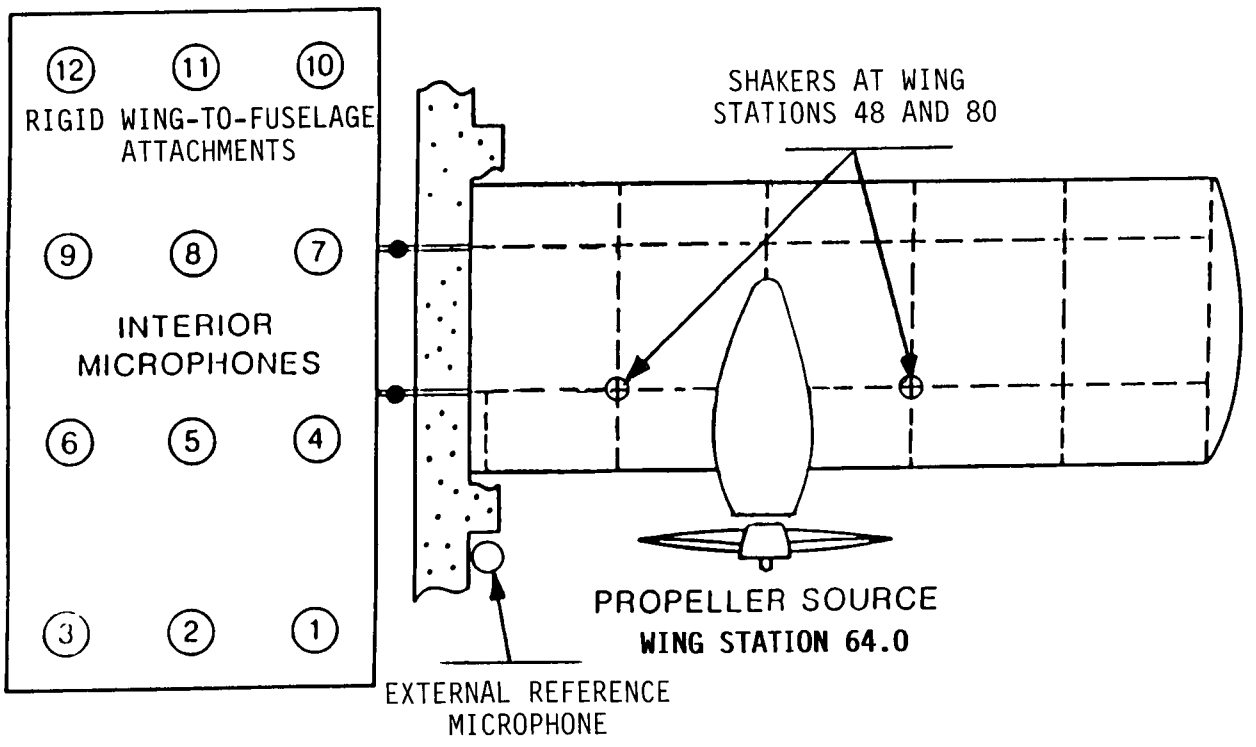

FIGURE 39. SCHEMATIC OF TEST SETUP FOR ACTIVE VIBRATION/NOISE CONTROL EVALUATION.

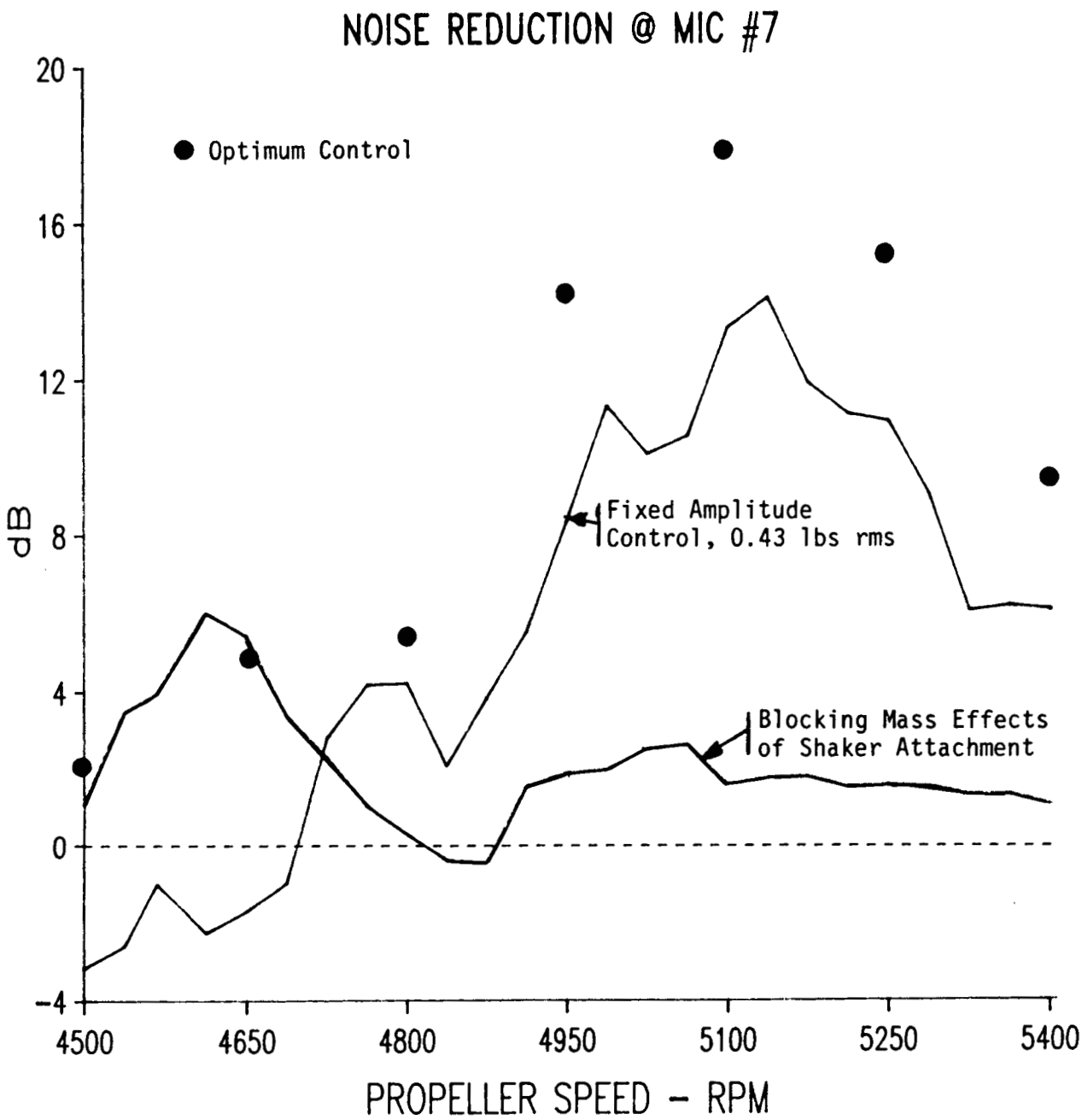

FIGURE 40. DUAL SHAKER STRUCTURE-BORNE NOISE CONTROL.

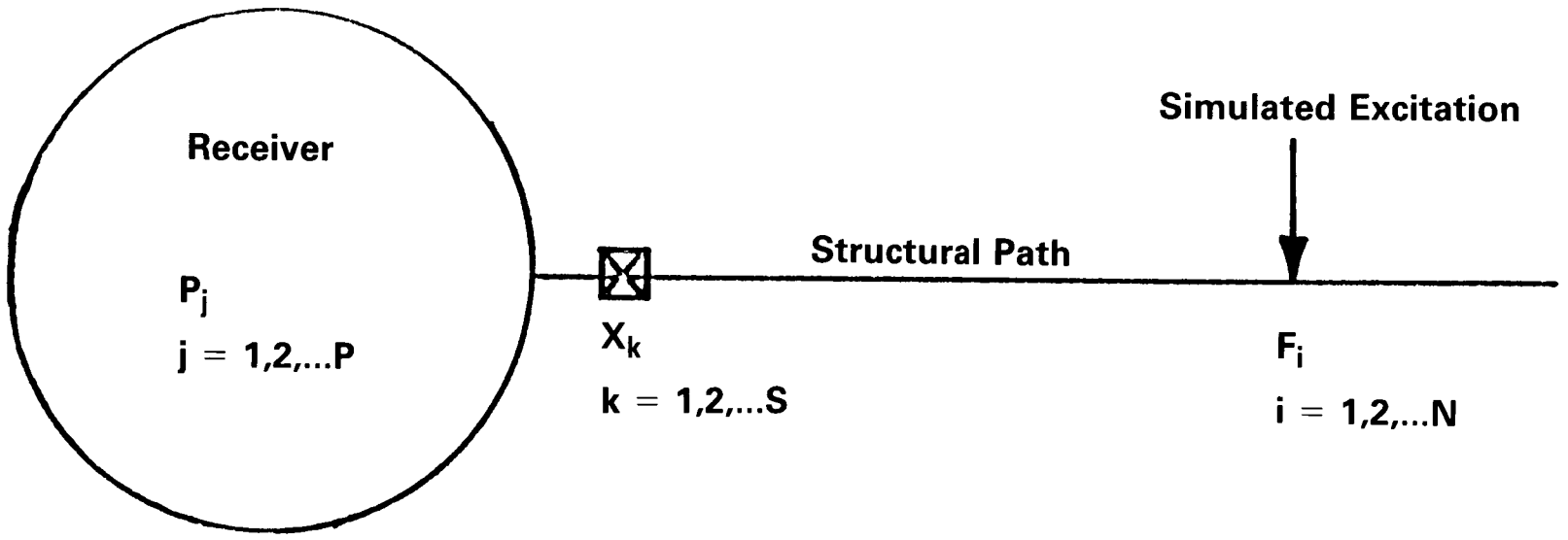

FIGURE 41. IN-FLIGHT STRUCTURE BORNE NOISE DETECTION CONCEPT.

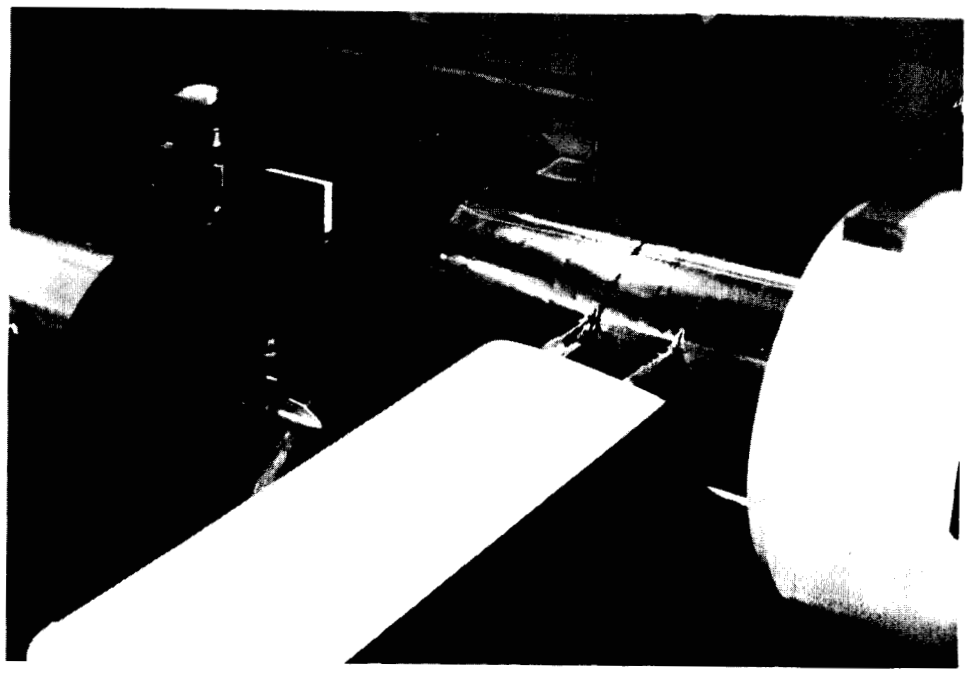

FIGURE 42. IN-FLIGHT SIMULATION TEST APPARATUS.

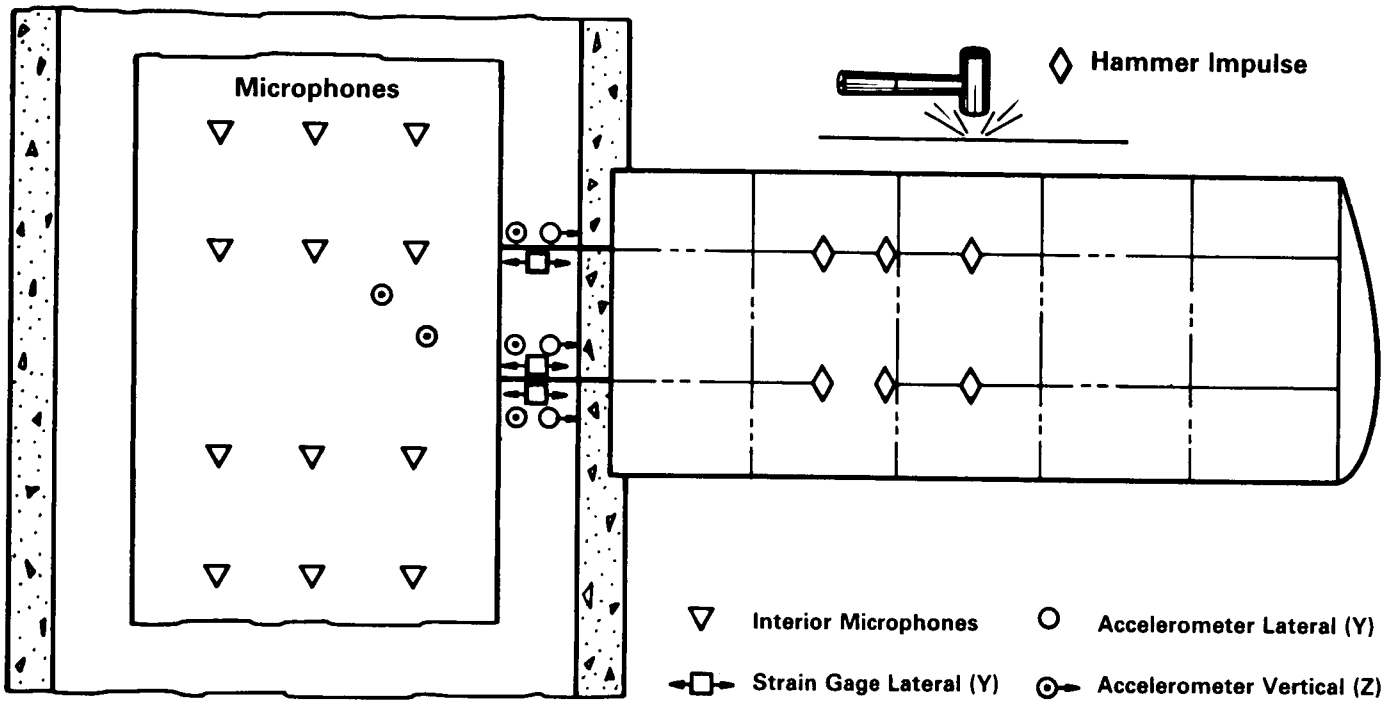

FIGURE 43. IN-FLIGHT STRUCTURE-BORNE NOISE DETECTION, TRANSDUCER LAYOUT.

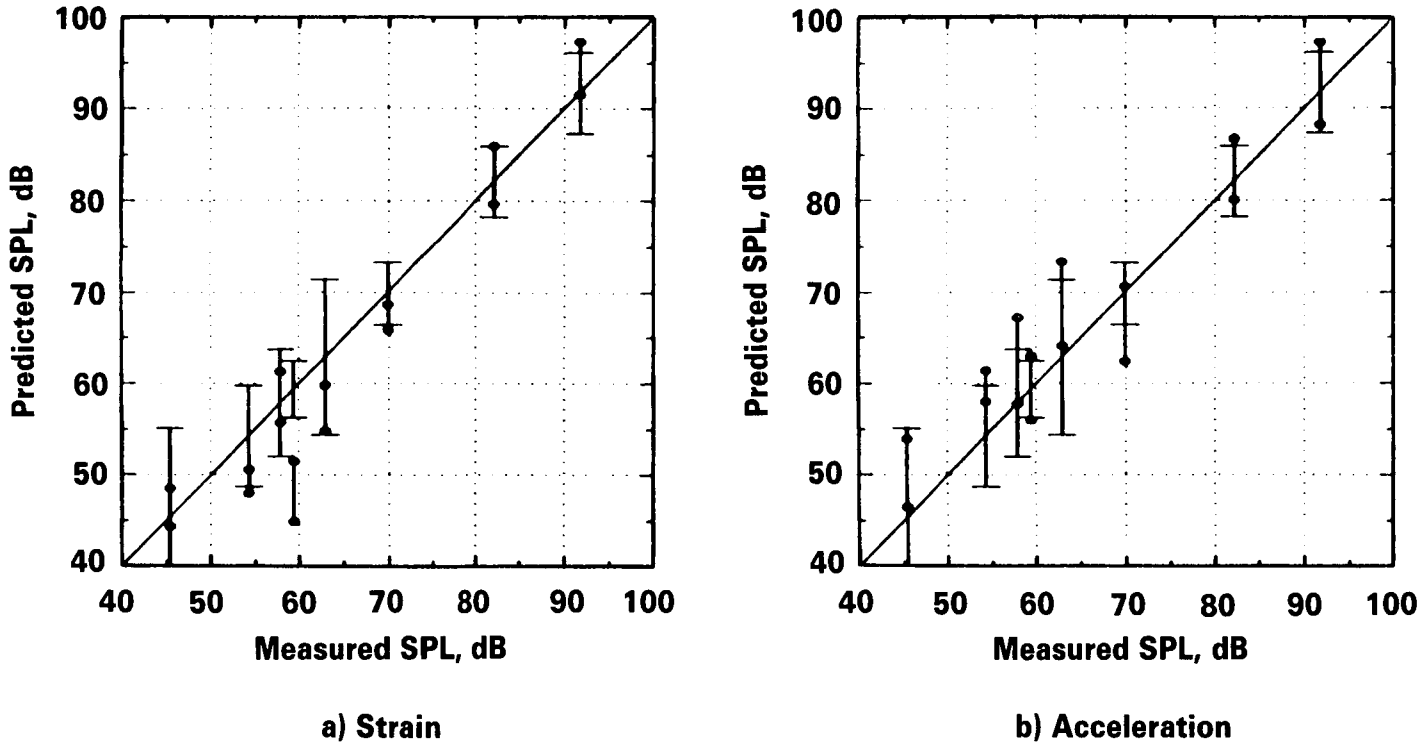

FIGURE 44. PREDICTED VERSUS MEASURED STRUCTURE-BORNE NOISE, WING FRONT SPAR LATERAL RESPONSE.

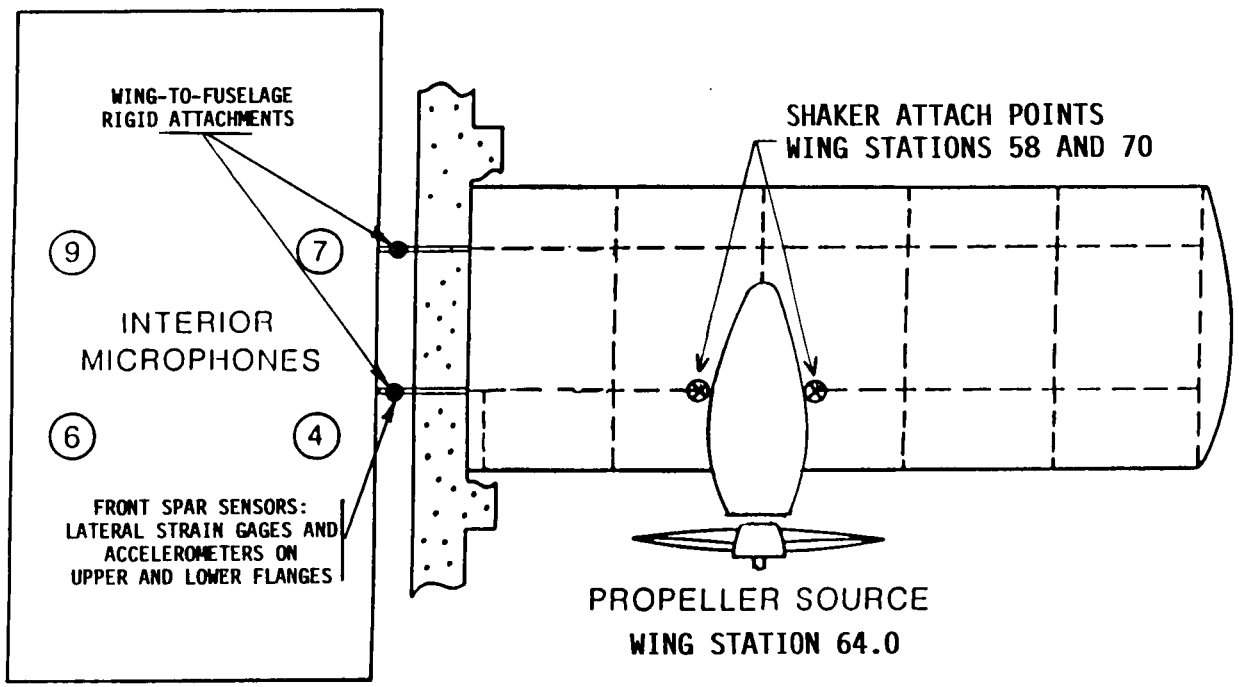

FIGURE 45. IMPROVED STRUCTURE-BORNE NOISE DETECTION PROCEDURES, TEST SETUP.

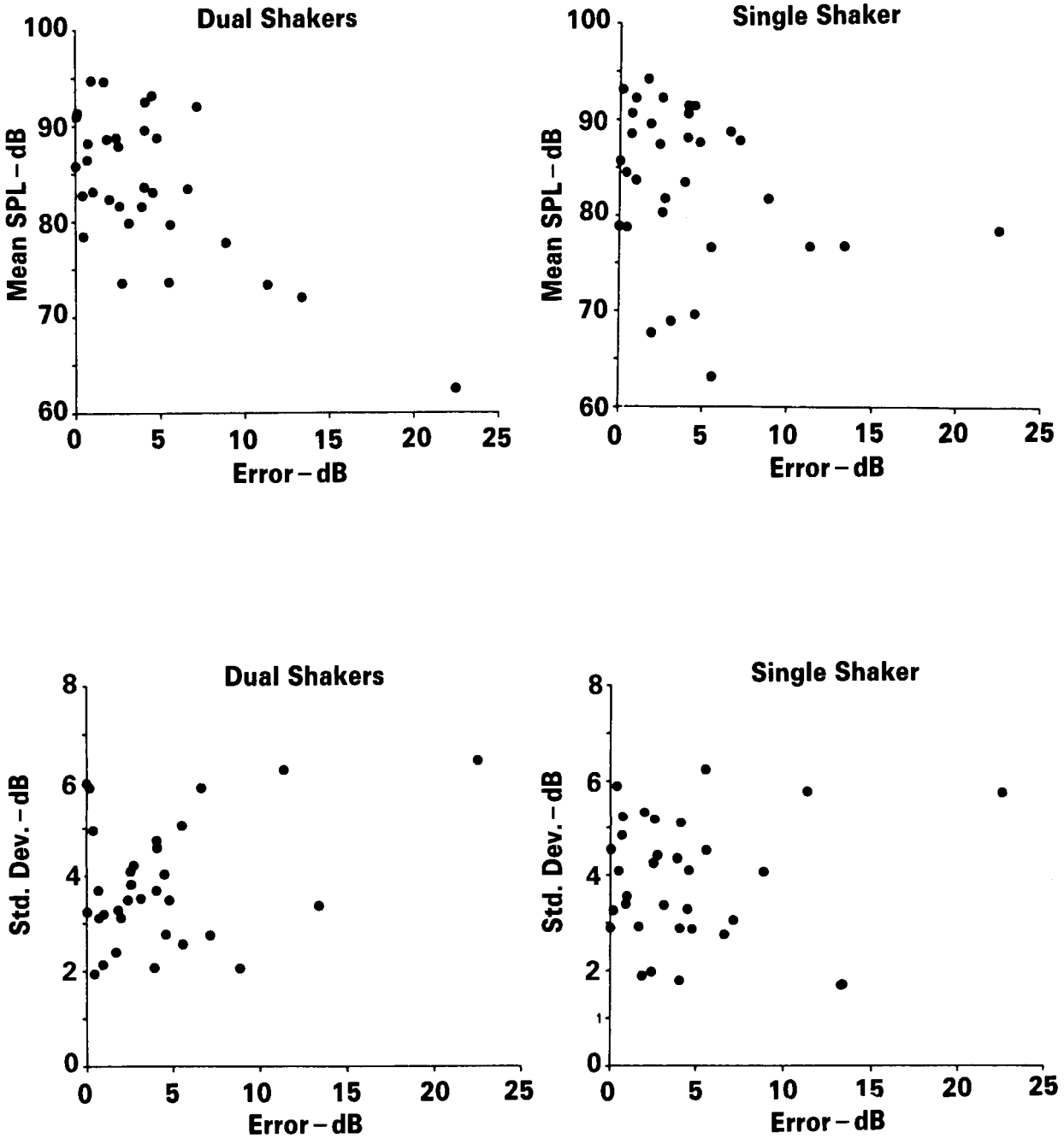

FIGURE 46. CORRELATION OF MICROPHONE MEAN ERROR WITH SOUND PRESSURE LEVEL AND STANDARD DEVIATION.

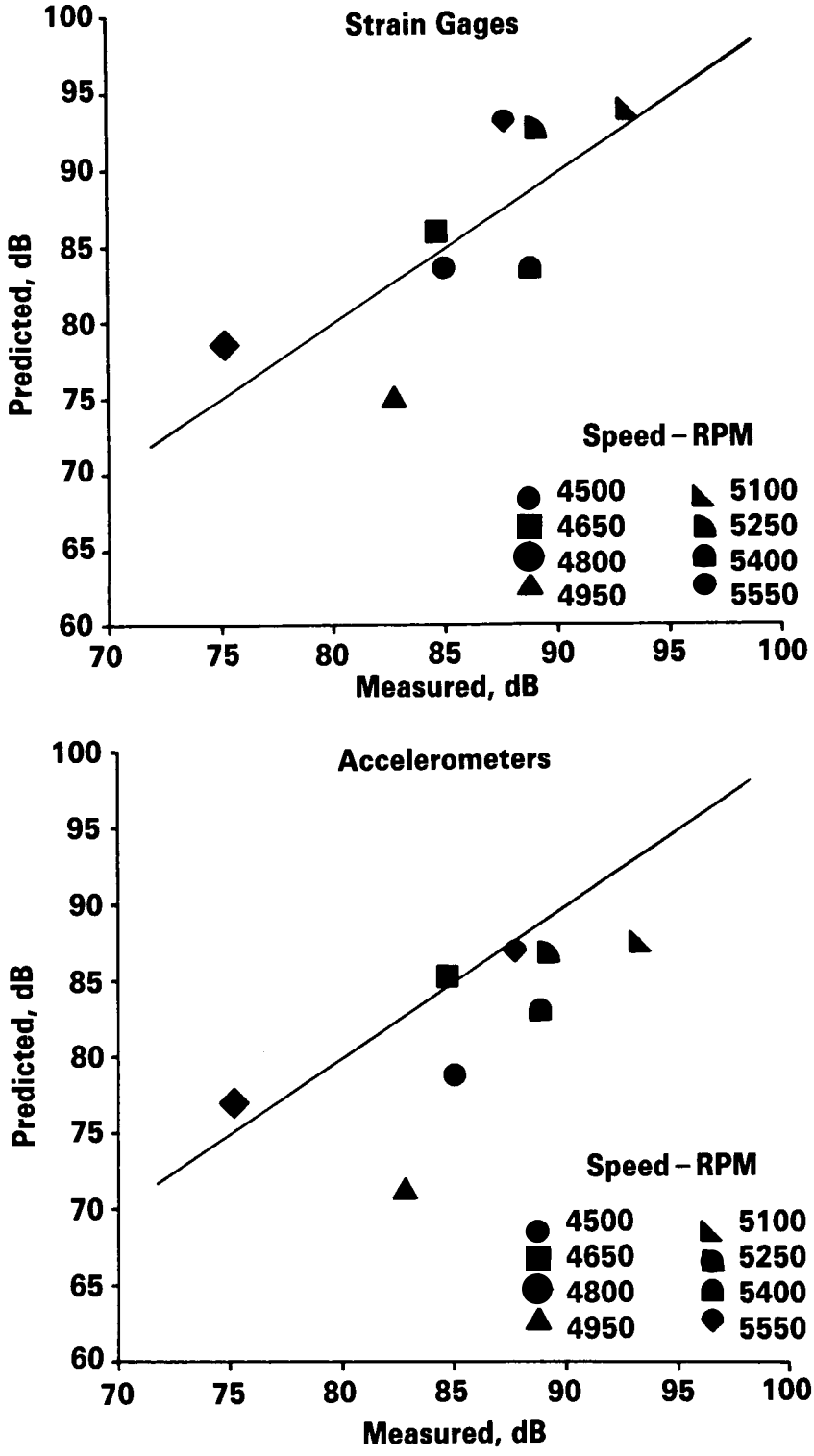

FIGURE 47. CORRELATION OF OVERALL SPATIAL AVERAGE STRUCTURE-BORNE NOISE TRANSMISSION, DUAL SHAKER EXCITATION.

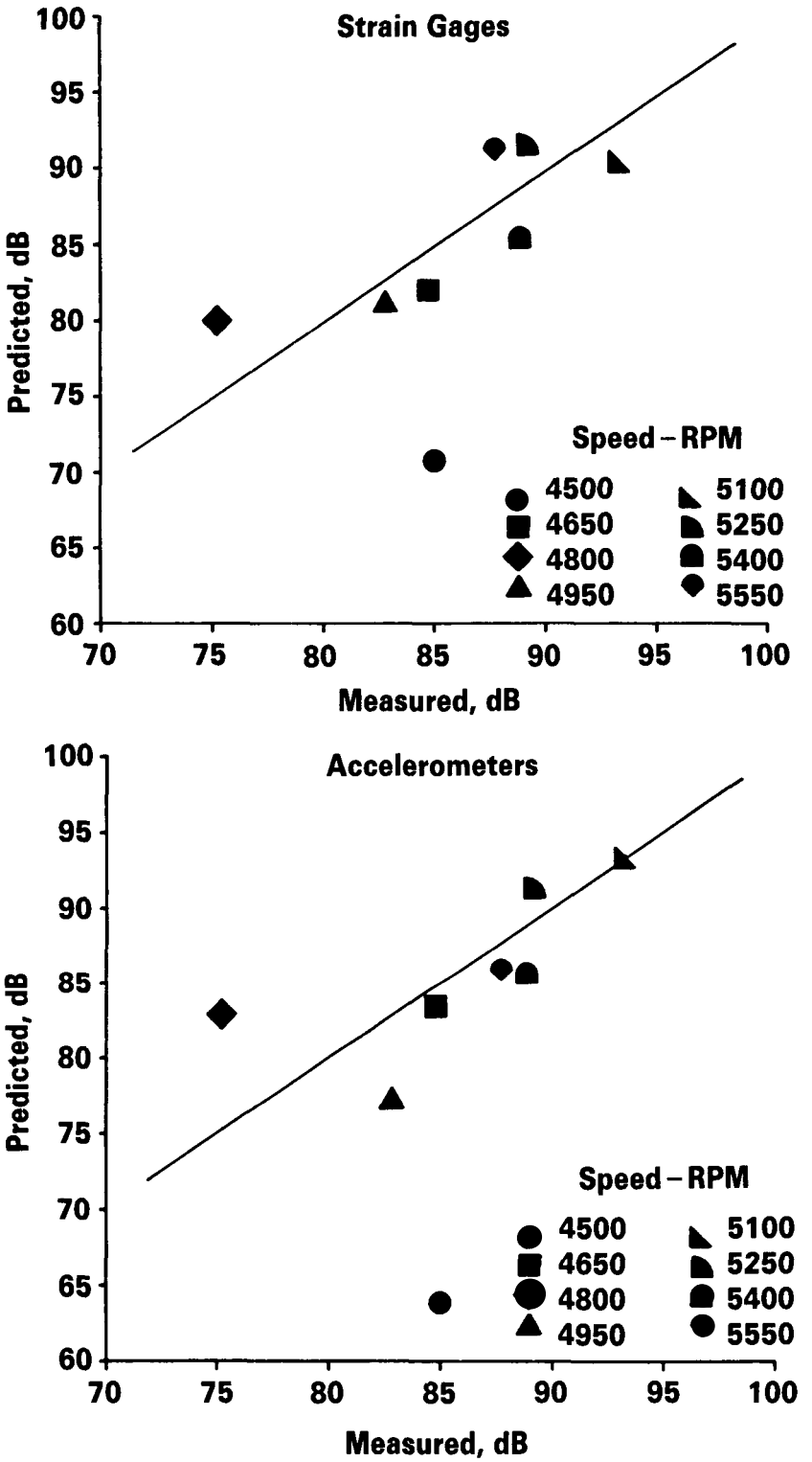

FIGURE 48. CORRELATION OF OVERALL SPATIAL AVERAGE STRUCTURE-BORNE NOISE TRANSMISSION, SINGLE SHAKER EXCITATION.

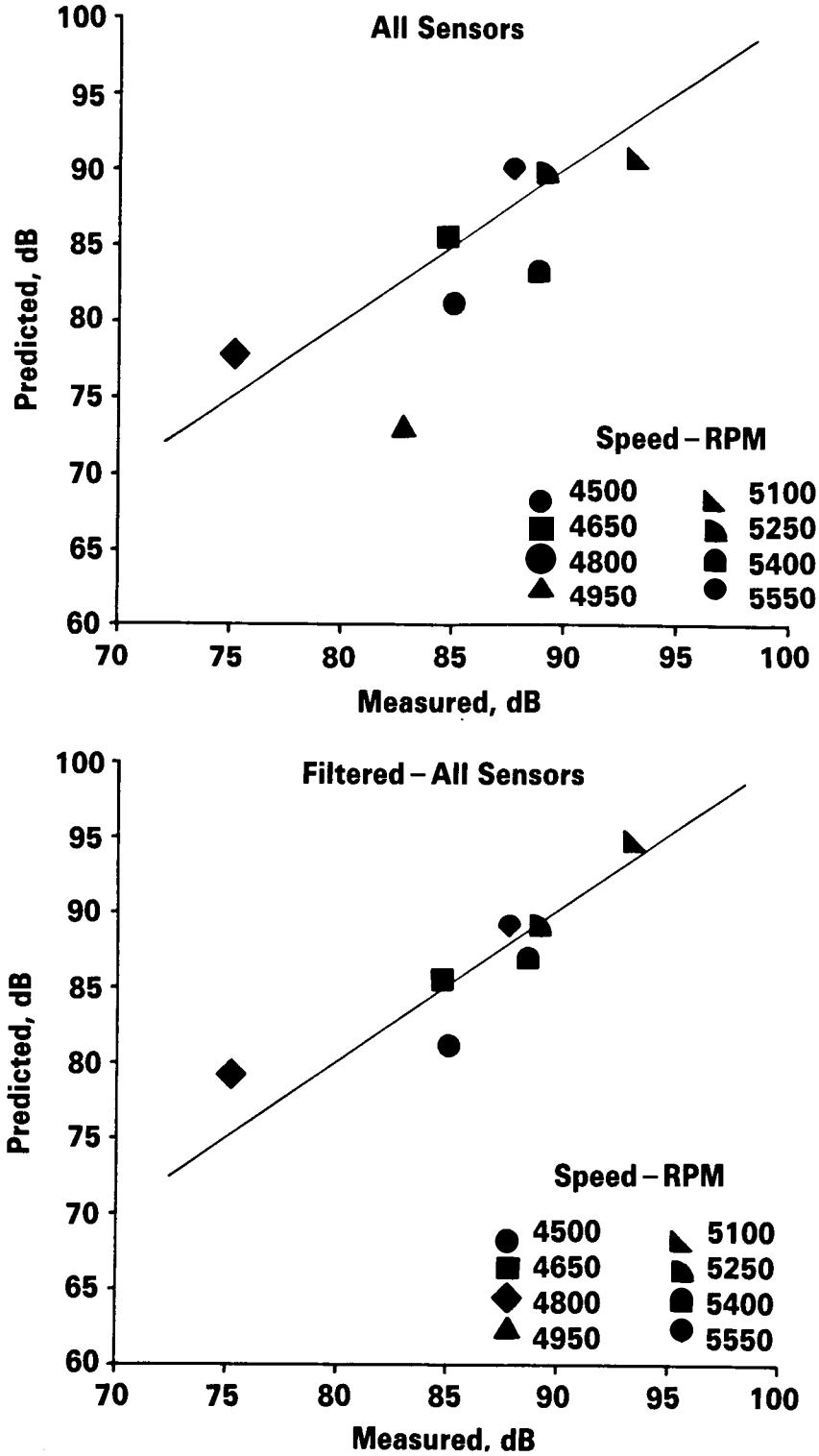

FIGURE 49. CORRELATION OF OVERALL SPATIAL AVERAGE STRUCTURE-BORNE NOISE TRANSMISSION, ALL SENSORS, DUAL SHAKER EXCITATION.

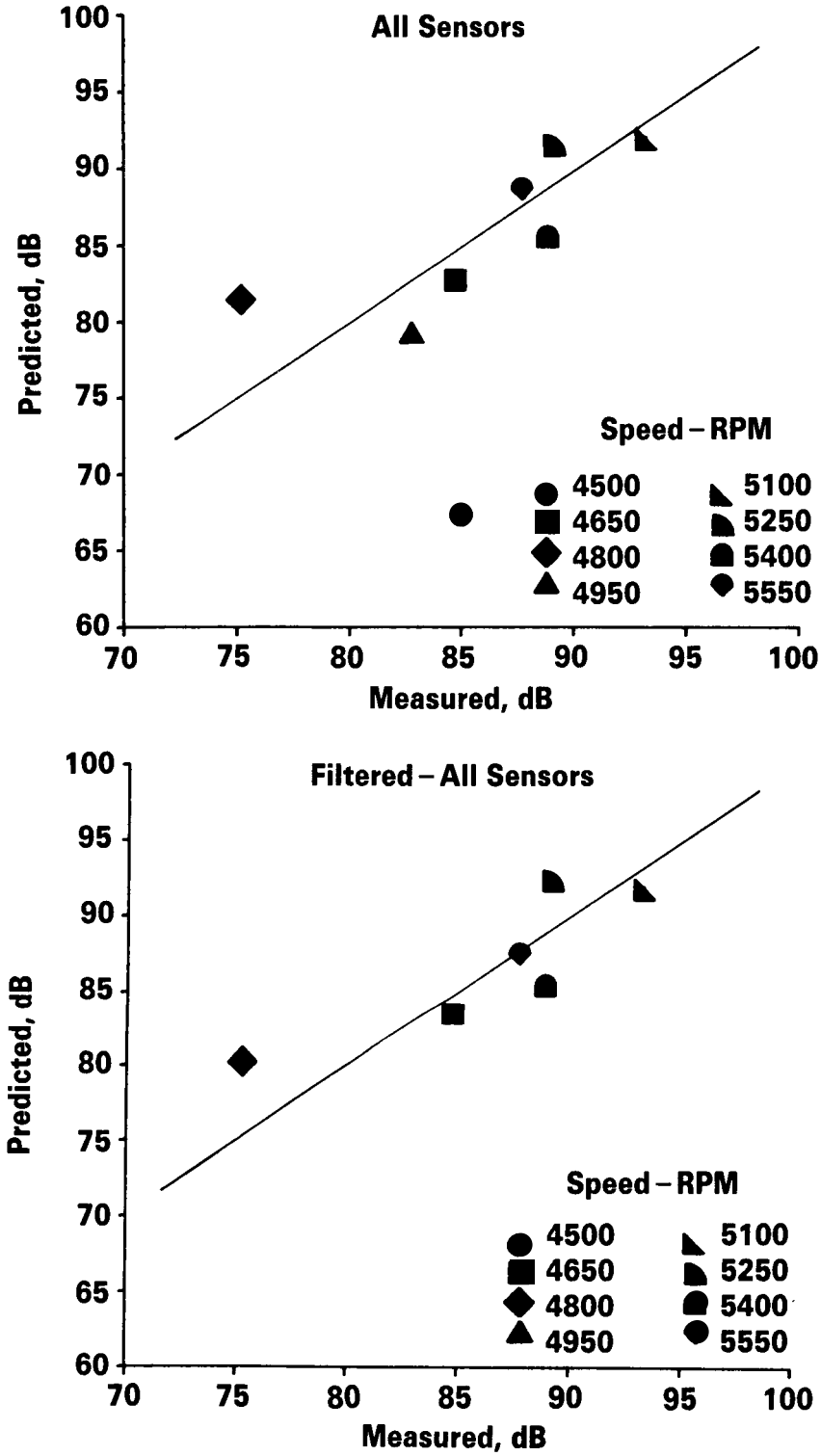

FIGURE 50. CORRELATION OF OVERALL SPATIAL AVERAGE STRUCTURE-BORNE NOISE TRANSMISSION, ALL SENSORS, SINGLE SHAKER EXCITATION.

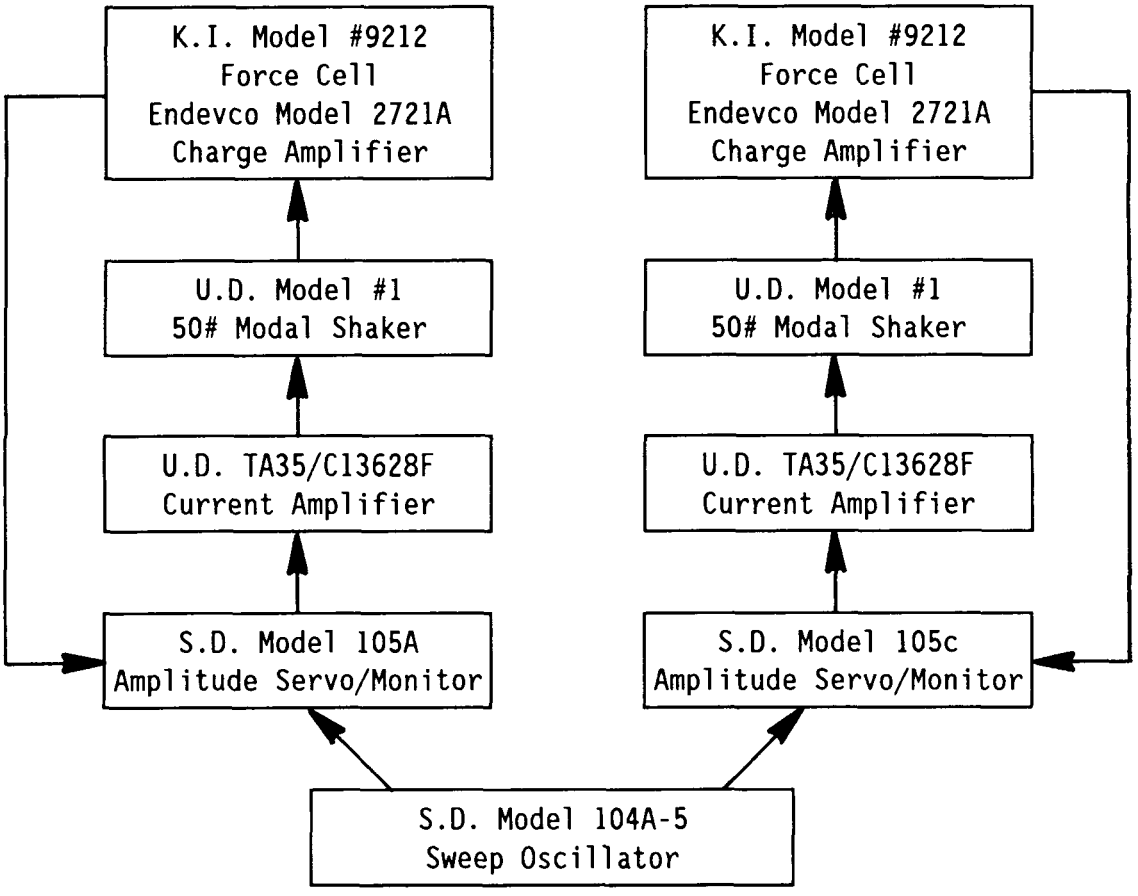

S.D. - Spectral Dynamics
K.I. - Kistler Instruments
U.D. - Unholtz-Dickie

FIGURE 51. DUAL SHAKER CONTROL INSTRUMENTATION

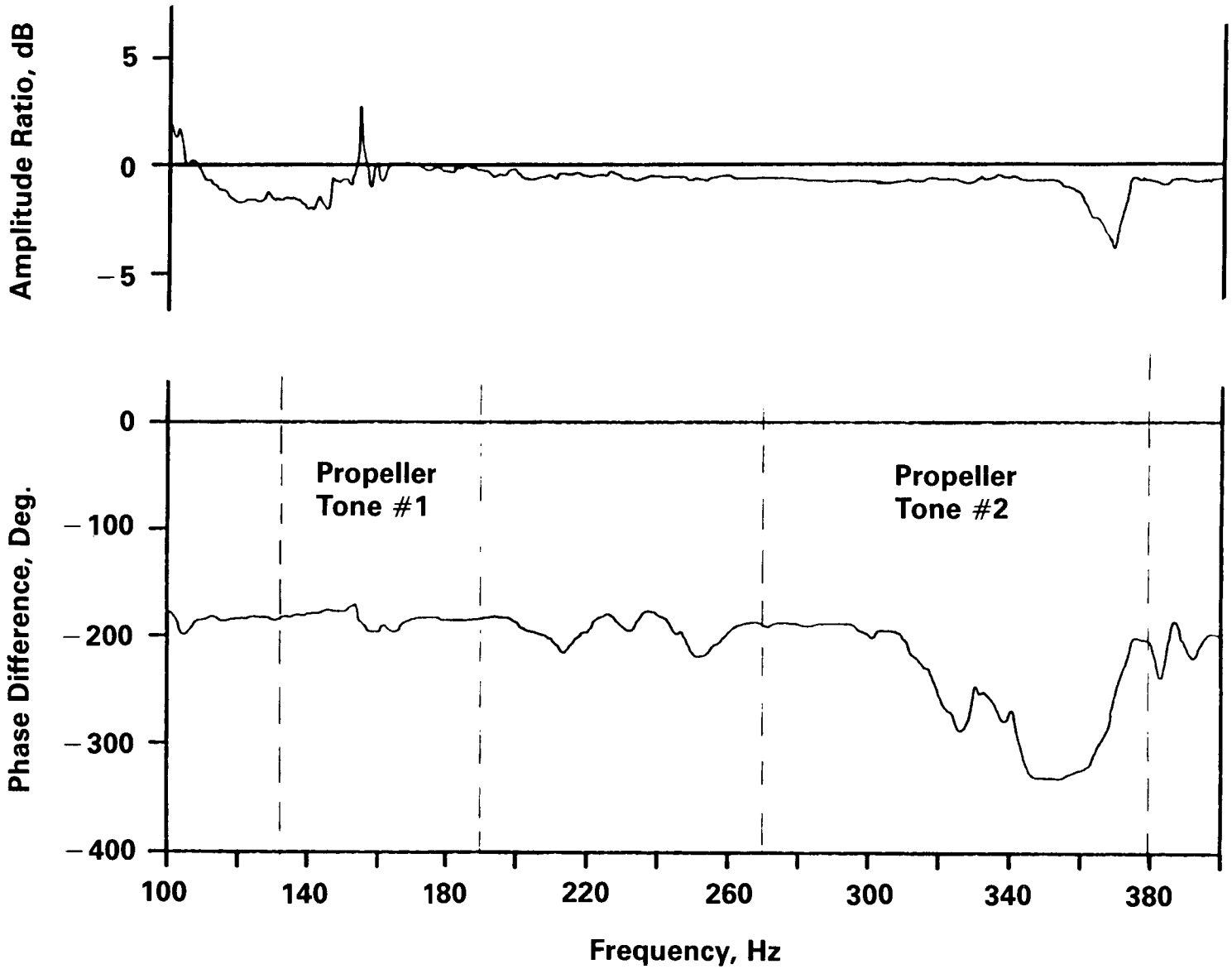

FIGURE 52. DUAL SHAKER CONTROL SIGNALS.

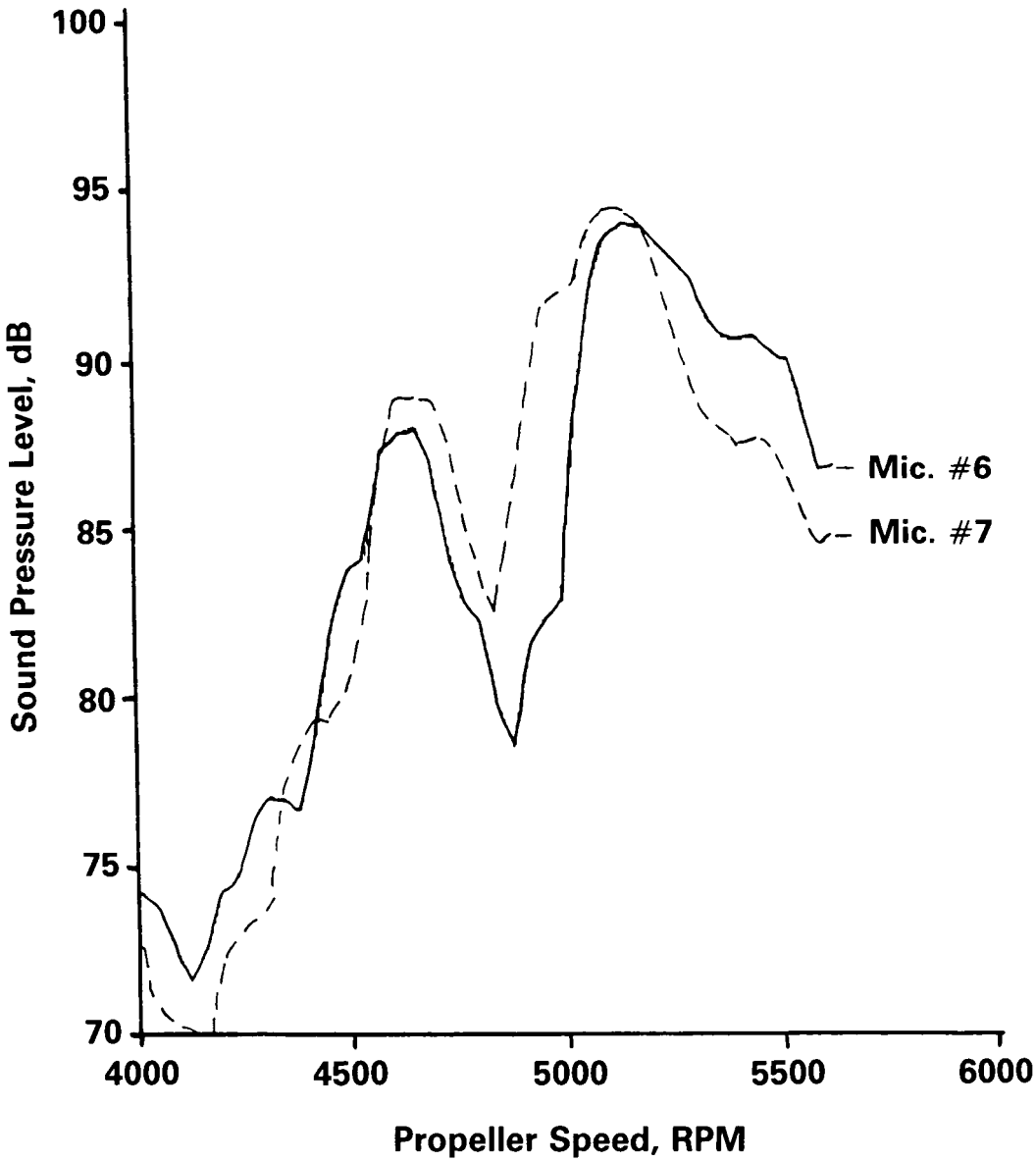

FIGURE 53. STRUCTURE-BORNE NOISE TRANSMISSION, PROPELLER EXCITATION WING STATION 64.

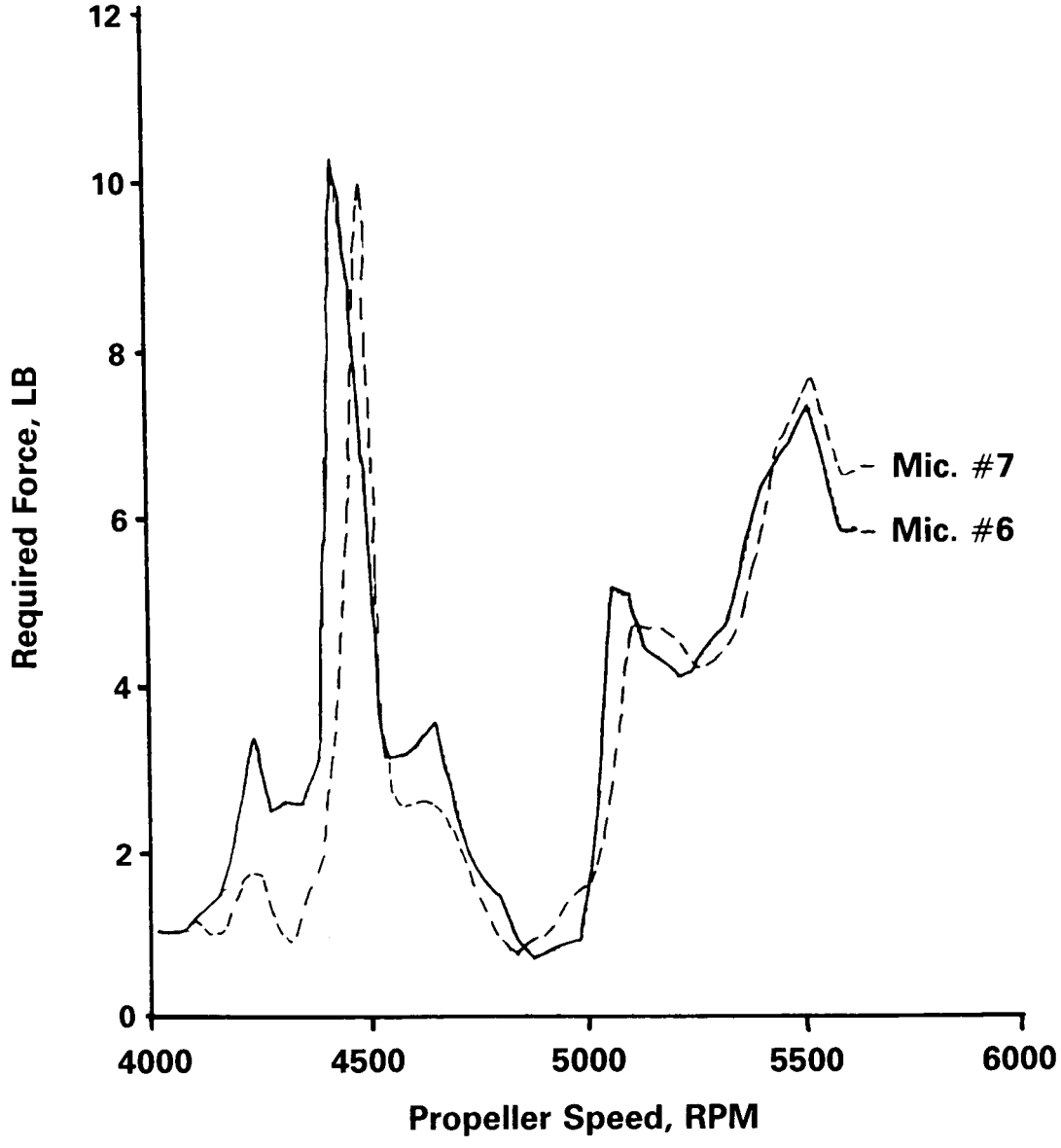

FIGURE 54. FORCE REQUIRED, SINGLE SHAKER EXCITATION WING STATION 70.

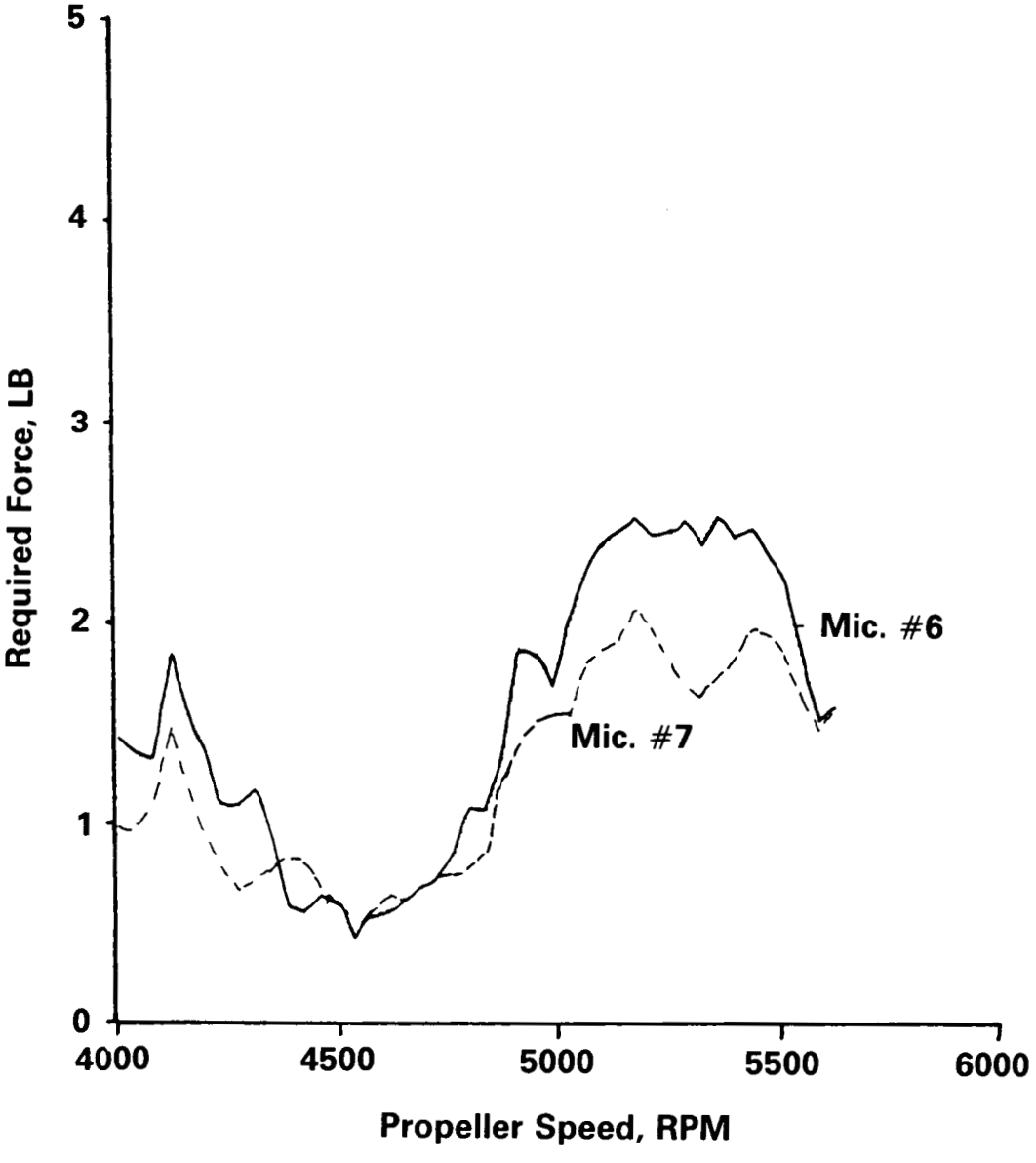

FIGURE 55. FORCE REQUIRED, DUAL SHAKER EXCITATION WING STATIONS 58 & 70.

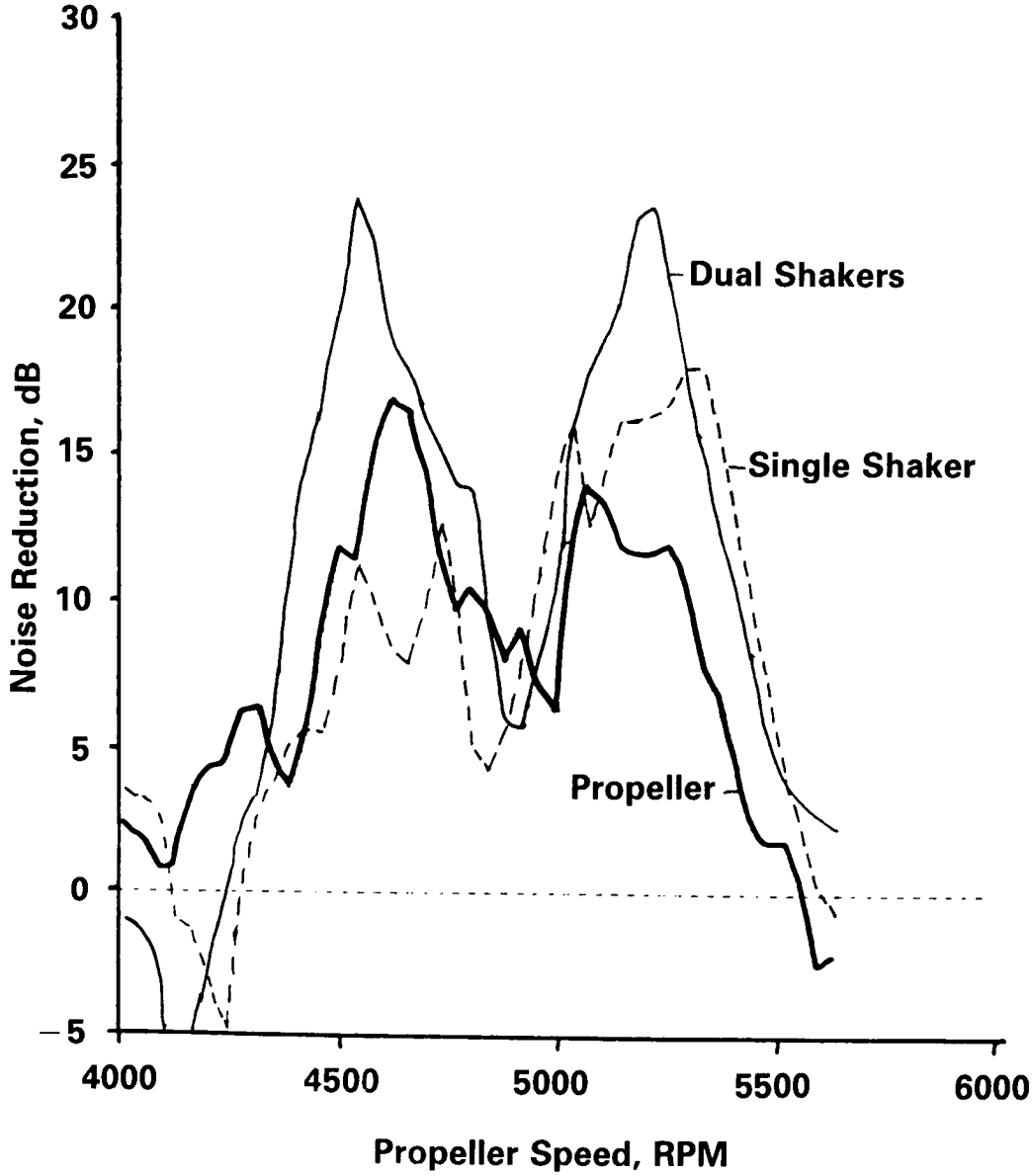

FIGURE 56. STRUCTURE-BORNE NOISE CONTROL EFFECTIVENESS, TUNED DAMPER, MICROPHONE #6.

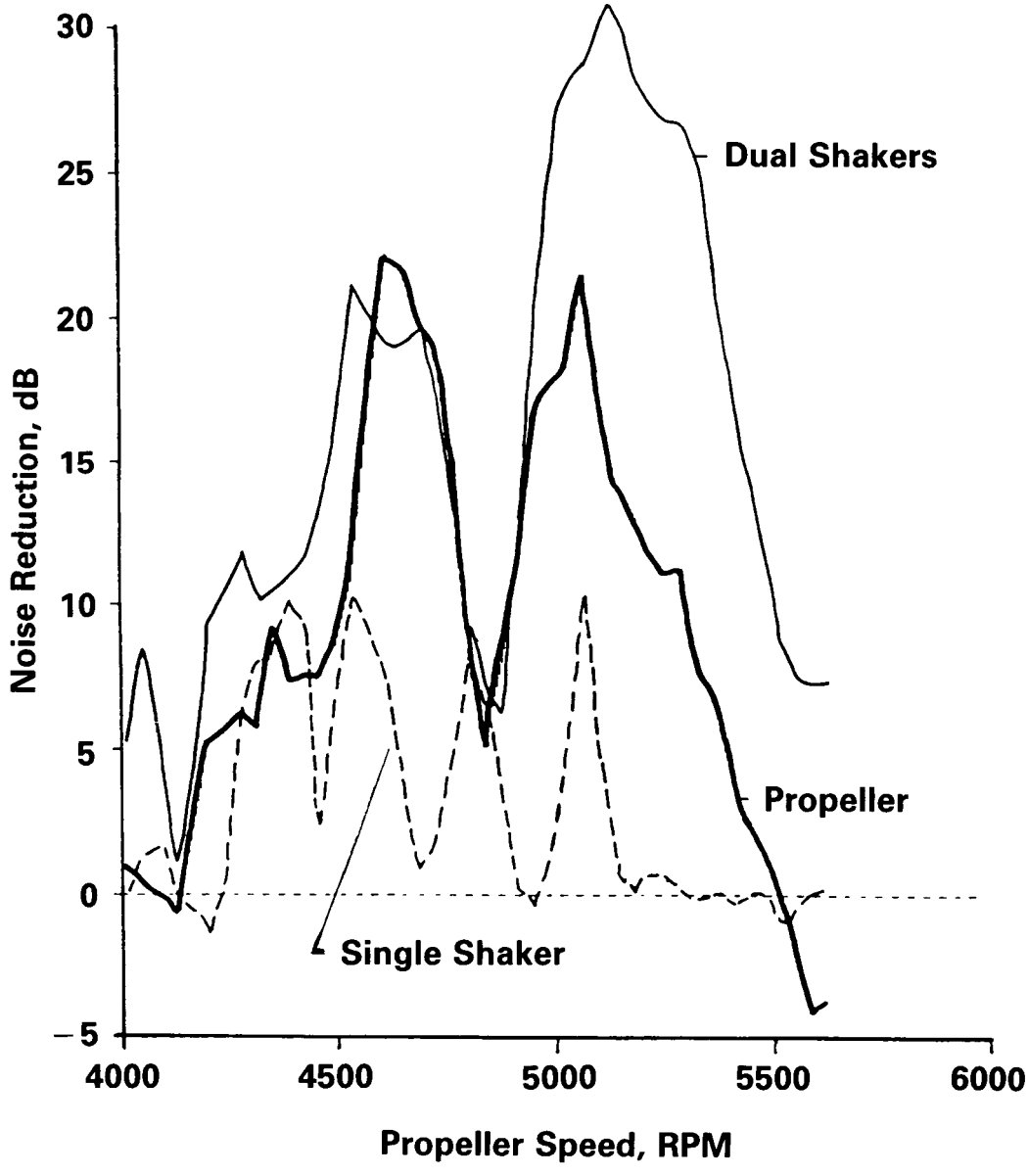

FIGURE 57. STRUCTURE-BORNE CONTROL EFFECTIVENESS, TUNED MECHANICAL DAMPER, MICROPHONE #7.

NASA National Aeronautics and Space Administration

Report Documentation Page

1. Report No.	2. Government Accession No.	3. Recipient's Catalog No.
NASA CR-4255		

4. Title and Subtitle

Aircraft Propeller Induced Structure-Borne Noise

5. Report Date

October 1989

6. Performing Organization Code

7. Author(s)

James F. Unruh

8. Performing Organization Report No.

04-8542-1

10. Work Unit No.

535-03-11-03

9. Performing Organization Name and Address

Southwest Research Institute
6220 Culebra Road, P. O. Box 28510
San Antonio, Texas 78228-0510

11. Contract or Grant No.

NAS1-17921

13. Type of Report and Period Covered

Contractor Report

12. Sponsoring Agency Name and Address

National Aeronautics and Space Administration
Langley Research Center
Hampton, VA 23665-5225

14. Sponsoring Agency Code

15. Supplementary Notes

Langley Technical Monitors: William H. Mayes (retired) and Vern L. Metcalf

16. Abstract

A laboratory-based test apparatus employing components typical of aircraft construction was developed that would allow the study of structure-borne noise transmission due to propeller induced wake/vortex excitation of in-wake structural appendages. The test apparatus was employed to evaluate several aircraft installation effects (power plant placement, engine/nacelle mass loading, and wing/fuselage attachment methods) and several structural response modifications for structure-borne noise control (the use of wing blocking mass/fuel, wing damping treatments, and tuned mechanical dampers). Most important was the development of in-flight structure-borne noise transmission detection techniques using a combination of ground-based frequency response function testing and in-flight structural response measurement. Propeller wake/vortex excitation simulation techniques for improved ground-based testing were also developed to support the in-flight structure-borne noise transmission detection development.

17. Key Words (Suggested by Author(s))	18. Distribution Statement
Structure-Borne Noise Aircraft Propellers	Unclassified-Unlimited Subject Category 71

19. Security Classif. (of this report)	20. Security Classif. (of this page)	21. No. of pages	22. Price
Unclassified	Unclassified	116	A06

For sale by the National Technical Information Service, Springfield, Virginia 22161-2171